2018

Daple Orients and Patterns Sensory Hair Bundles in the Inner Ear

Kimberly Siletti

DAPLE ORIENTS AND PATTERNS

SENSORY HAIR BUNDLES IN THE INNER EAR

A Thesis Presented to the Faculty of

The Rockefeller University

in Partial Fulfillment of the Requirements for

the degree of Doctor of Philosophy

by

Kimberly Siletti

June 2018

DAPLE ORIENTS AND PATTERNS

SENSORY HAIR BUNDLES IN THE INNER EAR

Kimberly Siletti, Ph.D.

The Rockefeller University 2018

The planar orientation of mammalian cells necessitates the integration of diverse pathways. In the inner ear, at least two systems regulate the planar polarity of the hair bundle. The core planar cell polarity (PCP) proteins coordinate the orientations of hair cells across the epithelial plane. The cell-intrinsic patterning of each hair bundle is implemented independently by a G-protein complex comprising the alpha subunit of heterotrimeric G-protein (Gαi) and Leu-Gly-Asn repeat-enriched protein (LGN). Classically known for orienting the mitotic spindle, these proteins form an apical blueprint for hair-bundle development. Although the primary cilium also participates in each of these pathways, the mechanism that links tissue-wide and cell-intrinsic polarity is not yet understood.

To address this issue, I initiated a yeast two-hybrid screen with a central component of the cell-intrinsic pathway, Gαi3. One of the most promising candidates, Dishevelled-associating protein with a high frequency of leucine residues (Daple), interacts with core PCP and cell-intrinsic signals. Here I show that Daple participates in the implementation of cell-intrinsic polarity. Regulated by G-protein signals, Daple is required for the correct positioning of the primary cilium at the apical surface. My results moreover suggest that the primary cilium or an associated structure influences the domain of Gαi3 expression that shapes the hair bundle. Daple is therefore essential to orient and pattern sensory hair bundles.

Acknowledgements

I would like to begin by thanking my advisor, Jim Hudspeth. During graduate school, I found a deep enthusiasm for science largely because Jim encouraged me to pursue my own ideas, explore new methods, and make new mistakes. I am grateful to him for his support, as well as for the matchless example he provides for his students. I feel privileged to have had the opportunity to learn from one of the best thinkers and communicators in scientific research.

In the same vein I would like to thank the members of my faculty advisory committee, Elaine Fuchs and Vanessa Ruta. I am deeply grateful for their thoughtful advice and for their enthusiasm for my project. I also thank Matthew Kelley for taking the time to serve on the committee as my external examiner.

Many other members of the Rockefeller community contributed to my graduate experience. The Flow Cytometry and Genomics Resources Centers made new technologies seem less intimidating; Alison North and the Bioimaging Resource Center taught me nearly everything I know about using a microscope. I also want to acknowledge the support of the Dean's office, especially Cristian Rosario, Marta Delgado, and Stephanie Fernandez for being endlessly helpful.

I additionally thank my undergraduate advisor, Jason Morris, whose infectious enthusiasm for science convinced me to attend graduate school. I remain sincerely grateful that he pointed me in this direction.

A special thanks also goes to my collaborator Basile Tarchini, whose mentorship near the end of my project was invaluable. Both the project and my graduate education were significantly improved by our many discussions.

I wish I had the space here to individually and elaborately thank each member of the Hudspeth group. I feel indescribably lucky to have worked in an environment where my colleagues answered my questions exhaustively and brightened the day. I truly looked forward to work because of the kindness and comedy I continually found there. A special thanks goes to Adedeji Afolalu, Maria Vologodskaia, Ksenia Gnedeva, Taeryn Kim, and Sean Low for greatly expanding my experimental abilities; Dáibhid Ó Maoiléidigh for the abundance of advice he has provided over the years; Beth Dougherty for providing administrative and other invaluable forms of assistance, including emotional support; and Brian Fabella for ordering materials, fixing every computer I touched, and finishing the crossword. I additionally thank Adrian Jacobo for hours upon hours of helpful discussion and collaboration. Lastly, I wish to extend my gratitude to Aaron Steiner for his mentorship. I never would have made it this far without his incessant advice, humor, and encouragement during my first years in the lab.

On a personal note, I am deeply grateful to my boyfriend for his constant care and understanding. I am incapable of expressing my appreciation for his honesty, humor, and optimism, which improve my each and every day. I also want to thank my best friend for her unconditional love and encouragement, and my nephews for keeping me grounded (often literally). I thank all of my childhood friends for believing in me, in that way only childhood friends do, and for pushing me through difficult times. I wish most especially to acknowledge James Kurinskas, to whose memory I lovingly dedicate this work. His honest, dependable character and wholehearted support still inspire me to be a better person and a better scientist.

Most importantly I owe an indescribable debt of gratitude to my family. My baby

sister is my role model, because she has always been stronger, braver, and more hilarious than I am. I also wish to acknowledge my parents but would not know where to begin. I should probably thank them for their unconditional love, for pushing me to be resilient, and for being proud of me when I fail. They say you should never meet your heroes, but I go home sometimes anyway.

Table of Contents

List of Figures

List of Tables

Chapter One: Introduction

Cellular polarity of the hair cell

The vast majority of our cells rely on asymmetries in shape and organelle distribution to function properly. These asymmetries are collectively referred to as cell polarity. Epithelial cells, for example, characteristically exhibit polarization along two axes. One axis separates the functions of the cell's apical surface—absorption, secretion, and motility, for example—from those of the basolateral surface—such as adhesion, intercellular communication, and synaptic transmission. The second axis lies within the plane of the epithelium and is therefore termed planar cell polarity (PCP).

A remarkable example of cell polarity is found in the vertebrate inner ear. Both the auditory system and the vestibular system rely on a sensory receptor cell called the hair cell to detect sound and acceleration. Like other epithelial cells, the hair cell is asymmetric along two axes. An apical organelle termed the hair bundle transduces mechanical stimuli into electrical signals. The middle portion of the cell holds the cell's nucleus and the organelles of protein synthesis, processing, and degradation. Finally, the cell's base contains ribbon synapses that mediate signaling to afferent nerve fibers.

Each hair cell is also precisely oriented within the epithelial plane. The hair bundle comprises a few tens to a few hundreds of rigid, actin-filled stereocilia arranged in a staircase pattern. The hair cell's primary cilium, the kinocilium, stands at the tall edge of the staircase. Deflection of the bundle toward its tall edge opens channels at the tips of the stereocilia, depolarizes the cell, and excites the associated nerve fibers[1]. Stimulation in the opposite direction elicits inhibition, and orthogonal deflection has no effect.

Because each hair bundle is thus responsive along a specific axis, hearing and balance require that this axis of sensitivity correspond with that of mechanical stimulation. Nevertheless the mechanisms that orient and pattern hair bundles remain poorly understood.

The Wnt/PCP pathway from flies to mammals

First studied in *Drosophila*, the factors that regulate PCP are also required for vertebrate development. The correct planar orientation of cells, for example, enables embryonic tissues to extend along a specific axis, a process referred to as convergent extension (CE). CE is essential to properly form a number of organs, including the central nervous system and the cochlea. Although PCP additionally contributes to the formation of ciliated organs such as the kidney and skin, planar polarity in mammals remains poorly understood[2].

In *Drosophila* the planar orientation of a cell is specified by the distribution of six core PCP proteins: Frizzled, Van Gogh, Flamingo, Dishevelled, Prickle, and Diego. Van Gogh and Prickle inhibit the formation of a Frizzled-Dishevelled complex, whereas Diego competes with Prickle to stabilize the complex. These interactions segregate the six proteins into two complexes, Frizzled–Dishevelled-Diego and Van Gogh-Prickle, on opposing sides of a cell. Flamingo interacts with both complexes. Frizzled, Van Gogh, and Flamingo additionally stabilize one another across cell membranes, propagating PCP across a tissue[3]. A long-range gradient of Wnt coordinates this propagation by providing a directional cue. Epithelial cells in multiple *Drosophila* tissues orient toward a source of Wnt expression. Because their ectopic expression moreover alters the localization of the

core PCP proteins, dWnt4 and Wg appear to play an instructive role in planar orientation[4].

Each core PCP gene has at least one homolog in mammals, and mutations of these genes disrupt the coordinated orientation of hair cells in the inner ear[5]. The organ of Corti, the sensory epithelium of the auditory system, is a spiral epithelium that contains four rows of hair cells. Three rows of outer hair cells and one row of inner hair cells are separated by tow rows of supporting cells. Acoustic stimulation evokes mechanical vibrations along an axis that runs radially from the center of the cochlea toward its periphery, or between the neural and abneural edges of the organ of Corti (Figure 1.1). Although all hair cells are oriented toward the abneural edge of the epithelium, the mutation of a core PCP protein affects each row of hair cells to a different extent. In the *Looptail* Vangl2 mutants, both inner hair cells and outer hair cells are misoriented. The last row of outer hair cells is most affected, whereas the first row of outer hair cells is least affected[6-8]. In contrast, *Frizzled-3;Frizzled-6* double mutants exhibit few misoriented outer hair cells, but many inner hair cells are oriented toward the neural edge of the epithelium[9]. A gradient of Wnt5a expression has also been implicated in mammalian planar polarity. Wnt5a is expressed at the neural edge of the cochlea, and its inhibition most severely perturbs the third, abneural row of outer hair cells[10].

Although the core PCP pathway is functionally conserved in mammals, the *Drosophila* and mammalian pathways exhibit notable differences. First, the proteins form different complexes in cochlear hair cells than in *Drosophila* wing cells. Although the mammalian isoforms of Frizzled and Van Gogh localize on the neural side of the hair cell (Figure 1.2A), Dishevelled occurs on the abneural side. Second, the localization of all six

factors within a cell is sufficient to specify polarity in *Drosophila* but not in the mammalian inner ear. Two of the sensory epithelia of the vestibular system, the saccule and the utricle, each contain a distinct line of polarity reversal across which hair cells are oppositely oriented. Localization of neither Prickle-like 2 nor Frizzled 6 differs between cells situated on either side of the reversal[11]. Thus the localization of core PCP factors is not sufficient for the establishment of mammalian planar polarity. An additional mechanism must specify polarity cell-autonomously.

Planar cell polarity and the primary cilium

Another salient difference between *Drosophila* and mammals is the importance of the primary cilium. Whereas most cells in *Drosophila* have no cilia, mammalian primary cilia have been implicated in multiple signaling pathways[12]. The mammalian Wnt/PCP pathway first numbered among these after the ciliary protein Inversin was found to regulate the localization of Dishevelled. By permitting the accumulation of Dishevelled at the cell membrane, Inversin acts as a molecular switch between the canonical Wnt and Wnt/PCP pathways[13]. The set of disorders termed ciliopathies, which are caused by defective primary cilia, have also been associated with PCP defects, and Dishevelled and Vangl2 localize to the cilia in some vertebrate cell types[13, 14].

Some of the most compelling evidence linking PCP to the primary cilium has emerged from the mammalian inner ear. The kinocilium is suggestively found at the apex of the hair bundle, and its genetic ablation disrupts hair-bundle orientation. The intraflagellar transport (IFT) proteins, for example, are necessary for the formation and maintenance of primary cilia. Conditional knockout of Ift88 causes defects in hair-bundle

orientation that correlate with mispositioning of the basal body[15]. A subset of cells with central basal bodies exhibits circular hair bundles. Because Vangl2 remains asymmetrically distributed, the mechanism by which Ift88 affects PCP remains unclear. Conditional knockout of the IFT motor Kif3a likewise results in misoriented hair bundles without significantly disrupting the asymmetric localization of Dishevelled[16]. Bundle orientation in *Kif3a* mutants, however, is uncoupled from rather than correlated with basal-body position. Because Kif3a may additionally position the basal body through Rac-PAK signaling, this discrepancy might reflect a non-ciliary role of the protein.

Indeed other ciliary factors are now known to function beyond the formation of the primary cilium. A recent study characterized the PCP defects apparent in mutants of Ift20 and Bbs8, a protein implicated in the ciliopathy Bardet-Biedl syndrome.[17]. Unlike the absence of Ift88 or Kif3a, Bbs8 and Ift20 deficiencies deplete Vangl-2 from the junctions between hair cells and supporting cells. Immunogold localization of Bbs2 and Ift20 in the cochlea moreover demonstrates that these proteins localize to stereocilia, microvilli, and other actin-based cellular structures in addition to the microtubule-based kinocilium. Because the authors demonstrate direct physical interactions between these proteins and Vangl-2, their results suggest that a subset of ciliary proteins is involved in intracellular trafficking. Thus the nature of the primary cilium's role in planar cell polarity signaling is yet to be fully understood.

Cell-intrinsic polarity in the inner ear

In a core PCP mutant, hair bundles are misoriented in the epithelial plane but maintain their normal shapes. An independent signaling system regulates the cell-intrinsic polarity

of the hair bundle. In particular, the apical surface of each hair cell is patterned by a molecular "blueprint" comprising proteins that are classically known for orienting the mitotic spindle during asymmetric cell division[18, 19]. Well characterized in *Caenorhabditis elegans* and *Drosophila*, an asymmetric cell division yields two daughter cells that adopt different fates. This process necessitates the coordination of multiple signaling complexes. First, the partitioning defective (Par) proteins and atypical protein kinase C (aPKC) establish cortical polarity in the mother cell. Secondly, the mammalian Inscuteable protein (mInsc) links the Par proteins to a second complex comprising the alpha subunit of heterotrimeric G-protein (Gαi) and Leu-Gly-Asn repeat-enriched protein (LGN). During mitosis, the G-protein complex aligns the mitotic spindle with polarity cues such that cell-fate determinants segregate into one daughter cell[20].

G-protein signals might orient the mitotic spindle through interactions with the minus end-directed motor Dynein and its activator Dynactin[21]. In *C. elegans,* a protein similar to the mammalian nuclear mitotic apparatus protein (NuMa) links an LGN homolog to the Dynein-Dynactin complex. Because Gαi is myristoylated and thereby attached to the cell membrane, the processive activity of Dynein along microtubules presumably generates a pulling force on the microtubule aster. This mechanism is moreover conserved in mammals; the absence of LGN, NuMA or Dynactin perturbs spindle orientation in mouse basal keratinocytes[22]. Whereas the loss of Par-3, mInsc, or Gαi causes mild orientation defects, the loss of both Gαi and mInsc mimics the more severe phenotype that is observed upon knockdown of LGN[23]. The results suggest that during mammalian asymmetric cell division, Gαi and mInsc orient the mitotic spindle by cooperating to recruit LGN to the cell cortex.

The machinery that orients the mitotic spindle is repurposed in the post-mitotic sensory cell of the cochlea. Par-3, Gαi, LGN, and mInsc localize on the abneural side of the hair bundle, whereas aPKC forms a complementary domain on the neural side of the bundle (Figure 1.1B, 1.2A). Unlike disruption of the core PCP pathway, the inhibition of a G-protein signal perturbs the intrinsic polarity of the hair cell (Figure 1.2B). Mutation of LGN or treatment with the G-protein inhibitor pertussis toxin perturbs the position of the kinocilium, resulting in hair cells with split or otherwise misshapen bundles[24, 25].

Upon the genetic expression of pertussis toxin in the cochlea, the first two rows of outer hair cells are inverted and orient neurally[18]. Consistent with this observation, G-protein signals might specify the orientation of hair cells with respect to the line of polarity reversal in the saccule and utricle. In these tissues, the homebox transcription factor Emx2 is expressed in hair cells on only one side of the line of polarity reversal. The line of polarity reversal disappears in the absence of Emx2, and all hair bundles orient in the same direction[26]. Because pertussis toxin perturbs the orientations of only those vestibular hair cells that express Emx2, the transcription factor appears to act through G-protein signals to specify hair-bundle orientation.

How does G-protein signaling orient the hair bundle? One possibility is that Gαi and LGN regulate the migration of the kinocilium using a similar mechanism to that employed for orienting the mitotic spindle. In support of this hypothesis, the asymmetric localization of Gαi3 appears to precede the movement of the kinocilium during development[19]. Several discrepancies, however, suggest that the true mechanism is more complex. First, the role of G-protein signals clearly extends beyond the positioning of the kinocilium on the hair-cell surface. Gαi and LGN also occur at the tips of hair-bundle

stereocilia, and recent studies demonstrate that both proteins promote the elongation of these structures during development[27, 28]. Myosin 15 and whirlin, which are known to participate in stereociliary growth, are necessary for the presence of Gαi and LGN at stereociliary tips but not at the apical cell surface[28]. Moreover, the total amounts of Gαi and LGN are balanced between the apical surface and the tips of the stereocilia. In *mInsc* mutants in which Gαi and LGN are depleted from the apical surface, the proteins accumulate at the tips of stereocilia[27]. G-protein signals are therefore positioned to coordinate the staircase structure of the hair bundle with the planar polarity of the hair cell.

Some evidence suggests that the migration of the kinocilium is not entirely downstream of G-protein signaling. Basal bodies are mislocalized in *Mkks*$^{-/-}$ and *Bbs8*$^{-/-}$ mice, and the expression domain of Gαi3 is accordingly expanded[17, 19]. The kinocilum or its appendages may therefore also regulate Gαi localization. Moreover the kinocilium undergoes multiple movements during hair-cell maturation; a shift toward the abneural cortex in immature hair cells is followed by a neural relocalization that precedes bundle development[18] (Figure 1.2C). Although the enrichment of Gαi3 at the abneural surface coincides with the initial shift of the kinocilium, the two are not perfectly correlated. Instead, the orientation of Gαi3 is refined as the kinocilium shifts neurally. These observations suggest a more complex relationship between G-protein signals and the positioning of the kinocilium.

Figure 1.1 Hair cells in the mammalian cochlea (A) A schematic diagram of the cochlear sensory epithelium, the organ of Corti, depicts one row of inner hair cells and three rows of outer hair cells surmounted by the gelatinous tectorial membrane. Up-and-down vibration of the basilar membrane causes mechanical stimulation along the neural-to-abneural axis (arrow). (B) A schematic representation of the surface of the organ of Corti portrays the single row of inner hair cells (IHC) and the three rows of outer hair cells (OHC). Each hair bundle (green) forms an arrowhead pointed toward the abneural edge of the tissue. A kinocilium (blue) stands at the apex of each bundle, and the domain of Gαi expression (pink) extends from the hair bundle to the abneural edge of the cell.

A

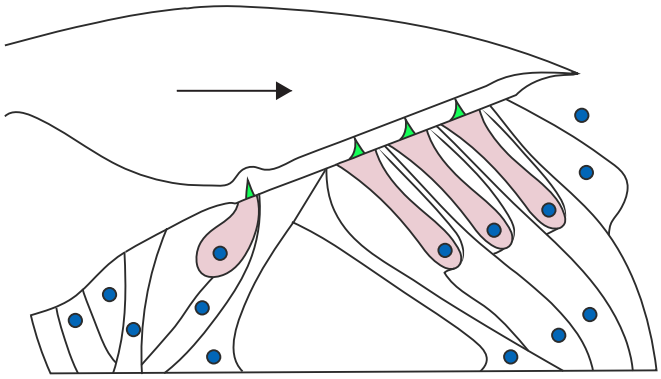

B

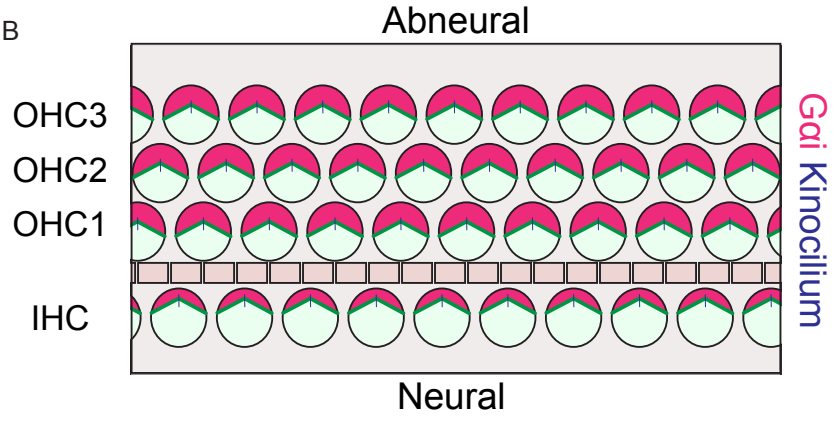

Figure 1.2 Core PCP and cell-intrinsic signals in cochlear hair cells (A) In wild-type cochleas, immunohistochemistry demonstrates the localizations of core PCP and cell-intrinsic factors. Phalloidin staining (gray) marks each actin-based hair bundle. Although Vangl2 (magenta, left) occurs in a thin crescent at the junction between a hair cell and supporting cell, Gαi3 and aPKC (green and magenta, right) distribute across the apical surface on either side of the hair bundle. Scale bar, 10 μm. (B) A schematic diagram demonstrates the divergent effects of core PCP proteins and cell-intrinsic signals on the cochlear hair bundle. Although the mutation of a core PCP protein misorients the hair bundle (middle), a cell-intrinsic defect disrupts hair-bundle morphology (right). The hair bundle (green), kinocilium (blue), and Gαi domain (pink) are depicted. (C) A schematic diagram depicts the sequence of hair-cell maturation. The kinocilium (green) lies at the center of an immature hair cell (left). The initial shift of the kinocilium toward the abneural edge of the cell coincides with the enrichment of Gαi (purple, middle). The domain of Gαi is then refined as the kinocilium relocates toward the center of the cell (right).

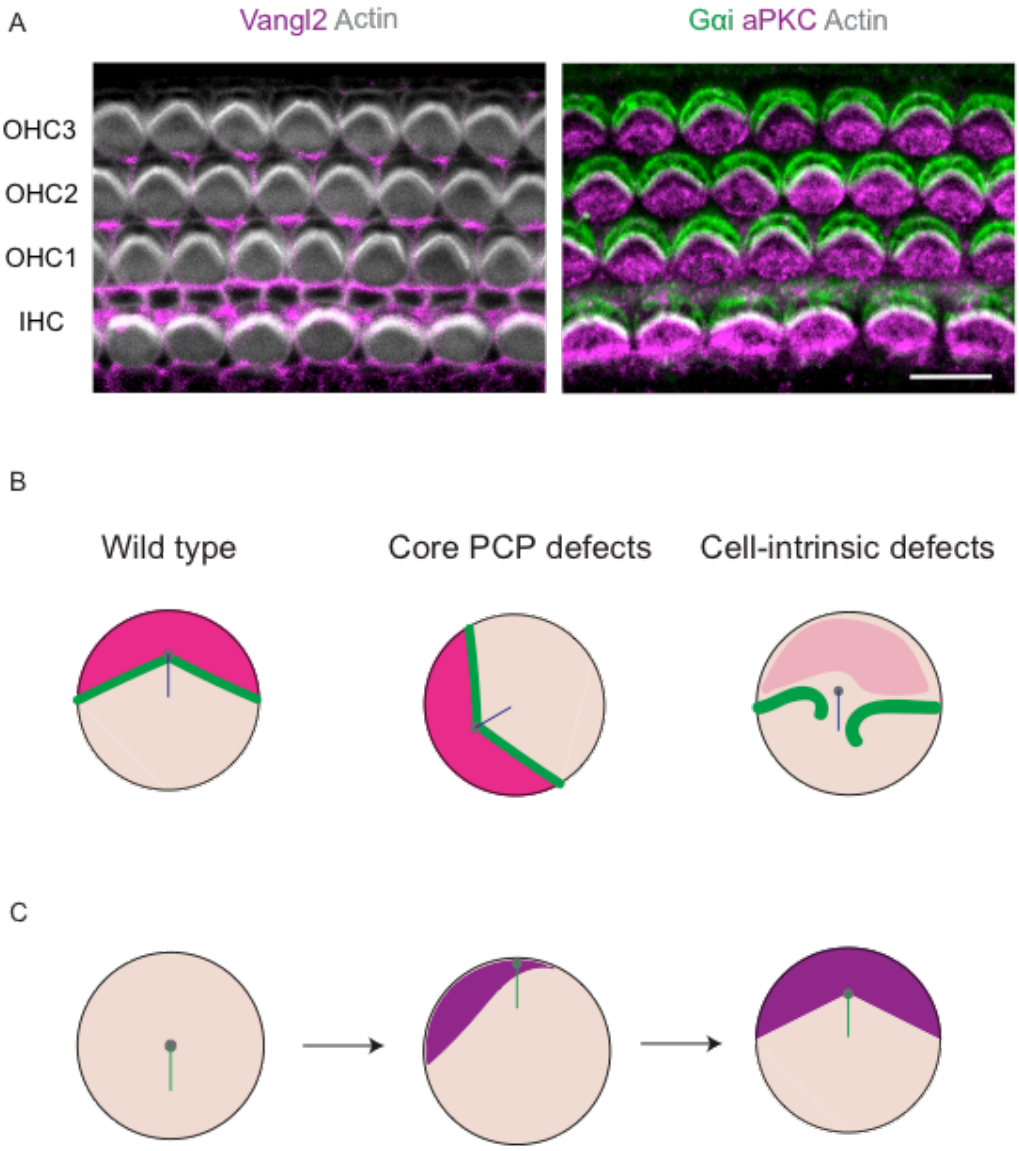
A
Vangl2 Actin
Gαi aPKC Actin
OHC3
OHC2
OHC1
IHC
B
Wild type
Core PCP defects
Cell-intrinsic defects
C

In summary, core PCP proteins and G-protein signals cooperate to orient hair bundles in the mammalian inner ear. Whereas the former appear to coordinate tissue-wide polarity, the latter participate in the cell-intrinsic patterning of hair bundles. How the two pathways are coordinated remains an open question. Additionally, the effects of the kinocilium on each pathway remain poorly understood. Although the absence of either tissue-wide or cell-intrinsic signals disrupts the positioning of the kinocilium, ciliary signals might conversely influence the tissue-wide and cell-intrinsic polarity of the each cell. A key remaining issue is therefore the mechanism by which these diverse signaling systems are reconciled. The sequence of events and the identity of additional regulators have yet to be elucidated.

Chapter Two: Materials and Methods

Animal care and strains

Experiments were conducted in accordance with the policies of The Rockefeller University's Institutional Animal Care and Use Committee. Pregnant C57BL/6J mice with embryos at stages E16 and E17 were obtained from Taconic. C57BL/6N-*Ccdc88c*$^{tm1(KOMP)Mbp}$ sperm was obtained from the University of California—Davis Komp Repository, and i*n vitro* fertilization in the B6 Taconic background was conducted at the Comparative Bioscience Center of The Rockefeller University. *Tg(CMV-cre)1Cgn* mice were obtained from the Jackson Laboratory. The LGN and *PTXa* transgenic lines were described previously[18, 27]. *Foxg1-Cre* (JAX JR#6084) transgenic animals were obtained from The Jackson Laboratory.

Yeast two-hybrid screening

Yeast two-hybrid screening was performed by Hybrigenics Services, S.A.S., Paris, France (http://www.hybrigenics-services.com). The coding sequence for *Mus musculus* Gαi3 (amino acids 2-354, GenBank reference NM_010306.3) was PCR-amplified and cloned into pB27 as a C-terminal fusion to LexA (LexA-Ccdc88c). The construct was checked by sequencing the entire insert and used as a bait to screen a randomly primed mouse inner-ear cDNA library constructed in pP6 plasmids. pB27 derives from the original pBTM116[29] and pP6 is based on the pGADGH plasmid[30].

68.6 million clones, approximately sevenfold the complexity of the library, were screened using the mating approach with YHGX13 (Y187 ade2-101::loxP-kanMX-loxP,

matα) and L40ΔGal4 (mata) yeast strains[31]. 144 His+ colonies were selected on a medium lacking tryptophan, leucine, and histidine and were supplemented with 0.5 mM 3-aminotriazole to avoid bait autoactivation. The prey fragments of the positive clones were amplified by PCR and sequenced at their 5¢ and 3¢ junctions. The resulting sequences were used to identify the corresponding interacting proteins in the GenBank database (NCBI) through a fully automated procedure. A confidence score was attributed to each interaction[32].

The coding sequence for *Mus musculus* Ccdc88c (amino acids 880-2009, GenBank reference NM_026681.4) was PCR-amplified and cloned into pB27 as a C-terminal fusion to LexA (LexA-Ccdc88c). The construct was checked by sequencing the entire insert and used as a bait to screen the library described above. 56.2 million clones, or about sixfold the library's complexity, were screened using the mating approach noted above. After 270 His+ colonies had been selected, the resulting sequences were used to identify the corresponding interacting proteins and a confidence score was assigned to each candidate.

The confidence score relies on two levels of analysis. First, a local score takes into account the redundancy and independency of prey fragments as well as the distribution of reading frames and stop codons in overlapping fragments. Second, a global score considers the interactions found for the same library in all the screens performed at Hybrigenics. This global score represents the probability that an interaction is nonspecific. For practical use, the scores are divided into four categories, from A (highest confidence) to D (lowest confidence). A fifth category, E, notes interactions involving highly connected prey domains found several times in screens performed on

libraries derived from the same organism. Several of these highly connected domains have been confirmed as false positives of the technique and are assigned to category F. The confidence scores have been shown to positively correlate with the biological significance of interactions[33, 34].

Morpholino injections

Zebrafish embryos at the one-cell stage were injected with 34 ng of a splice-blocking morpholino against the first exon of *Daple* transcript ENSDART00000062010. The morpoholino solution contained 12.5 % phenol red and was injected into the yolk sac. Following injections, embryos were raised at room temperature.

Immunolabeling and confocal microscopy

Inner ears were dissected and fixed in 2 % paraformaldehyde for 45 min at 4 ˚C. After three 15 min rinses, cochleas were dissected and permeabilized in phosphate-buffered saline solution (PBS) containing 0.5 % Tween for 30 min at room temperature. Samples were then blocked for 1 hr at room temperature with a PBS solution containing 0.5 % Tween and 10 % normal donkey serum. Primary antibodies were diluted in a PBS solution containing 0.5 % Tween and 2 % serum and applied overnight at 4 ˚C. After three rinses with the permeabilization solution, secondary antibodies were diluted in the permeabilization solution and applied for 45 min at room temperature. Samples were rinsed with PBS and fixed for 15 min with 4 % paraformaldehyde before mounting.

A different protocol was used for immunostaining with the anti-Dishevelled and the Bethyl Laboratories anti-Daple antibodies. Inner ears were fixed for 45 min on ice

with 10 % trichloroacetic acid in distilled water. The ears were washed three times in cold PBS on ice. After dissection, cochleas were incubated for 1 hr at room temperature with a PBS solution containing 0.5 % Triton-X and 1% BSA. Primary antibodies were diluted in PBS and applied overnight at 4 ˚C. Samples were rinsed and incubated overnight with secondary antibodies in PBS at 4 ˚C.

The following antibodies were used: anti-ABTB2 (1:100, Novusbio NBP1-84141), anti-acetylated tubulin (1:500, Sigma T6793), anti-ANKRD13B (1:100, Proteintech 25737-1-AP), anti-aPKC (1:400, Santa Cruz Biotechnology C-20 sc-216), anti-Beta-catenin (1:100, Bethyl Laboratories A302-010A-T), anti-Daple (1:100, Bethyl Laboratories A302-951A-T), anti-Daple (1:100, Santa Cruz Biotechnology sc-137416), anti-Dishevelled2 (1:100, Cell Signaling 3216), anti-EB1 (1:100, EMD Millipore AB6057), anti-Eya4 (1:100, Abcam ab110148), anti-Frizzled-6 (1:500, R&D Systems AF1526), anti-Gαi3 (1:600, Sigma G4040), anti-GAI3 (1:200, GeneTex), anti-Girdin (1:100, Abcam ab113890), anti-LGN (1:300 Sigma HPA007327), anti-Nucleobindin1 (1:100, Abcam ab154262), anti-Pericentrin (1:100, Covance PRB-432C), anti-Rgs14 (1:100, Novusbio NBP2-20148), and anti-Vangl2 (1:500, EMD Millipore ABN373). Signals were detected with donkey secondary antibodies conjugated to Alexa Fluor 488 or Alexa Fluor 555. Phalloidin conjugated to Alexa Fluor 633 (Molecular Probes) was used to label actin.

Confocal imaging was performed with an Olympus IX81 microscope equipped with a Fluoview FV1000 laser-scanning system (Olympus America). Z-stacks were acquired at 1- or 2- micron intervals.

Quantification of Gαi3 expression and kinociliary position

Cochleas from four postnatal *Daple*$^{-/-}$ mice and four heterozygous littermates were stained with phalloidin and immunolabeled for Gαi3 and acetylated tubulin. For each cochlea two confocal Z-stacks were imaged near the base, one near the middle, and three near the apex.

Each Z-stack was analyzed with a custom Python program that presented the stack to the user and paused for input. The user's first click near the center of a cell prompted the program to estimate the radius of the cell's apical surface by means of the phalloidin signal. The program next estimated the angle from the cell's center to the middle of the Gαi3 domain, then paused again for input. The user marked the position of the kinocilium with a second click and proceeded to the next cell. Any cell for which the estimates did not appear accurate was immediately discarded.

When the user exited the program, the results were saved into a comma-separated file. The data recorded for each cell included: the cell's X and Y coordinates, the cell's radius, the angles from the cell's center to the middle of the Gαi3 domain and to the kinocilium, and the distance of the kinocilium from the cell's center.

Cochleas from three E17.5 *Daple*$^{-/-}$ mice and three heterozygous littermates were immunolabeled for phalloidin and pericentrin. For each hair cell, the angle of the basal body was estimated using an ImageJ measuring tool. Only basal bodies near the boundary of a hair cell were included in the analysis. One of the three cochleas was also immunolabeled for Gαi3, and the angle of the Gαi3 domain was estimated.

The statistical significance of a circular distribution was determined using Watson's two-sample test of homogeneity implemented in the R CircStats library. The

statistical significance of a distribution between 0˚ and 180˚ was determined using the Kolmogorov-Smirnov test implemented in the R Stats library.

Cochlear explant electroporation and culture

Temporal bones from E14.5 C57BL/6J- FVB/NJ outbred fetuses were extracted and collected in HBSS/Hepes. Circular plasmid DNA at 2-3 mg/ml was mixed with Fast Green and injected into the cochlear duct using the Drummond Wiretrol II plunger/capillary system. Using home-made platinum wire electrodes, the whole temporal bone was electroporated in PBS with 6x 27 V square pulses of 27 ms at 950 ms intervals (BTX ECM830). The cochlea was then dissected away from the surrounding condensed mesenchyme and embedded into 50 % Matrigel in DMEM. Cochleas were cultured for 6 days in DMEM + 10% FBS and ciprofloxacin, before fixation with 4% PFA for 15 min and immunostaining.

Figure 2.1 Representation of the method used to quantify orientation and kinociliary defects (A-B) A custom script is used to annotate Z-stacks of a cochlea immunolabeled for Gαi3 (green) and acetylated tubulin (red). Phalloiding staning reveals hair bundles (blue). When the user clicks upon the image of each cell, the program estimates the radius of the cell (white dotted lines) and finds the angle from the cell's center to the middle of the crescent of Gαi3 (white arrows). Any cell that the script does not properly trace is excluded from the dataset. The user's second click marks the position of the kinocilium (red dots). Keyboard commands permit the user to scroll through the full Z-stack. (A) An analysis of the second row of outer hair cells is performed near the apex of a *Daple*$^{-/-}$ cochlea. Yellow lines are drawn between the position of the kinocilium in an annotated image (top) and the corresponding kinocilium in an unannotated, more apical image (bottom) from the same stack. (B) An analysis of the second row of outer hair cells is performed near the base of a *Daple*$^{-/-}$ cochlea. Yellow lines are drawn between the position of the kinocilium in an annotated image (top) and the corresponding kinocilium in an unannotated, more apical image (bottom) from the same stack. Scale bars, 10 μm.

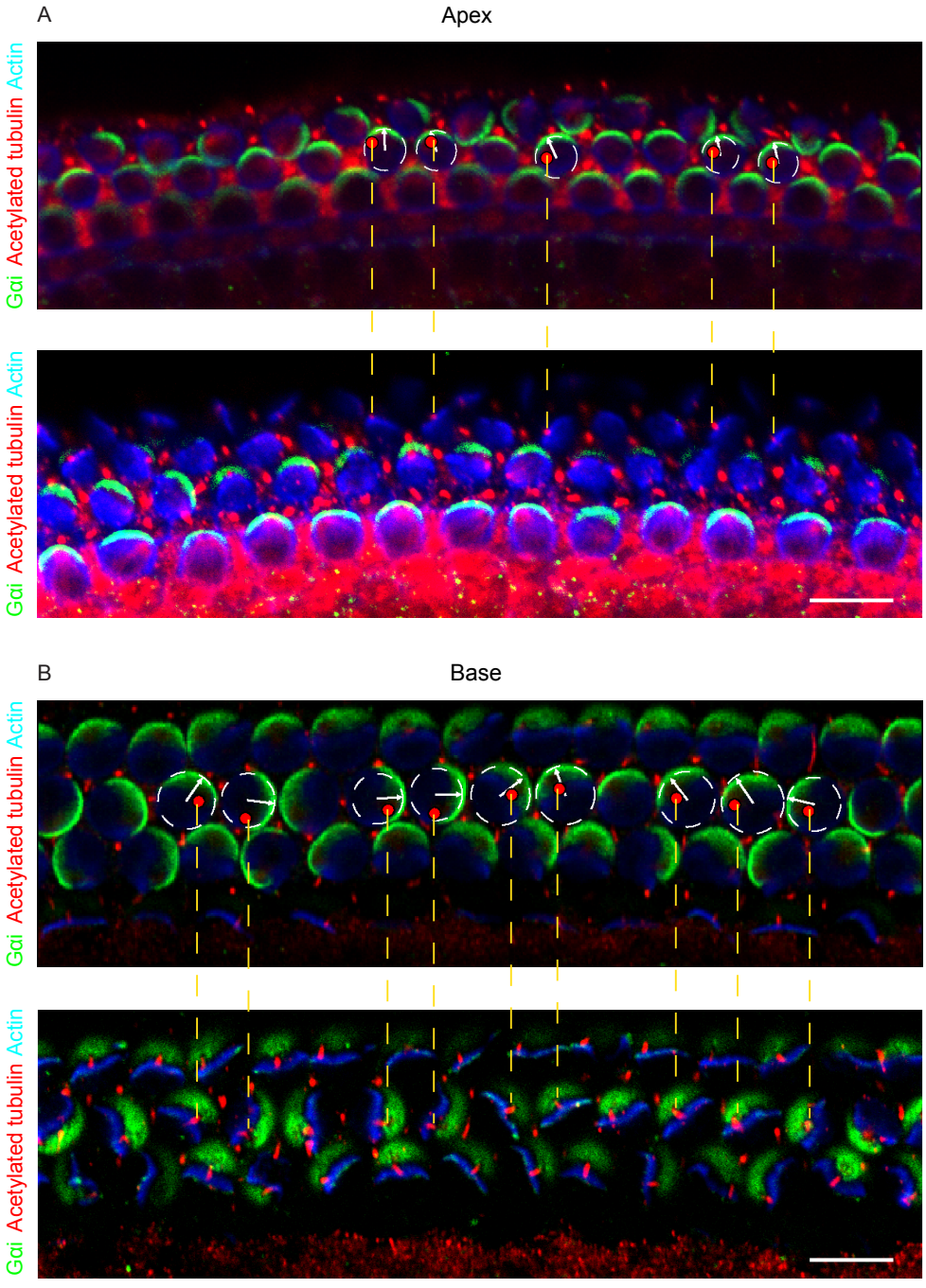
A
Apex
Gαi Acetylated tubulin Actin
Gαi Acetylated tubulin Actin
B
Base
Gαi Acetylated tubulin Actin
Gαi Acetylated tubulin Actin

Chapter Three: Daple orients and shapes cochlear hair bundles

A yeast two-hybrid approach suggests binding partners of Gαi3 in the murine inner ear.

To initiate a yeast-two hybrid screen, I cloned a full-length Gαi3 cDNA and submitted the construct to the company Hybrigenics. Using Gαi3 as bait, Hybrigenics screened a cDNA library derived from 600 inner ears of mice aged two to six days (P2-P6; Table 3.1). As expected, the screen detected the interaction of Gαi3 with LGN. Immunohistochemical localization of several candidates revealed expression in the nucleus, membrane-bounded organelles, and the cellular cortex (Figure 3.1). Two centrosomal proteins were also identified in the screen, centrosomal protein 250 and a regulator of G-protein signaling Rgs14[35-37]. In the cochlea, Rgs14 localized to the microtubule asters of both hair cells and supporting cells (Figure 3.1G).

Prominent among the products of the screen was the coiled-coil domain-containing protein 88c (Ccdc88c), also termed Dishevelled-associating protein with a high frequency of leucine residues (Daple). Daple was discovered as a negative regulator of the canonical Wnt pathway in cultured cells and *Xenopus* embryos[38]. In this context, Daple binds Dishevelled and inhibits Wnt3a-dependent accumulation of β-catenin. Overexpression of Daple causes the ventralization of *Xenopus* embryos. Because morpholino knockdown of Daple is lethal in *Danio rerio*, this function may be conserved in zebrafish (Figure 3.2).

Daple also directs cell migration through non-canonical Wnt signaling[10, 39, 40]. In Vero cells cultured with Wnt5a, Daple activates Rac by facilitating the association of Dishevelled and aPKC. Moreover, Daple is a guanine exchange factor (GEF) that can

activate G-protein signaling downstream of Wnt5a in cell culture[41]. GEFs stimulate the release of GDP from Gαi and permit GTP to bind[41, 42]. Because Daple can therefore regulate both Wnt signals and G-proteins, I sought to characterize the protein's role in hair-bundle orientation and development.

Table 3.1 Candidates revealed by a yeast two-hybrid screen with Gαi

Gene symbol	Gene name	Accession number	Score
Abtb2	Ankyrin repeat and BTB (POZ) domain containing 2	NM_178890.3	A
Ankrd13b	Ankyrin repeat domain 13b	XM_006533393.2	A
Gpsm1_var1	G-protein signalling modulator 1 (AGS3-like, *C. elegans*)	NM_153410.5	A
Gpsm1_var2	G-protein signalling modulator 1 (AGS3-like, *C. elegans*)	NM_001199146.1	A
Gpsm2 (LGN)	G-protein signalling modulator 2 (AGS3-like, *C. elegans*)	NM_029522.2	A
Nucb1	Nucleobindin 1	NM_001163662.1	A
Rgs12	Regulator of G-protein signaling 12 (Rgs12)	NM_173402.2	A
Ccdc88a	Coiled-coil domain containing 88A	NM_176841.4	B
Ccdc88c	Coiled-coil domain containing 88C	NM_026681.4	B
Cep250	Centrosomal protein 250	NM_008383.3	B
Btbd1	BTB (POZ) domain containing 11	NM_028709.2	D
Eya4	Eyes absent 4 homolog	NM_010167.4	D
Fads1	Fatty acid desaturase 1	NM_146094.2	D
Ranbp6	RAN binding protein 6	NM_177721.4	D
Rap1gap_var1	Rap1 GTPase-activating protein	NM_001081155.2	D
Rcn2	Reticulocalbin 2	NM_011992.2	D
Rgs14	Regulator of G-protein signaling 14	NM_016758.3	D
Snx5	Sorting nexin 5	NM_001199188.1	D

Figure 3.1 Candidates revealed by a yeast two-hybrid screen with Gαi (A) A schematic diagram, reproduced from Figure 1.1, illustrates the layout of the cochlea. Three rows of outer hair cells and a row of inner hair cells are separated by two rows of supporting cells. (B-G) Immunohistochemistry reveals the localizations of six candidate regulators of Gαi in the inner ear. Maximal intensity projections of a Z-stack are shown. (B) Abtb2 (green) appears to localize to hair-cell nuclei. Phalloidin (gray) labels actin at cell boundaries. (C) Ankrd13B (green) is expressed in hair cells and appears in a pattern similar to that of heterochromatin. Phalloidin (gray) labels actin at cell boundaries. (D) Eya4 (green) occurs in hair-cell nuclei. Phalloidin (gray) labels actin at cell boundaries. (E) Nucb1 (green) localizes to membrane-bounded organelles in the cell bodies of hair cells and supporting cells. Phalloidin (gray) labels actin at cell boundaries. (F) Girdin (green) is distributed along the junctions between hair cells and supporting cells. The protein also localizes near the centers of hair cells in a pattern consistent with the stereociliary tips. (G) RGS14 (magenta) is expressed in hair cells and supporting cells. Co-labeling with acetylated tubulin (green) suggests that RGS14 accumulates at the base of the kinocilia near apical microtubules. Scale bar, 10 μm.

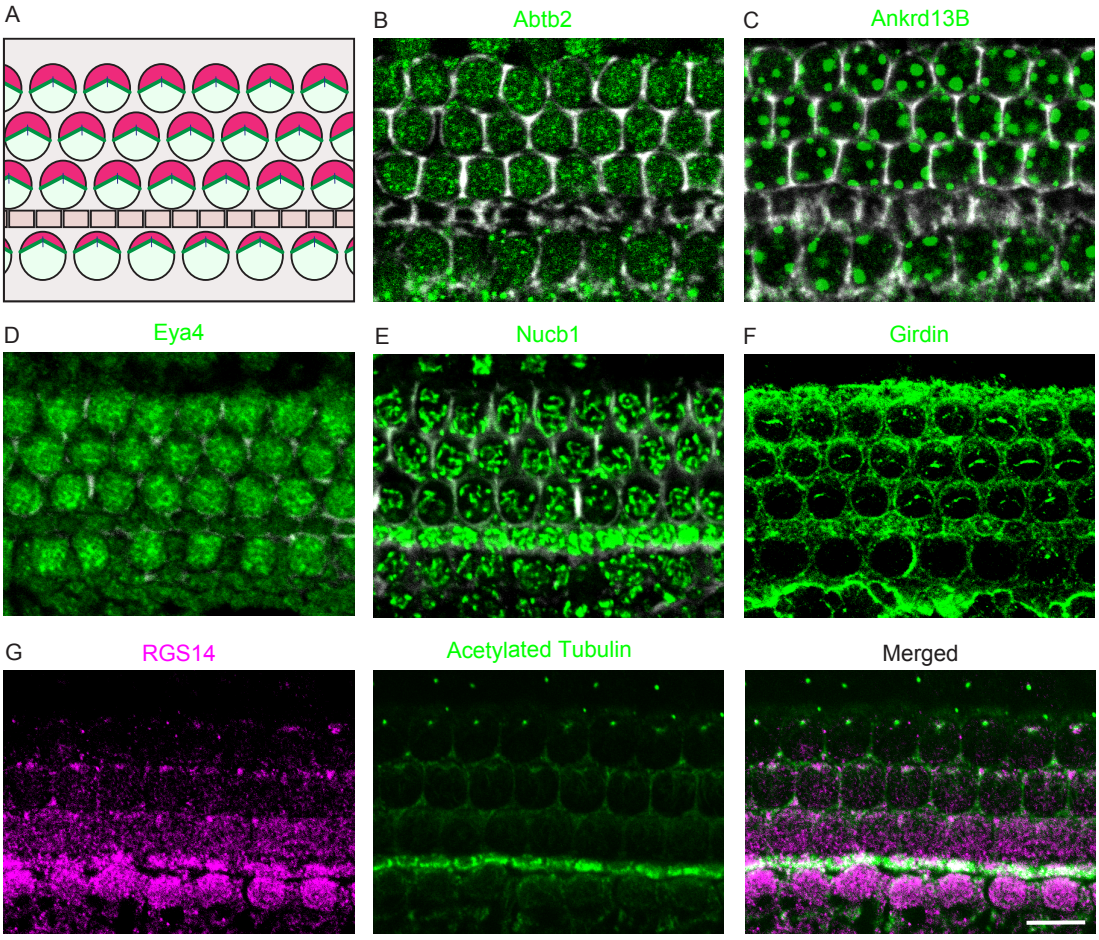
A
B
Abtb2
C
Ankrd13B
D
Eya4
E
Nucb1
F
Girdin
G
RGS14
Acetylated Tubulin
Merged

Figure 3.2 A role for Daple in zebrafish development (A) Uninjected zebrafish embryos have undergone gastrulation by approximately 24 hours post fertilization. The head and tail bud regions are prominent at this stage (arrows). (B-C) Stage-matched embyros injected with a morpholino against Daple exhibit developmental defects. (B) A subset of embryos arrests prior to gastrulation. (C) Most embryos complete gastrulation but exhibit defects during the segmentation period. The head and tail bud fail to become prominent (arrows).

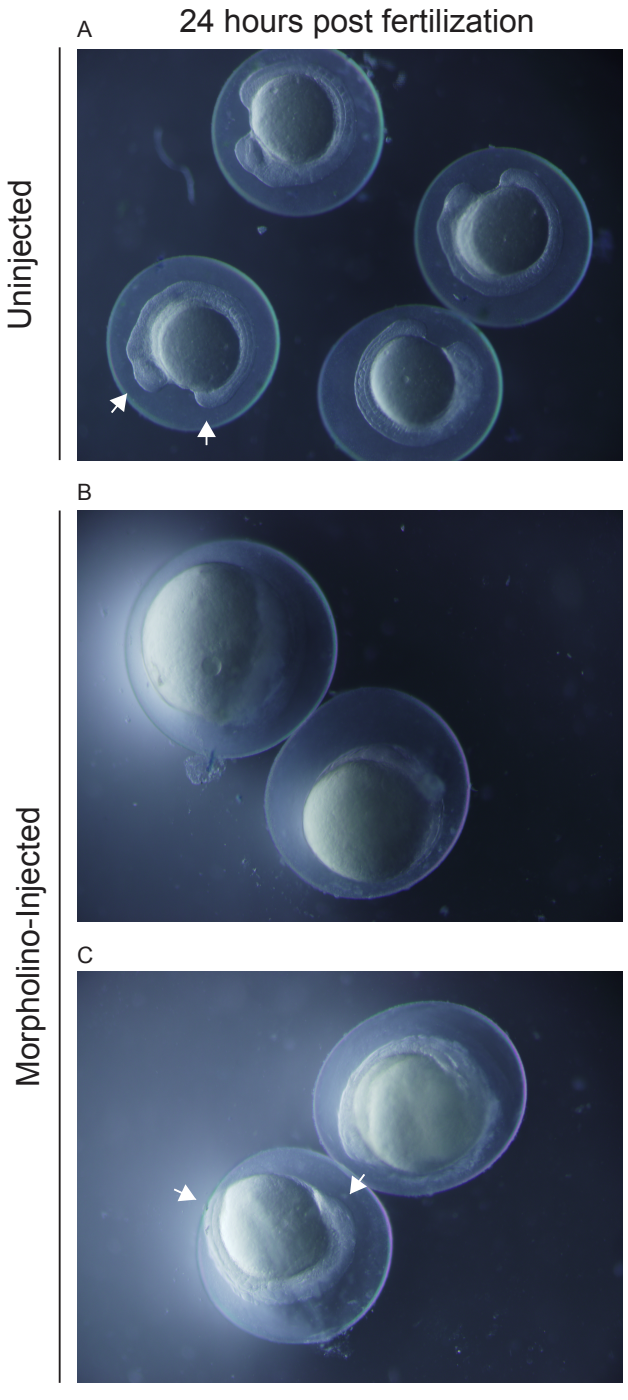
24 hours post fertilization
A
Uninjected
B
Morpholino-Injected
C

Daple regulates hair-bundle morphogenesis in the cochlea.

Adult animals of the *Ccdc88c*$^{tm1(KOMP)Mbp}$ strain, subsequently referred to as *Daple*$^{-/-}$ animals, were fertile and resembled their heterozygous littermates. Although their cochleas did not exhibit defects in convergent extension (Figure 3.3A), *Daple*$^{-/-}$ mice displayed striking defects in their hair bundles (Figure 3.3B). The staircase of stereocilia was both misoriented and grossly misshapen. Because the *Ccdc88c*$^{tm1(KOMP)Mbp}$ strain contains a floxed neomycin-resistance cassette, I crossed the mice to *CMV-cre* transgenic mice to confirm that the neomycin-resistance gene or its promoter did not cause the hair-bundle phenotype. The CMV promoter drives expression in all tissues. *CMV-cre*;*Daple*$^{-/-}$ cochleas with no detectable neomycin-resistance amplicon also exhibited hair-bundle defects (Figure 3.4).

To confirm that the genetic deletion caused a loss of function, I conducted immunohistochemistry with two antibodies that target Daple protein in regions outside the genetic deletion. Each antibody exhibited some residual labeling in *Daple*$^{-/-}$ cochleas; one antibody occasionally labeled cell junctions and the other consistently marked kinocilia. Because the patterns were distinct for each antibody, however, I considered these interactions non-specific (Figure 3.5A-B). Both antibodies revealed Daple in the abneural cortex of the hair cell, an enrichment not visible in *Daple*$^{-/-}$ mice at either the base or the apex of the cochlea (Figure 3.5C). Additionally, the domain of Daple expression was more asymmetric near the middle turn and base of the cochlea than in immature hair cells near the apex.

Figure 3.3 Daple in cochlear hair-bundle development (A) The dissected cochleas of *Daple*$^{+/-}$ (top) and *Daple*$^{-/-}$ (bottom) mice resemble one another. (B) Phalloidin labeling (green) reveals hair bundles in a P0 wild-type cochlea (top) and a *Daple*$^{-/-}$ littermate (bottom). Although wild-type bundles orient toward the abneural edge of the cochlea, *Daple*$^{-/-}$ hair bundles are misshapen and do not orient uniformly. Scale bar, 10 μm.

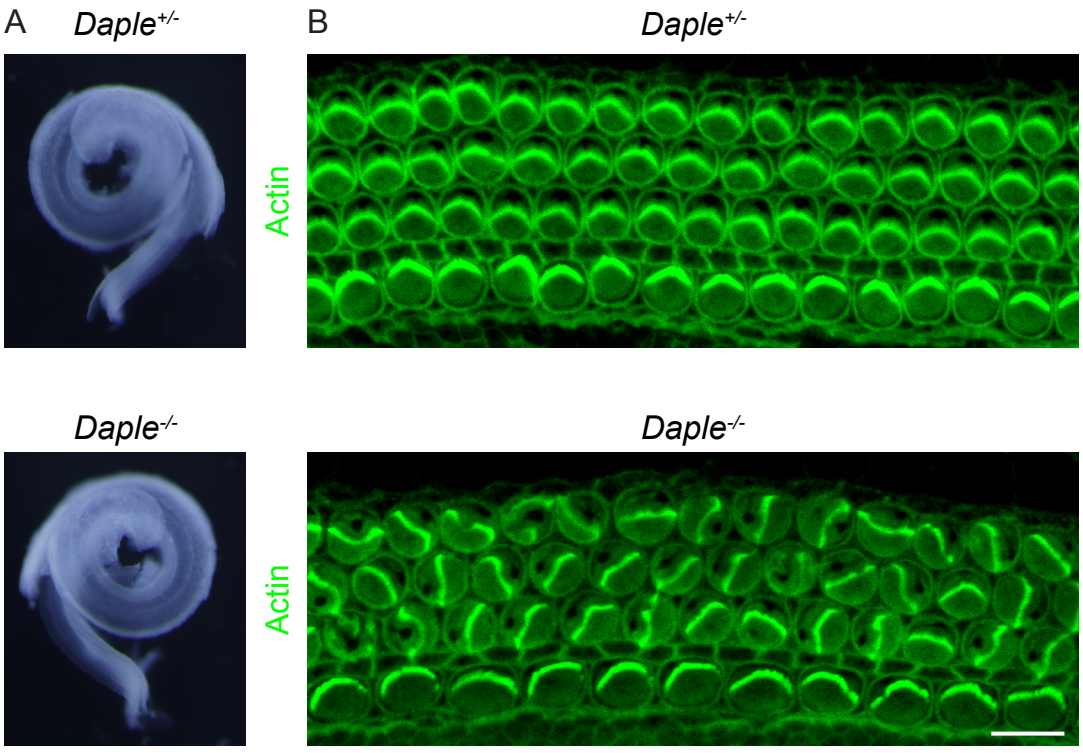
A
Daple+/-
B
Daple+/-
Actin
Daple-/-
Daple-/-
Actin

Figure 3.4 Characterization of Daple mutants (A) The schematic diagram depicts the genetic insertion that replaces exons five through ten in *Ccdc88c*$^{tm1(KOMP)Mbp}$ mice. The insertion contains a floxed neomycin cassette that may contain a cryptic splice site. (B) The results of a genotyping PCR reveal two P1 animals of interest. The first (yellow dotted box) is a wild-type *Cmv-cre; Daple*$^{+/-}$ mouse identified by amplicons from *LacZ*, wild-type *Daple*, and *Cre* sequences. The second (blue dotted box) is a *Cmv-cre; Daple*$^{-/-}$ mouse identified by amplicons from *LacZ* and *Cre* sequences. Although a faint wild-type *Daple* amplicon is also present in this lane, it is comparable to the negative control (last lane of the gel). (C) Immunohistochemistry labels cochlear hair bundles (green) of the two mice described in panel *B*. Although *Cmv-cre; Daple*$^{+/-}$ hair cells exhibit wild-type bundles (top), *Cmv-cre; Daple*$^{-/-}$ hair bundles are misoriented and misshapen (bottom). The latter resemble *Daple*$^{-/-}$ hair bundles (See Figure 1). Scale bar, 10 μm.

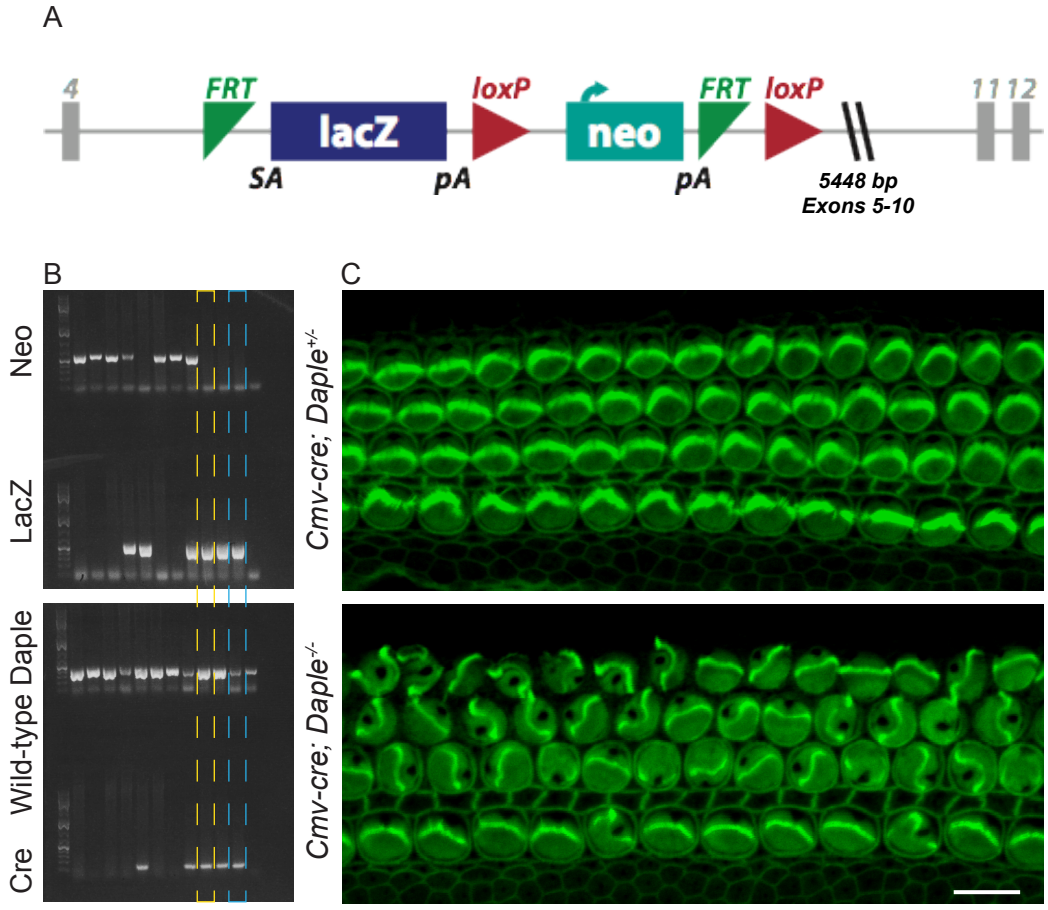
A
4
FRT
lacZ
loxP
neo
FRT
loxP
11 12
SA
pA
pA
5448 bp
Exons 5-10
B
C
Neo
LacZ
Wild-type Daple
Cre
Cmv-cre; Daple+/-
Cmv-cre; Daple-/-

Figure 3.5 Localization of Daple in the cochlea Postnatal cochleas were immunolabeled for Daple using two antibodies. (A) The first antibody (Santa Cruz, green) labels hair-cell junctions and the kinocilium in wild-type cochleas (bottom left). In the absence of Daple only the kinocilium is visible (bottom right). (B) The second antibody (Bethyl Laboratories, magenta) labels hair-cell junctions near the apex and middle turn of wild-type cochleas (top left and bottom left, respectively). This distribution is absent from *Daple*$^{-/-}$ mice (right). Some residual immunolabeling is apparent at cell junctions near the middle turn (bottom right) but not near the apex (top right) (C) Near the base of a cochlea, immunohistochemistry reveals Daple (magenta) at the abneural boundaries of wild-type hair cells (left and inset). No residual immunloabeling is visible at cell junctions in *Daple*$^{-/-}$ littermates (right). Scale bars, 10 μm.

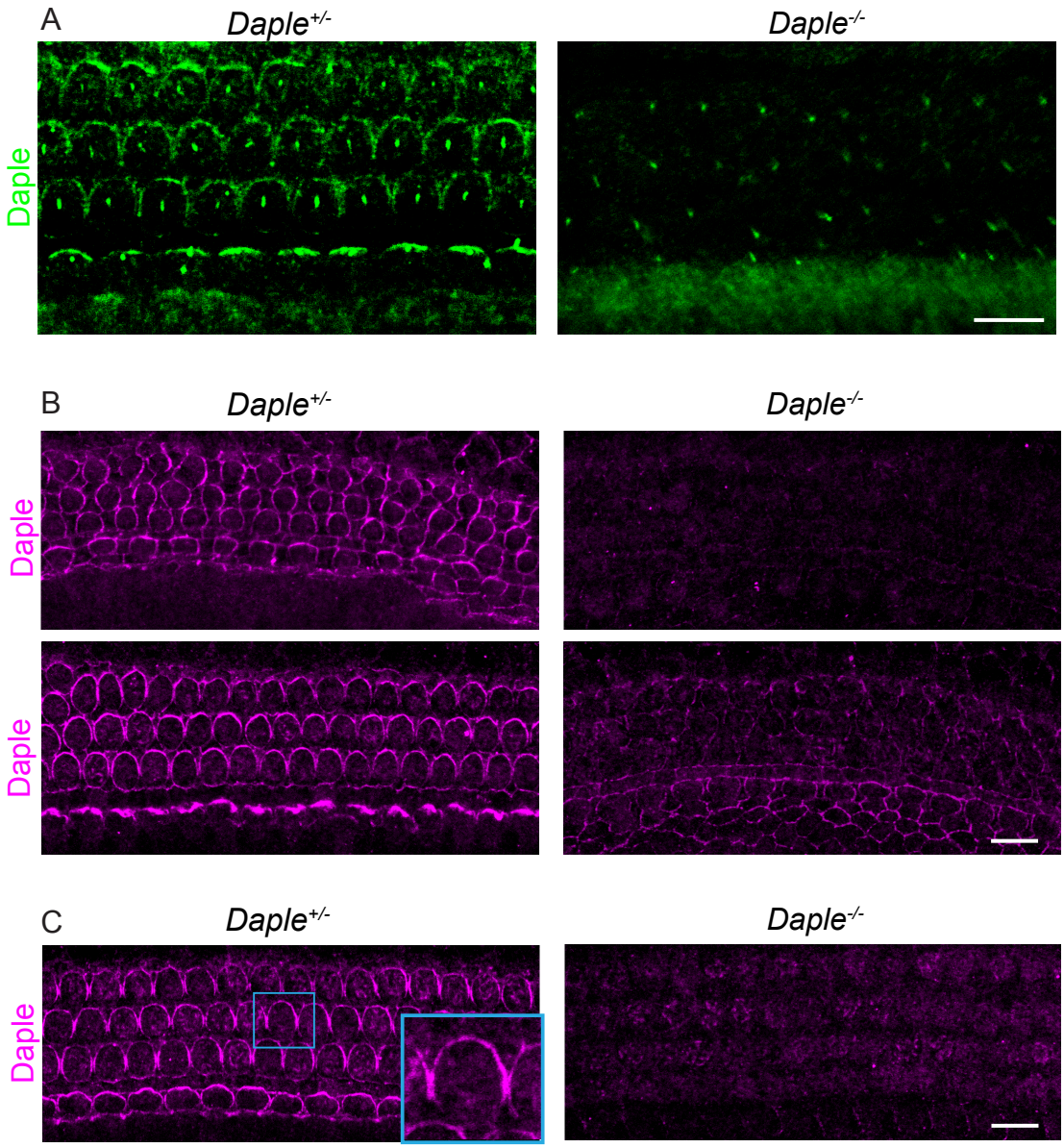
A
Daple+/-
Daple-/-
Daple
B
Daple+/-
Daple-/-
Daple
Daple
C
Daple+/-
Daple-/-
Daple

Discussion

Because Daple is a Dishevelled-associated protein that interacts with Gαi3 in a yeast two-hybrid assay, I investigated the role of Daple in hair-cell development. Unlike mutations of the core PCP proteins, the absence of Daple does not appear to disrupt convergent extension of the cochlea. Howevever, Daple is necessary to orient and shape cochlear hair bundles. The protein is also asymmetrically distributed at the apical surfaces of hair cells; the distribution of Daple is more abneural along the base of the cochlea than near the apex, indicating that the refinement of Daple localization coincides with the maturation of the hair bundle. Daple therefore likely plays a hair cell-specific role in development. Notably, because both Dishevelled and Gαi also localize on the abneural side of cochlear hair cells, Daple is well positioned to interact both with core PCP proteins and with cell-intrinsic signals. Consistent with this possibility, *Daple*$^{-/-}$ hair bundles appear both misoriented and misshapen. My results therefore merit a careful characterization of the contributions of tissue-wide and cell-intrinsic defects to the *Daple*$^{-/-}$ phenotype.

Chapter Four: Daple coordinates G-protein signals with the position of the kinocilium.

Gαi3 and the kinocilium shape the sensory hair bundle.

Because postnatal *Daple*$^{-/-}$ hair bundles were severely misshapen, I asked whether the apical enrichment of cell-intrinsic signals was diminished. Surprisingly, I found the G-protein complex present at the apical surface of each *Daple*$^{-/-}$ hair cell. Gαi3 and LGN occurred at stereociliary tips, implying that the loss of Daple did not eliminate their participation in the elongation of stereocilia (Figure 4.1A). Moreover LGN colocalized with Gαi3, and aPKC formed a complementary domain (Figure 4.1A,B). The apical blueprints formed by these proteins, however, were severely mispatterned.

In mature wild-type cells, the kinocilium was always centered within the Gαi3 domain (Figure 4.2A). In contrast, postnatal *Daple*$^{-/-}$ hair cells exhibited a variety of hair-bundle shapes characterized by altered relationships between Gαi3 and the kinocilium. In some *Daple*$^{-/-}$ cells, the kinocilia lay near the edges of the Gαi3 domains, resulting in S-shaped bundles (Figure 4.2B). In other cells the kinocilia more closely aligned with the Gαi3 domain but were shifted toward the centers of the apical surfaces. Gαi3 spread to encompass the kinocilia, resulting in bundles with a C-shaped appearance (Figure 4.2C). In a final subset of cells the kinocilia adopted approximately normal positions and the hair bundles resembled those of wild-type animals (Figure 4.2D).

In some hair cells Gαi3 was entirely uncoupled from the kinocilia (Figure 4.2E). In each of these cells the kinocilium localized to the neural edge, whereas Gαi3 formed an abneural crescent. Although in most hair cells the stereocilia bordered the domains of

Gαi3 expression (Figure 4.2A-D), the stereocilia of these cells grew in a fragmented pattern, extending from the border of the Gαi3 domain toward the kinocilium and encircling it.

Daple$^{-/-}$ cochleas exhibit hair-cell orientation and kinociliary positioning defects.

I sought to compare tissue-wide and cell-intrinsic defects by immunolabeling Gαi3 and the kinocilia (Figure 4.3A). Unlike the kinocilia of heterozygous littermates, which occurred at the abneural edges of hair bundles, the kinocilia of *Daple$^{-/-}$* outer hair cells were distributed across the apical surfaces (Figure 4.3B). Inner hair cells exhibited less severe defects, although some kinocilia were found in the neural half of the cell (Figure 4.3C). Because disruption of the core PCP pathway significantly affects the positions of the kinocilia but not their distances from the cellular boundaries, the randomized distribution of kinocilia in outer hair cells signaled a defect in cell-intrinsic polarity.

To quantify the defects associated with tissue-wide orientation, I used the localization of Gαi3 to denote the orientations of hair cells within the cochlear sensory epithelium. For individual hair cells from four *Daple$^{+/-}$* and four *Daple$^{-/-}$* P1 littermates, I plotted the angle of the Gαi3 domains with respect to the centers of the apical surfaces. Each cochlea contains one row of inner hair cells and three rows of outer hair cells. Although the absence of Daple did not affect the organization of these four rows, the domain of Gαi3 was misoriented in both outer and inner hair cells (Fig 4.3D,E), with more significant defects in the former ($p < 0.001$ and $p < 0.01$, respectively). Because

Gαi3 was clearly biased toward the abneural edges of both types of hair cells, however, additional mechanisms evidently localized Gαi in the absence of Daple.

By comparing orientation defects among the three rows of outer hair cells, I further examined the contributions of tissue-wide and cell-intrinsic signals. In *Looptail* mutants lacking the core PCP protein Vangl2, both inner and outer hair cells are misoriented. The third, most abneural row of outer hair cells is the most affected, whereas the first row is least disturbed[6-8]. This trend was also apparent near the apices of *Daple*$^{-/-}$ cochleas, where a greater number of hair cells was reversed in the third row of outer hair cells than in the other two rows (Figure 4.4A,B). In contrast, near the base of *Daple*$^{-/-}$ cochleas the third row exhibited milder orientation defects than did the other two (Figure 4.4C,D). Increased severity of misorientation in the first row of outer hair cells, rather than the third row, occurs in conditional knockouts of the kinociliary transport protein Ift88 and after exposure to the G-protein inhibitor pertussis toxin[18, 19]. The latter treatment in particular disrupts cell-intrinsic signals. Thus the apices of *Daple*$^{-/-}$ cochleas resembled those of core PCP mutants, whereas the bases of *Daple*$^{-/-}$ cochleas suggested cell-intrinsic defects. My data therefore implicated both tissue-wide and cell-intrinsic defects in the phenotype of Daple mutants.

Figure 4.1 G-protein signals in the absence of Daple (A) Immunohistochemistry demonstrates that Gαi (green) and LGN (magenta) localize to the hair-cell surface in *Daple*$^{+/-}$ (top) and *Daple*$^{-/-}$ (bottom) littermates. Note that Gαi and LGN occur at the tips of stereocilia in both wild-type and *Daple*$^{-/-}$ hair cells (arrows). (B) Gαi (green) and aPKC (magenta) form complementary domains in *Daple*$^{+/-}$ (top) and *Daple*$^{-/-}$ (bottom) littermates. Scale bars, 10 μm.

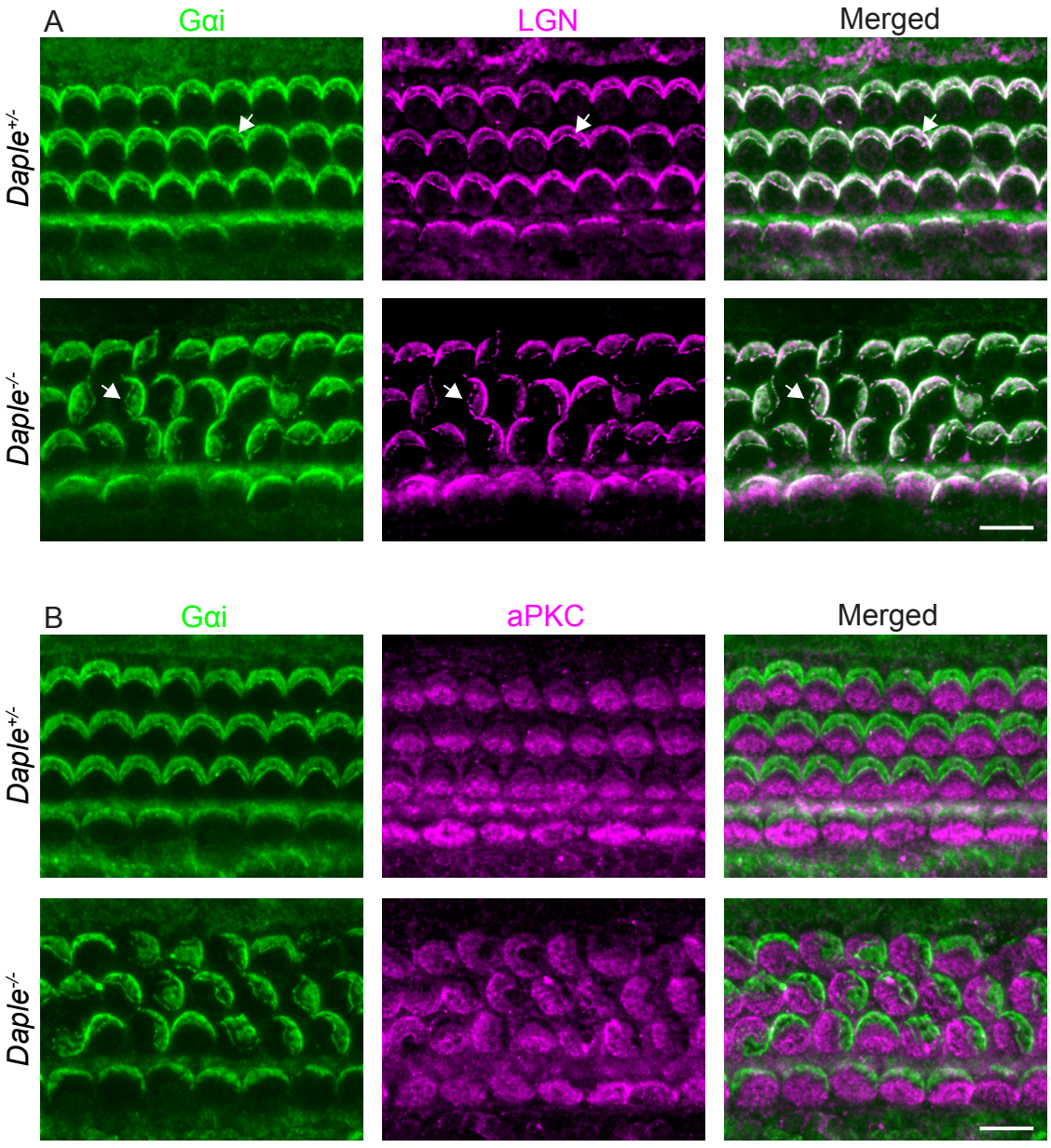
A
Gαi
LGN
Merged
Daple+/-
Daple-/-
B
Gαi
aPKC
Merged
Daple+/-
Daple-/-

Figure 4.2 Hair bundles in *Daple*$^{-/-}$ cochleas (A) In a postnatal wild-type hair cell, immunohistochemistry demonstrates that the kinocilium (acetylated tubulin, green) is centered within the domain of Gαi expression (magenta). Phalloidin (gray) labels the actin-filled hair bundle. (B-D) Postnatal hair cells in a *Daple*$^{-/-}$ mutant are immunolabeled for Gαi (magenta) and acetylated tubulin (green). Phalloidin staining (gray) reveals that, as in panel *A*, the hair bundles border the edges of the Gαi domains. (B) The kinocilium lies near the edge of the Gαi domain in an S-shaped bundle. (C) The kinocilium occurs near the center of the hair cell in a C-shaped bundle. (D) The kinocilium is centered within the domain of Gαi expression in a hair bundle that resembles the wild-type. (E) A postnatal *Daple*$^{-/-}$ hair cell is immunolabeled for Gαi (magenta) and acetylated tubulin (green). Phalloidin staining (gray) demonstrates that the bundle is fragmented when the kinocilium opposes the crescent of Gαi expression in a mature cell. Scale bar, 2 μm.

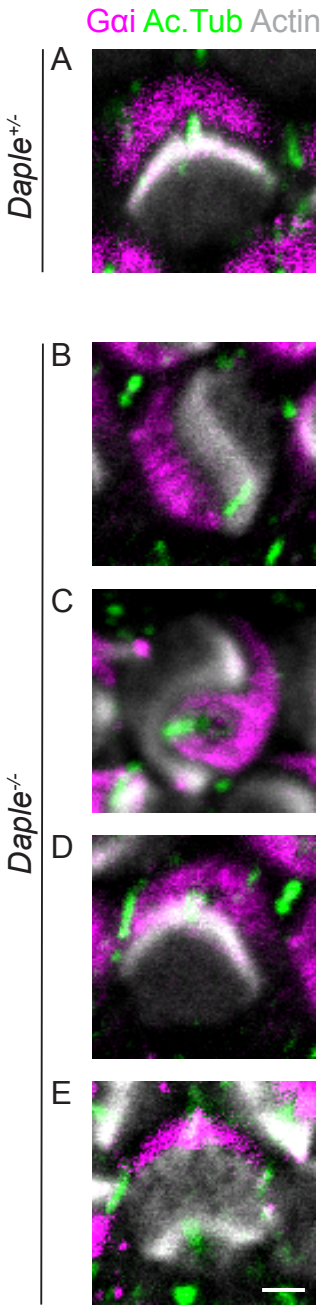
Gαi Ac.Tub Actin
A
Daple+/-
B
C
D
E
Daple-/-

Figure 4.3 Kinociliary defects in the absence of Daple (A) Immunolabeling of acetylated tubulin reveals the position of the kinocilia (green) near the base (top) and apex (bottom) of the cochlea in *Daple*$^{+/-}$ (left) and *Daple*$^{-/-}$ (right) littermates. Phalloidin staining (gray) and antibodies against Gαi (magenta) label the apical surface of each hair cell. (B) The position of the kinocilium (green) is plotted with respect to the apical surface for each of 350 wild-type and 495 *Daple*$^{-/-}$ outer hair cells. Whereas kinocilia localize near the abneural edges of *Daple*$^{+/-}$ hair cells (left), kinocilia adorn the entire apical surfaces in the absence of Daple (right). (C) For each of 88 wild-type and 105 *Daple*$^{-/-}$ inner hair cells, the positions of the kinocilia (green) are plotted with respect to the apical surfaces. Whereas the kinocilia localize near the abneural edge of a wild-type hair cell (left), some kinocilia occur in the neural half of the cell in the absence of Daple (right). (D) For each outer hair cell, the angle of the center of the Gαi3 domain is summarized in a polar histogram. Although Gαi is biased toward the abneural edge in both *Daple*$^{+/-}$ (left) and *Daple*$^{-/-}$ (right) littermates, the latter exhibit orientation defects. Whereas in wild-type cochleas the most abneural bin captures nearly 30 % of the hair cells, in *Daple*$^{-/-}$ cochleas the most abneural bin captures fewer than 14 %. (E) For each inner hair cell, the angle from the cell center to the middle of the Gαi3 domain is summarized in a polar histogram. The Gαi3 domain is only mildly misoriented in *Daple*$^{-/-}$ inner hair cells (left) compared to heterozygous littermates (right). Scale bars, 10 μm.

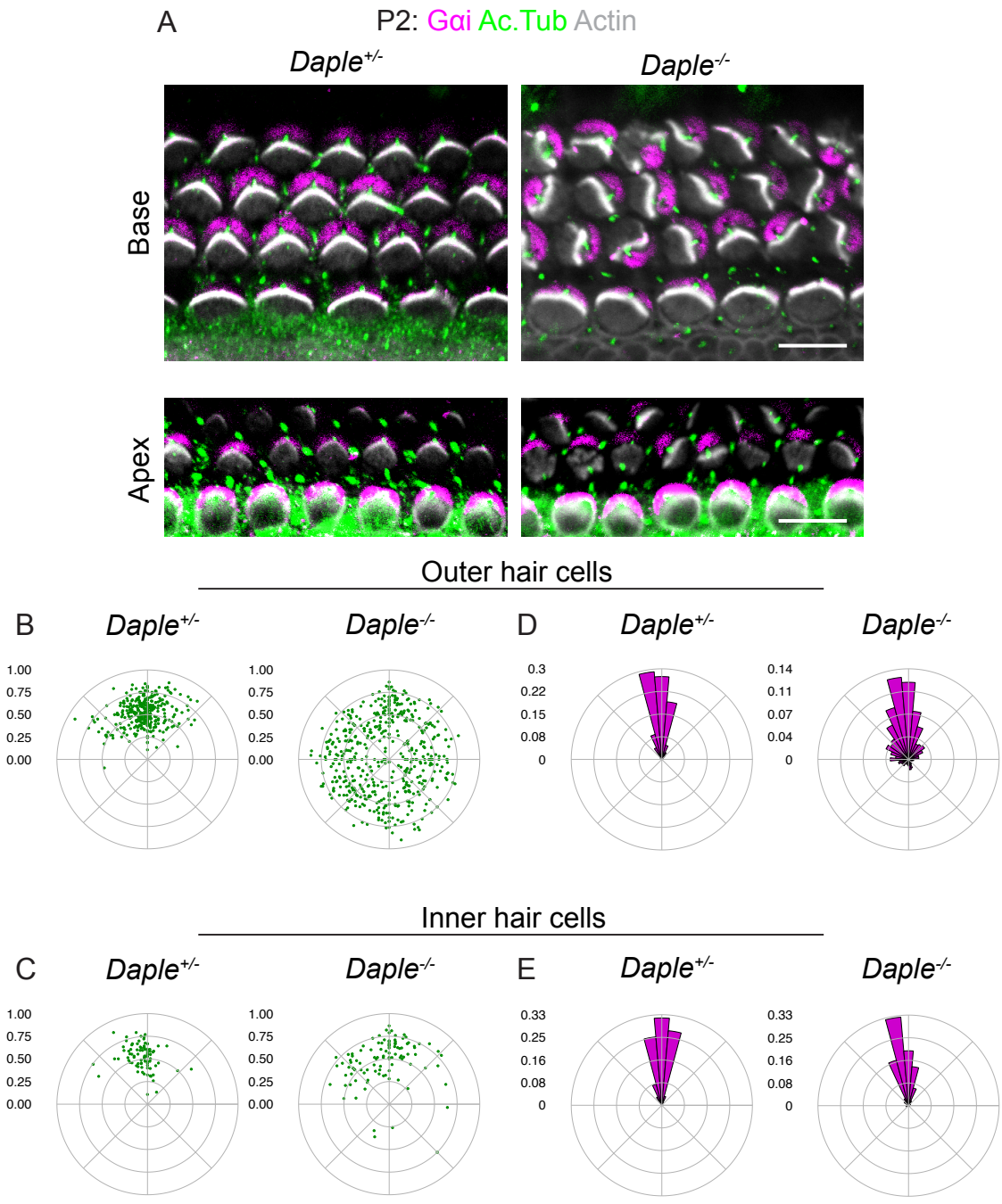
A
P2: Gαi Ac.Tub Actin
Daple+/-
Daple-/-
Base
Apex
Outer hair cells
B
Daple+/-
Daple-/-
D
Daple+/-
Daple-/-
1.00
0.75
0.50
0.25
0.00
0.3
0.22
0.15
0.08
0
0.14
0.11
0.07
0.04
Inner hair cells
C
Daple+/-
Daple-/-
E
Daple+/-
Daple-/-
0.33
0.25
0.16
0.08

Figure 4.4 Comparison of orientation defects among hair-cell rows (A) For each row of outer hair cells near the apex of the cochlea, the angles from the cell centers to the middles of the Gαi3 domains are summarized in a polar histogram. Compared with heterozygous littermates (top three panels), Daple mutants exhibit the most severe orientation defects in the third row of outer hair cells (bottom three panels). A single neural bin captures nearly 10 % of hair cells in the third row. (B) Near the apex of the cochlea, maximal-intensity projections of the Z-stacks shown in panel *4.3A* demonstrate the domain of Gαi expression in each hair cell. (C) For each row of outer hair cells near the base of the cochlea, the angles from the cell centers to the middles of the Gαi3 domains are summarized in a polar histogram. Compared with heterozygous littermates (top three panels), *Daple*$^{-/-}$ mutants exhibit the most severe orientation defects in the first two rows of outer hair cells (bottom three panels). (D) Near the base of the cochlea, maximal-intensity projections of the Z-stacks shown in panel *4.3C* reveal the domain of Gαi expression in each hair cell. Scale bars, 10 μm.

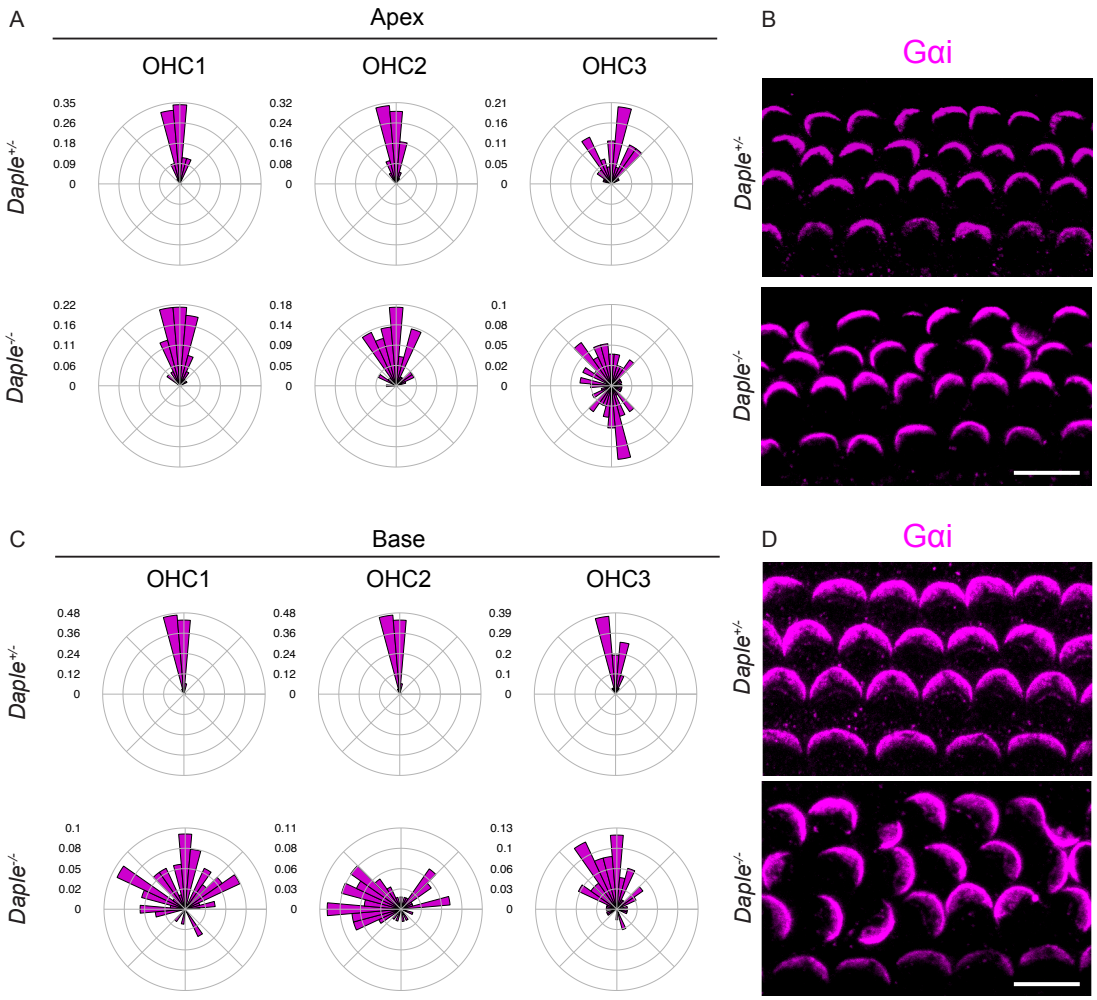
A
Apex
OHC1
OHC2
OHC3
Daple+/-
Daple-/-
0.35
0.26
0.18
0.09
0
0.32
0.24
0.16
0.08
0
0.21
0.16
0.11
0.05
0
0.22
0.16
0.11
0.06
0
0.18
0.14
0.09
0.05
0
0.1
0.08
0.05
0.02
0
B
Gαi
Daple+/-
Daple-/-
C
Base
OHC1
OHC2
OHC3
Daple+/-
Daple-/-
0.48
0.36
0.24
0.12
0
0.48
0.36
0.24
0.12
0
0.39
0.29
0.2
0.1
0
0.1
0.08
0.05
0.02
0
0.11
0.08
0.06
0.03
0
0.13
0.1
0.06
0.03
0
D
Gαi
Daple+/-
Daple-/-

Kinociliary defects precede Gαi3 misorientation in Daple$^{-/-}$ hair cells.

Because the kinocilia in postnatal *Daple*$^{-/-}$ hair cells were not displaced in the abneural direction, I wondered whether localization of the kinocilia remained correlated with G-protein signals. I therefore compared the angle of the Gαi3 domain and the corresponding angular position of the kinocilium with respect to each cell's center (Figure 4.5A). Although the two angles were correlated in both *Daple*$^{-/-}$ mice and heterozygous littermates, the correlation was imperfect in the absence of Daple (Figure 4.5B,C). When the domain of Gαi3 expression was oriented toward the abneural edge of the hair cell, the kinocilium could be found in either half of that domain. This relationship changed when the domain of Gαi3 shifted from the abneural edge: the kinocilium occurred in the neural half of the Gαi3 domain when Gαi3 was misoriented.

To explain this trend, I investigated the progression of the relationship between Gαi3 and the kinocilium in embryonic mice. As maturation proceeds in a gradient from the cochlear base toward the apex, each kinocilium first moves toward the abneural cellular edge, then migrates partway back toward the cell's center as the stereociliary cluster forms[18] (Figure 4.6A). Although in both *Daple*$^{+/-}$ and *Daple*$^{-/-}$ cochleas at E17.5 nearly all basal bodies were located near the centers of hair cells at the apex, I found very few central basal bodies at the cochlear base (Figure 4.6B-D). The initial shift of the kinocilium toward the abneural cellular boundary therefore occurred in the absence of Daple. Because basal bodies lay near the centers of postnatal *Daple*$^{-/-}$ hair cells, the second shift of the kinocilium also likely occurred.

Both shifts likely exhibited directional errors. Near both the middle turn and the base of E17.5 cochleas, the loss of Daple significantly affected the angular distribution of

basal bodies with respect to the center of the cell ($p < 0.0001$ and $p < 0.0001$). In approximately 47 of 141 hair cells near the middle turn of an E17.5 *Daple*$^{-/-}$ cochlea, the basal bodies were displaced in the neural direction (Figure 4.6C). In heterozygous littermates, only 3 of 134 basal bodies occurred in the neural half of a hair cell. Near the base of *Daple*$^{-/-}$ cochleas, 66 of 119 basal bodies were displaced in the neural direction, whereas the basal bodies of heterozygous littermates were uniformly abneural (Figure 4.6D). Because mature *Daple*$^{-/-}$ hair cells were more likely than immature *Daple*$^{-/-}$ hair cells to exhibit neural basal bodies, the data suggested that early errors in the initial shift of the kinocilia were augmented by relocalization defects as hair cells matured.

Although most basal bodies occurred abneurally near the middle turn of an E17.5 wild-type cochlea, the domains of Gαi3 expression were still misoriented in a subset of immature hair cells (Figure 4.7A). Crescents of Gαi3 expression were comparably misoriented near the middle turn of an E17.5 *Daple*$^{-/-}$ cochlea ($p > 0.5$). As each hair cell matured near the base of a wild-type cochlea, the domain of Gαi3 expression occurred at the abneural edge (Figure 4.7B). Although near the base of a *Daple*$^{-/-}$ cochlea about half of the basal bodies occurred in the neural halves of developing hair cells (Figure 4.6D), Gαi3 was only mildly misoriented in the same region ($p > 0.1$, Figure 4.7B). Moreover the Gαi3 domain was not grossly misshapen. As in some postnatal hair cells, in a subset of embryonic *Daple*$^{-/-}$ cells the basal body lay opposite the crescent of Gαi3 expression.

To characterize the relationship between Gαi3 and the basal body in embryonic mice, I compared the angle of the Gαi3 domain and the corresponding angular position of the basal body with respect to each cell's center. Near the middle turn of a wild-type E17.5 cochlea, the basal body was either aligned with the Gαi3 domain or found closer to

the abneural edge (Figure 4.8A). In the absence of Daple, this relationship nearly reversed. The center of the Gαi3 domain was frequently found closer to the abneural edge of the hair cell than the basal body. Near the base of a wild-type E17.5 cochlea, Gαi3 and the basal body began to align at the abneural edge of each hair cell (Figure 4.8B). In contrast, near the base of an E17.5 *Daple*$^{-/-}$ cochlea, the center of the Gαi3 domain was almost always found closer to the abneural edge of the hair cell than the basal body. The data implied that the basal body sometimes preceded the Gαi3 domain at the abneural edge of a wild-type hair cell, whereas in the absence of Daple Gαi3 was enriched at the abneural edge independently of the basal body.

Figure 4.5 Correlation between Gαi3 and the kinocilium in postnatal mice (A) In a schematic diagram, an angle of 0˚ denotes the abneural edge in a wild-type hair cell. Gαi expression (pink) and the kinocilium (green) are depicted. (B) The angle of the kinocilium with respect to each hair cell's center is plotted against the angle of the center of the Gαi3 domain in the same cell. Although the data from heterozygous littermates cluster about the blue identity line (left), the data from *Daple*$^{-/-}$ mice suggest a more complex relationship between the two angles (right). (C) *Daple*$^{-/-}$ hair bundles are displayed from different regions of the graph in panel *B*, where each bundle can be identified by its associated color (blue, orange, green, pink). Scale bar, 2 μm.

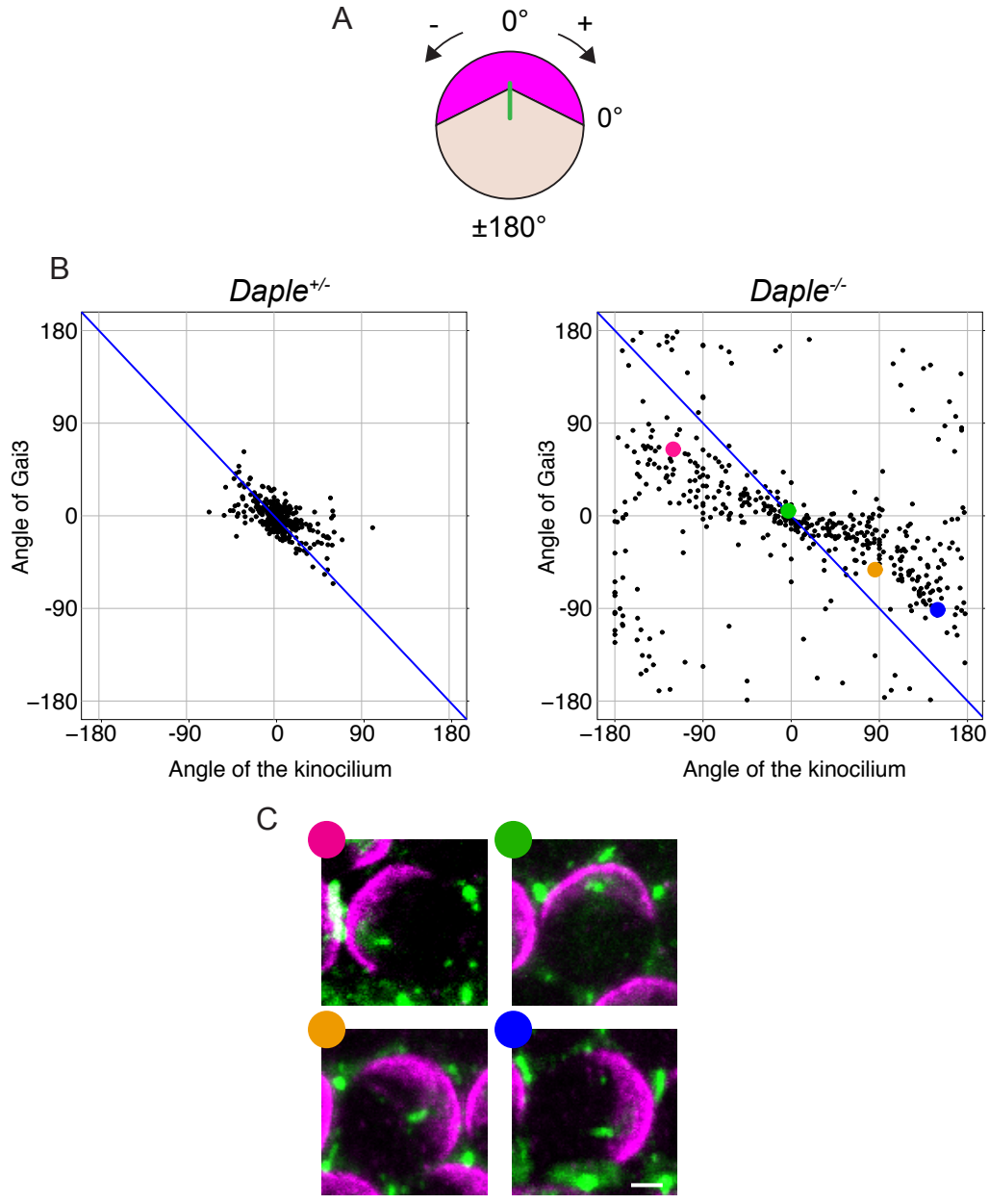
A
-
0°
+
0°
±180°
B
Daple+/-
Daple-/-
180
90
0
-90
−180
−180
-90
0
90
180
Angle of Gai3
Angle of the kinocilium
C

Figure 4.6 Migration of the kinocilium in the absence of Daple (A) A schematic diagram, reproduced from Figure 1.2, depicts the sequence of hair-cell maturation. The kinocilium lies at the center of an immature hair cell (left). The initial shift of the kinocilium (blue) toward the abneural edge of the cell coincides with the enrichment of Gαi (purple, middle). The domain of Gαi is then refined as the kinocilium relocates toward the center of the cell (right). (B-D) Immunolabeling of pericentrin (red) and phalloidin staining (blue) reveals the position of the basal body relative to intercellular junctions in E17.5 *Daple*$^{+/-}$ (left column) and *Daple*$^{-/-}$ (right column) littermates. Basal bodies lie near the centers of cells at the cochlear apex in both genetic backgrounds (top row). Near the middle and base of the cochlea, the hair cells of heterozygous animals exhibit basal bodies primarily at their abneural edges, whereas some *Daple*$^{-/-}$ basal bodies occur at the neural edges (arrows, middle and bottom rows). On the right-hand side of each panel, the angular position of each basal body with respect to the center of the cell is summarized in a radial histogram. The absolute value of each angle is shown. Quantification emphasizes that the number of basal bodies in the neural half of a hair cell increases toward the base of an E17.5 *Daple*$^{-/-}$ cochlea. Scale bar, 10 μm.

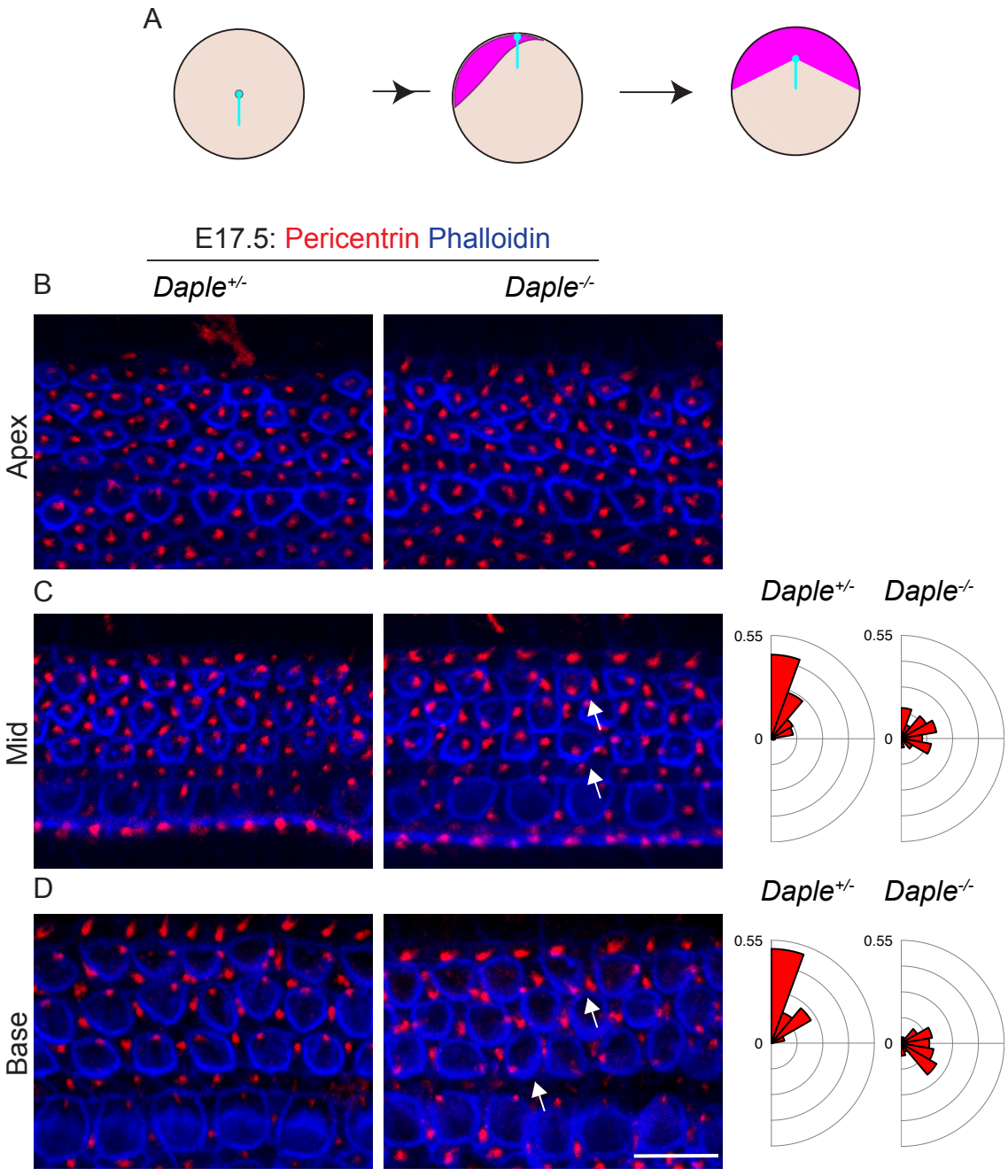
A
E17.5: Pericentrin Phalloidin
B
Daple+/-
Daple-/-
Apex
C
Daple+/-
Daple-/-
0.55
0
Mid
D
Daple+/-
Daple-/-
0.55
0
Base

Figure 4.7 Misalignment of Gαi and the kinocilium during *Daple*$^{-/-}$ hair-cell development (A) The middle turn of an E17.5 cochlea is immunolabeled for Gαi (green) and pericentrin (magenta). Although the Gαi3 domain is misoriented in a subset of immature wild-type hair cells (top), the kinocilium occurs at the abneural edge of the same cell (arrow). The Gαi3 domain is also misoriented in *Daple*$^{-/-}$ hair cells (bottom). On the right-hand side of each panel, the angular position of the Gαi3 domain with respect to the center of each hair cell is summarized in a radial histogram. The absolute value of each angle is shown. Quantification emphasizes that Gαi3 is mildly misoriented in both *Daple*$^{-/-}$ mice and heterozygous littermates. (B) The base of an E17.5 cochlea is immunolabeled for Gαi (green) and pericentrin (magenta). Although basal bodies occur near the centers of the Gαi domains in all heterozygous hair cells (top), the basal bodies lie near the edges of the Gαi domains in many *Daple*$^{-/-}$ hair cells (bottom). One of a hundred hair cells was inverted (yellow arrow). In a few cells the basal body is opposite the crescent of Gαi (white arrow). On the right-hand side of each panel, the angular position of the Gαi3 domain with respect to the center of each hair cell is summarized in a radial histogram. The absolute value of each angle is shown. Quantification emphasizes that Gαi3 is mildly misoriented in both *Daple*$^{-/-}$ mice and heterozygous littermates. Scale bars, 10 μm.

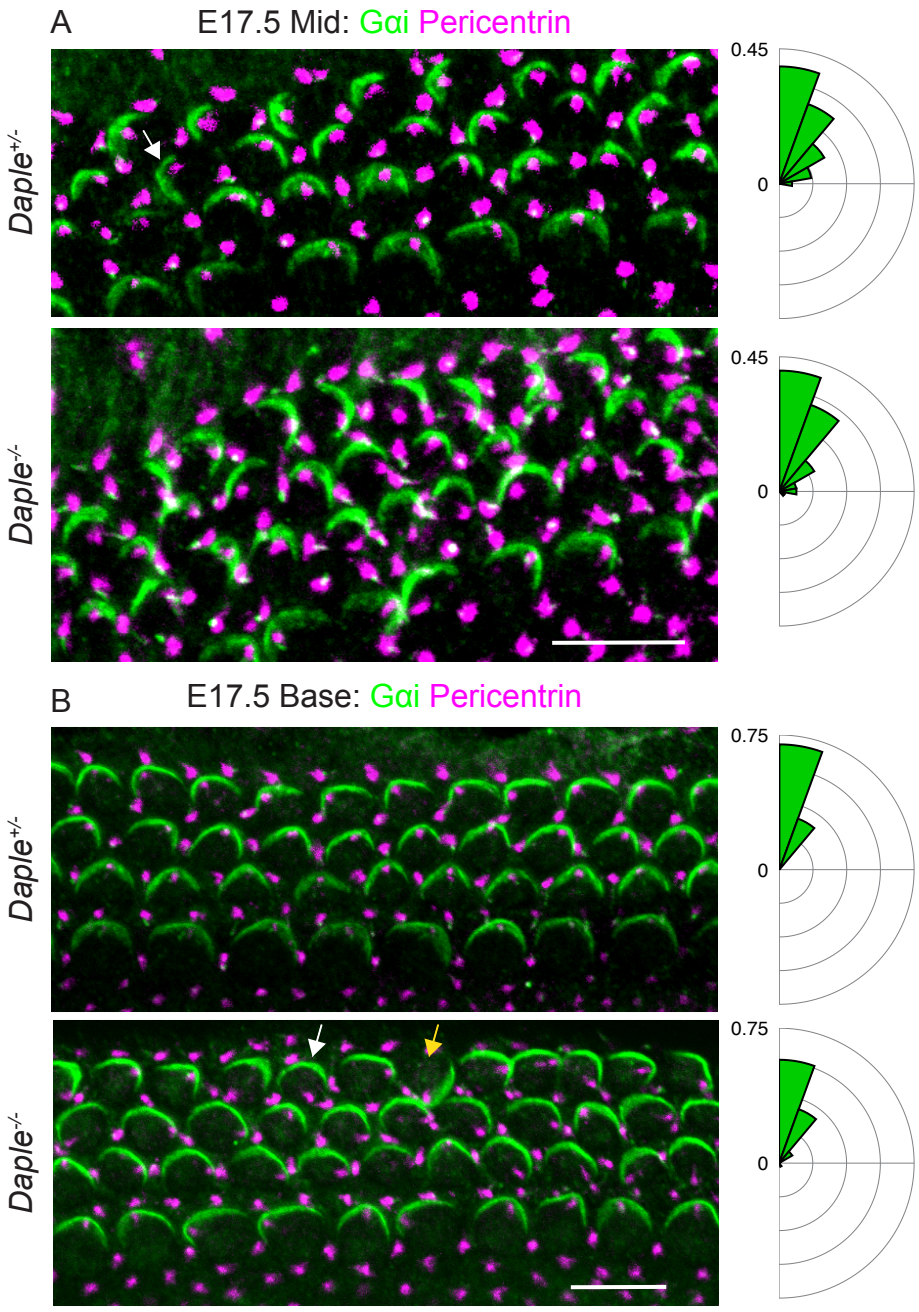
A
E17.5 Mid: Gαi Pericentrin
Daple+/-
Daple-/-
0.45
0
0.45
0
B
E17.5 Base: Gαi Pericentrin
Daple+/-
Daple-/-
0.75
0
0.75
0

Figure 4.8 Correlation between Gαi3 and the basal body in embryonic mice (A) Near the middle turn of an embryonic cochlea, the angle of the basal body with respect to each hair cell's center is plotted against the angle of the center of the Gαi3 domain in the same cell. Although the data from heterozygous littermates cluster near or below the blue identity line (left), the data from *Daple*$^{-/-}$ mice are distributed near or above the identity line (right). (A) Near the base of an embryonic cochlea, the angle of the basal body with respect to each hair cell's center is plotted against the angle of the center of the Gαi3 domain in the same cell. Although the data from heterozygous littermates cluster about the blue identity line (left), the data from *Daple*$^{-/-}$ mice are distributed above the blue identity line (right).

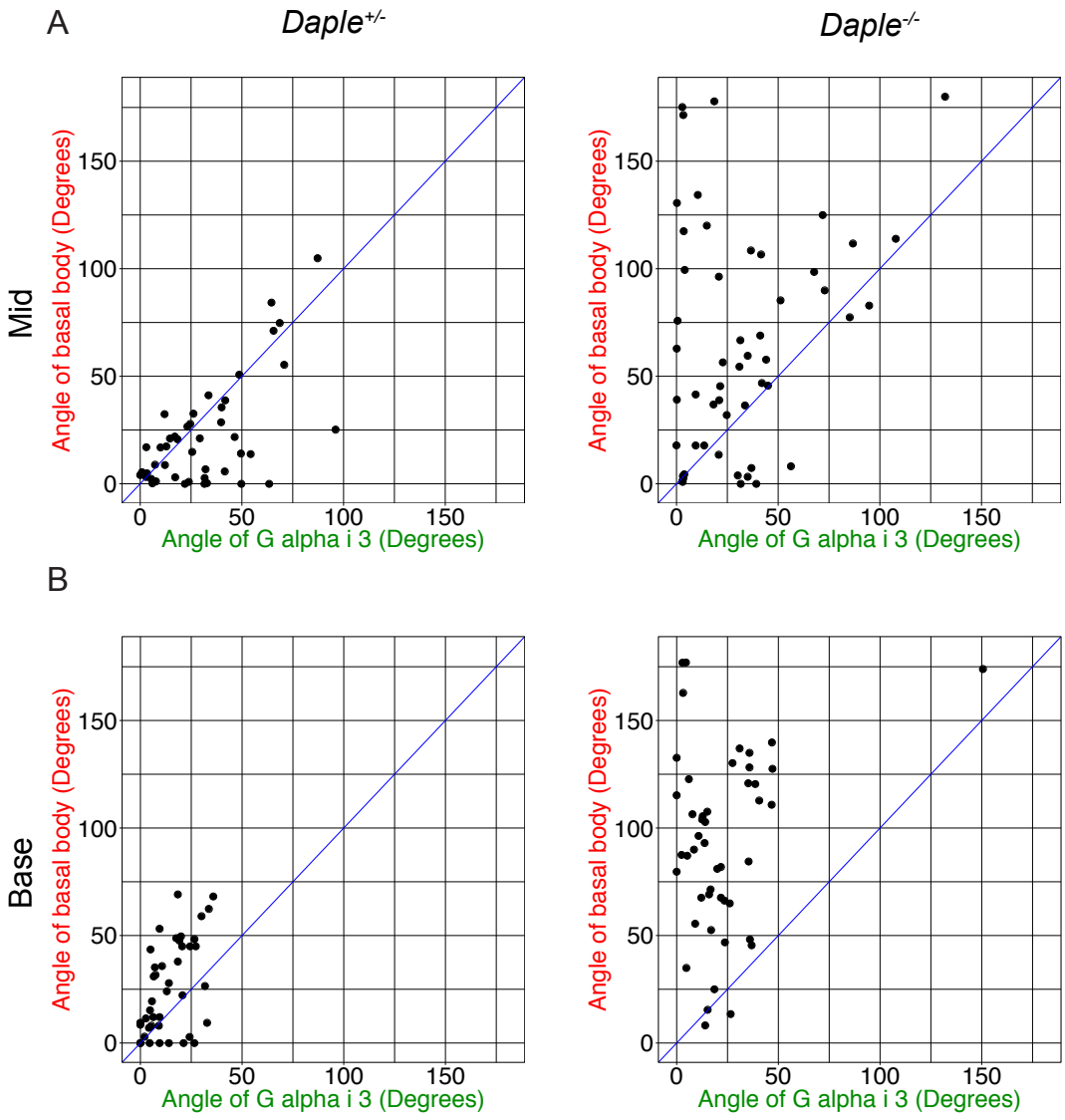
A
Daple+/-
Daple-/-
Mid
B
Base
Angle of basal body (Degrees)
Angle of G alpha i 3 (Degrees)
0
50
100
150

Discussion

Daple$^{-/-}$ postnatal hair cells appear to exhibit both tissue-wide and cell-intrinsic polarity defects. In contrast, *Daple*$^{-/-}$ embryonic hair cells are dominated by cell-intrinsic defects. Although the initial abneural shift and the subsequent neural relocation of the kinocilium are abnormal in E17.5 *Daple*$^{-/-}$ cochleas, the abneural crescent of Gαi does not differ dramatically between embryonic *Daple*$^{-/-}$ mice and heterozygous littermates. I therefore propose that *Daple*$^{-/-}$ postnatal defects in the orientation and patterning of G-protein signals result at least in part from feedback from the kinocilium, the basal body, or the associated microtubules. It is interesting in this regard that the yeast two-hybrid screen identified Rgs14, a regulator of G-protein signaling previously characterized as a centrosomal protein[35, 36]. Although the kinocilium has previously been implicated in Gαi expression, the experiments genetically targeted the basal body and only mildly disrupted kinociliary positioning. In contrast *Daple*$^{-/-}$ kinocilia are mislocalized across hair-cell surfaces despite the presence of apical G-proteins.

My results show that during embryonic development Gαi is enriched in a crescent at the abneural surface of the hair cell; this initial pattern is then modulated by the kinocilium or its appendages as the hair cell matures. When kinocilia are mispositioned in the absence of Daple, G-protein signals are evidently reoriented and expanded toward the kinocilia. This hypothesis explains the tendency in a postnatal *Daple*$^{-/-}$ hair cell for the kinocilium to occur in the neural half of the Gαi3 domain; the postnatal orientation of the Gαi3 domain represents a compromise between its embryonic abneural distribution and the angular position of the kinocilium. Also consistent with this hypothesis, some postnatal *Daple*$^{-/-}$ hair cells exhibit an abneural crescent of Gαi3 but a neural kinocilium.

These cells likely result from defects in the initial shift of the kinocilium; mislocation in the neural direction would preclude the kinocilium from modulating abneural Gαi expression. Daple therefore shapes the domain of Gαi by coordinating the early movements of the kinocilium with the crescent of Gαi expression in immature hair cells.

Daple also coordinates the growth of the hair bundle. In both wild-type cells and most Daple-deficient cells, growing stereocilia abut the domain of Gαi3 expression. When Gαi and the kinocilium occur on opposite sides of a hair cell, however, the hair bundle becomes highly fragmented. A ring of stunted stereocilia often encircles the kinocilium, suggesting that both Gαi and the kinocilium can promote stereociliary elongation. Together with the observation that wild-type positioning of the kinocilium in a *Daple*$^{-/-}$ mutant rescues bundle shape, these results imply that Gαi3 and the kinocilium cooperate to shape the hair bundle and that Daple coordinates these signals.

Chapter Five: Daple interacts with core PCP and cell-intrinsic signals.

Many of this chapter's experiments were performed in collaboration with Basile Tarchini. One of the first researchers to describe the role of Gαi and LGN in the cochlea, Dr. Tarchini maintains a variety of mouse models and reagents that permitted the exploration of Daple's role in the cell-intrinsic pathway.

Daple is not required for the asymmetric localization of Vangl2 or Frizzled6.

Daple is well established as a Dishevelled-binding protein. I therefore investigated whether Daple is necessary for the localization of PCP proteins. The core PCP components Vangl2 and Frizzled6, homologues of *Drosophila* Van Gogh and Frizzled, were distributed asymmetrically in both *Daple*$^{+/-}$ and *Daple*$^{-/-}$ hair cells (Figure 5.1). Even *Daple*$^{-/-}$ hair cells that were clearly misoriented exhibited both proteins at the neural edges of the junctions between hair cells and supporting cells.

Daple maintains the asymmetric localization of Dishevelled.

Because the PCP proteins are generally interdependent for their localization, core PCP signaling was apparently intact in *Daple*$^{-/-}$ mutants. We found that Dishevelled-2 was also detected by immunohistochemistry in hair cells near the apex of *Daple*$^{-/-}$ cochleas (Figure 5.2). However, Dishevelled could not be detected at the abneural edges of hair cells near the base of *Daple*$^{-/-}$ cochleas (Figure 5.3). Because hair-cell maturation proceeds in a gradient toward the apex of the cochlea, Daple might maintain the localization of Dishevelled during development.

Consistent with this hypothesis, immunohistochemistry demonstrated that Daple co-localized with Dishevelled at intercellular junctions (Figure 5.4A). Because the antibody provided inconsistent labeling, we additionally confirmed that a *Dvl2-EGFP* fusion construct co-localized with Daple in cochlear explants (Figure 5.4B). Thus Daple and Dishevelled likely interact during cochlear development.

Figure 5.1 Localization of Vangl2 and Frizzled6 in the absence of Daple Immunohistochemistry shows that Vangl2 (green) and Frizzled6 (magenta) occur at the abneural edge of junctions between hair cells and supporting cells in both wild-type (left) and *Daple*$^{-/-}$ (right) P2 littermates. Phalloidin labeling (gray) emphasizes that both proteins are asymmetrically distributed despite the severe bundle defects apparent in *Daple*$^{-/-}$ mice (arrows, right). Scale bar, 10 μm.

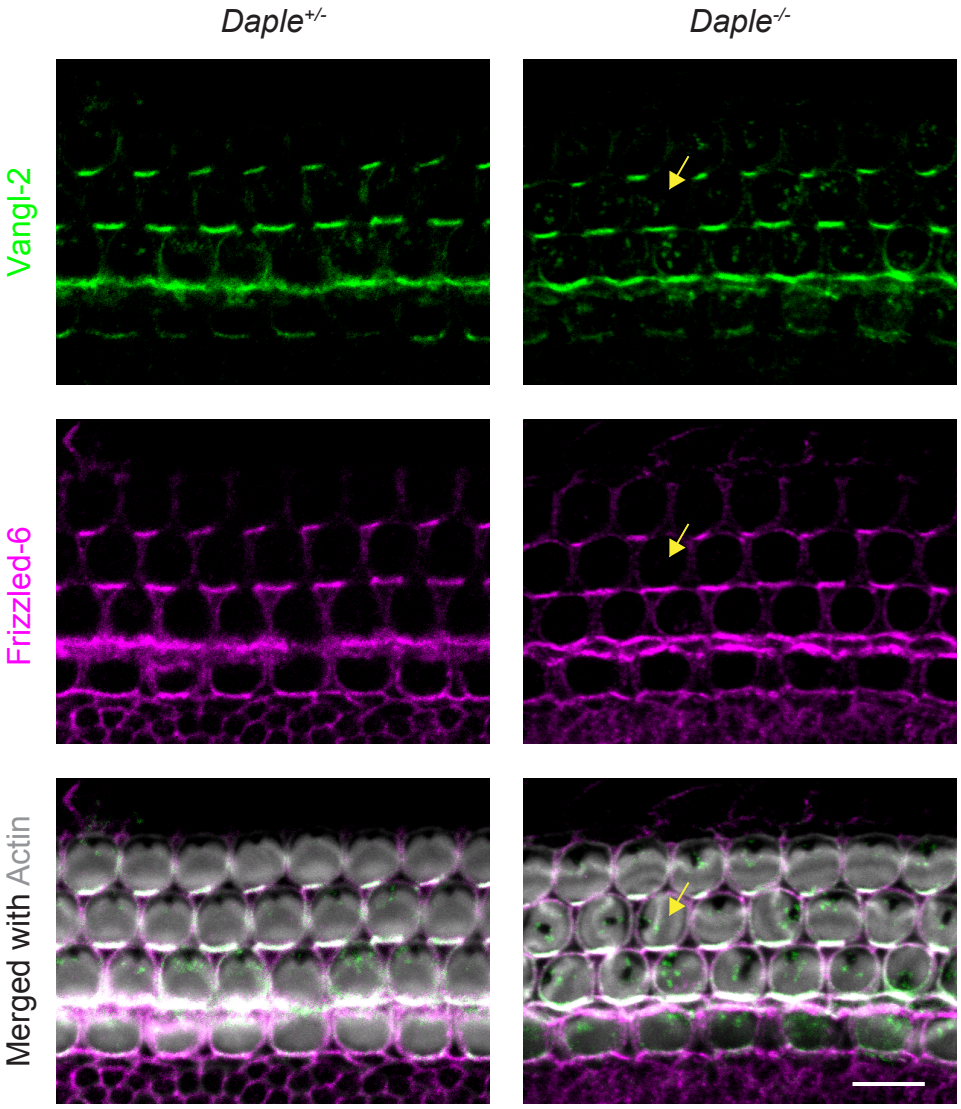
Daple+/-
Daple-/-
Vangl-2
Frizzled-6
Merged with Actin

Figure 5.2 Dishevelled localization near the apex of *Daple*$^{-/-}$ cochleas ZO1 (green) and Dishevelled (magenta) are immunolabeled near the apex of wild-type (left) and *Daple*$^{-/-}$ (right) P0 cochleas. ZO1 denotes intercellular junctions. Dishevelled occurs at the abneural edges of hair cells. Scale bar, 10 μm.

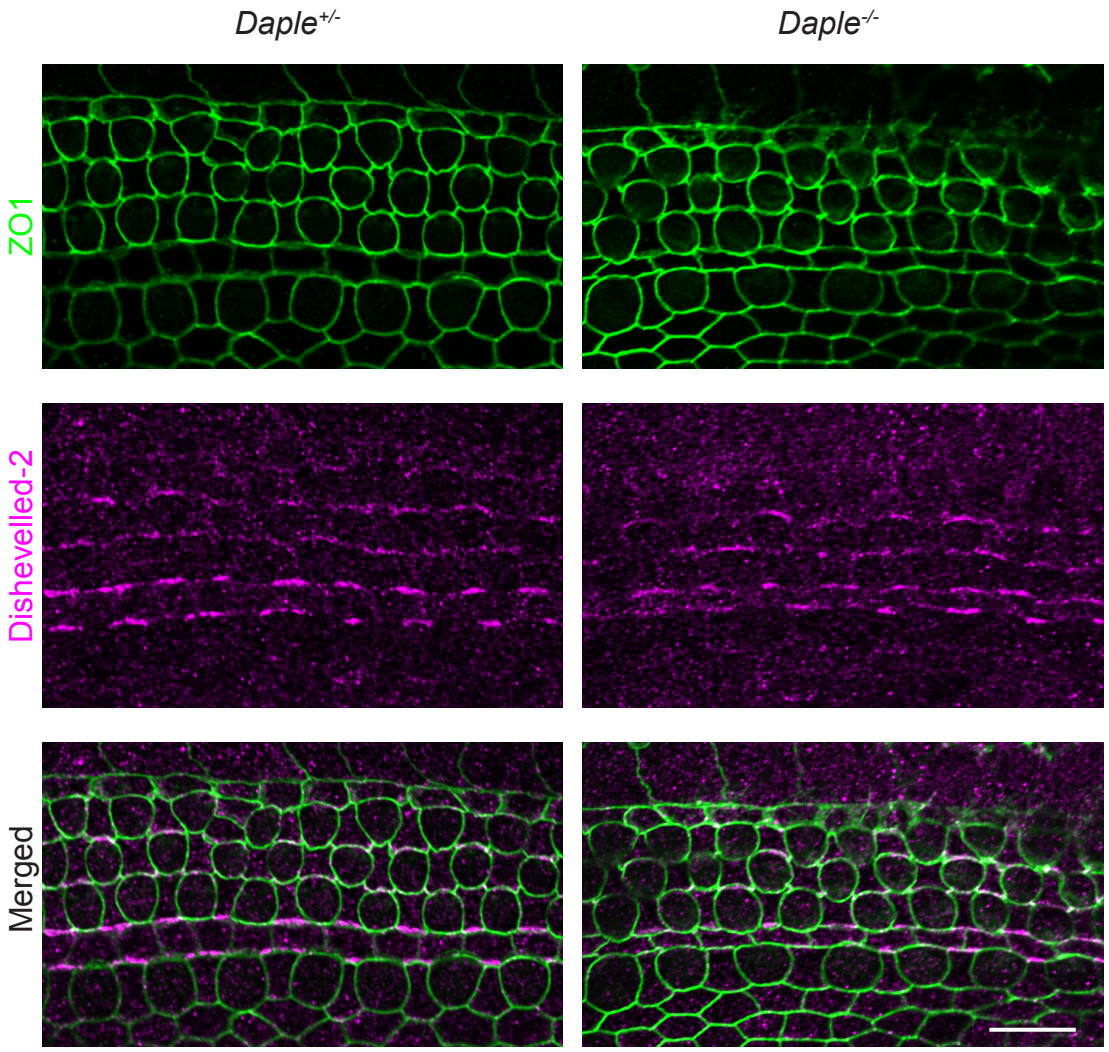
Daple+/-
Daple-/-
ZO1
Dishevelled-2
Merged

Figure 5.3 Dishevelled localization near the base of *Daple*$^{-/-}$ cochleas ZO1 (green) and Dishevelled (magenta) are immunolabeled near the base of wild-type (left) and *Daple*$^{-/-}$ (right) P0 cochleas. ZO1 denotes intercellular junctions. Although Dishevelled localizes asymmetrically in wild-type cochleas, the protein is absent from the abneural edges of *Daple*$^{-/-}$ hair cells. Scale bar, 10 μm.

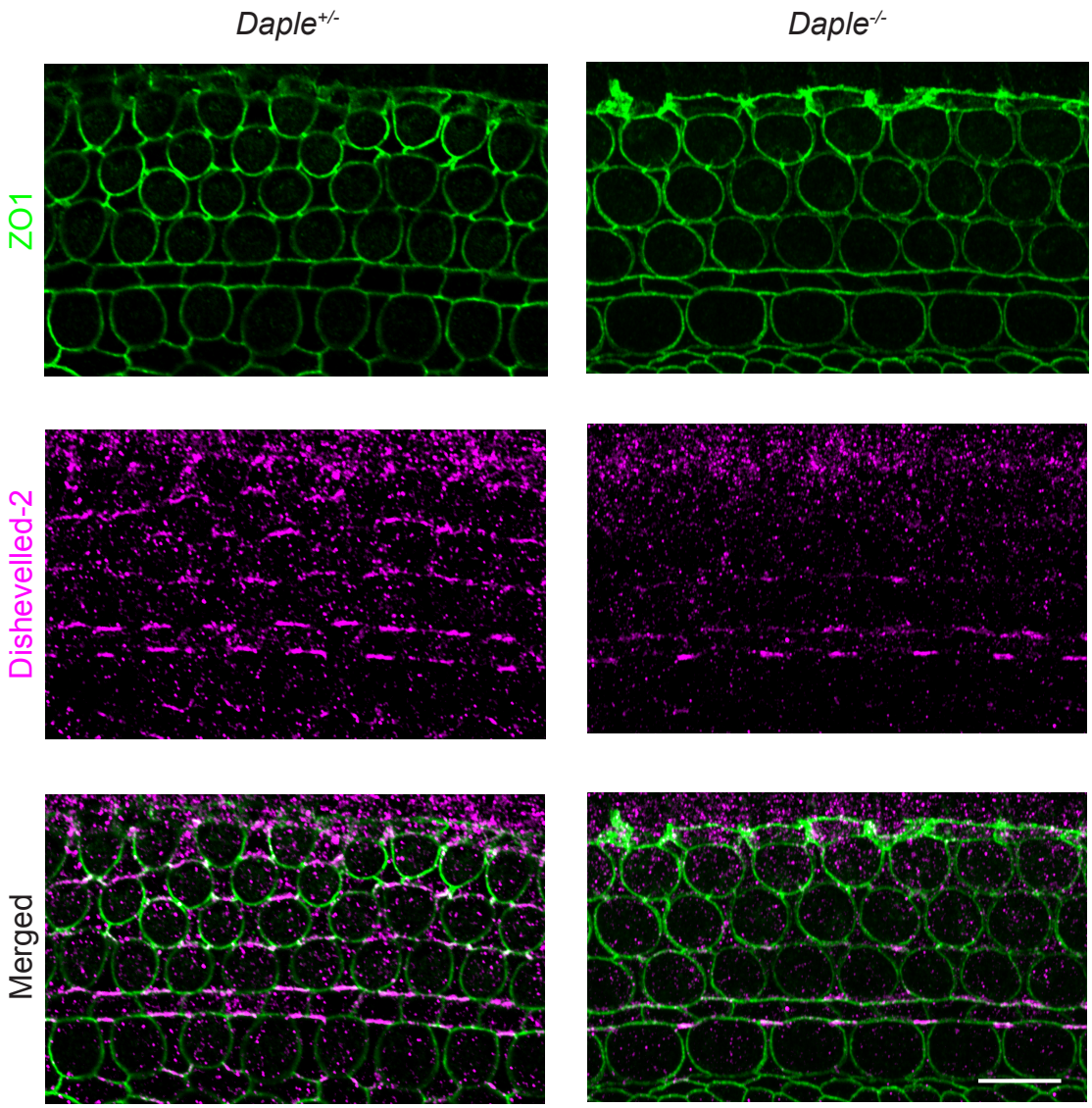
Daple+/-
Daple-/-
ZO1
Dishevelled-2
Merged

Figure 5.4 Co-localization of Daple and Dishevelled (A) Immunohistochemistry demonstrates that Dishevelled (green) and Daple (magenta) co-localize at the abneural edges of P0 cochlear hair cells. (B) A cochlear explant is electroporated with a *Dvl2-EGFP* construct (green) and immunolabeled for Daple (magenta). Because a hair-cell specific promoter drives the expression of *Dvl2-EGFP*, Daple and Dvl2-EGFP are colocalized at the abneural junctions of endogenous hair cells. Scale bars, 10 μm.

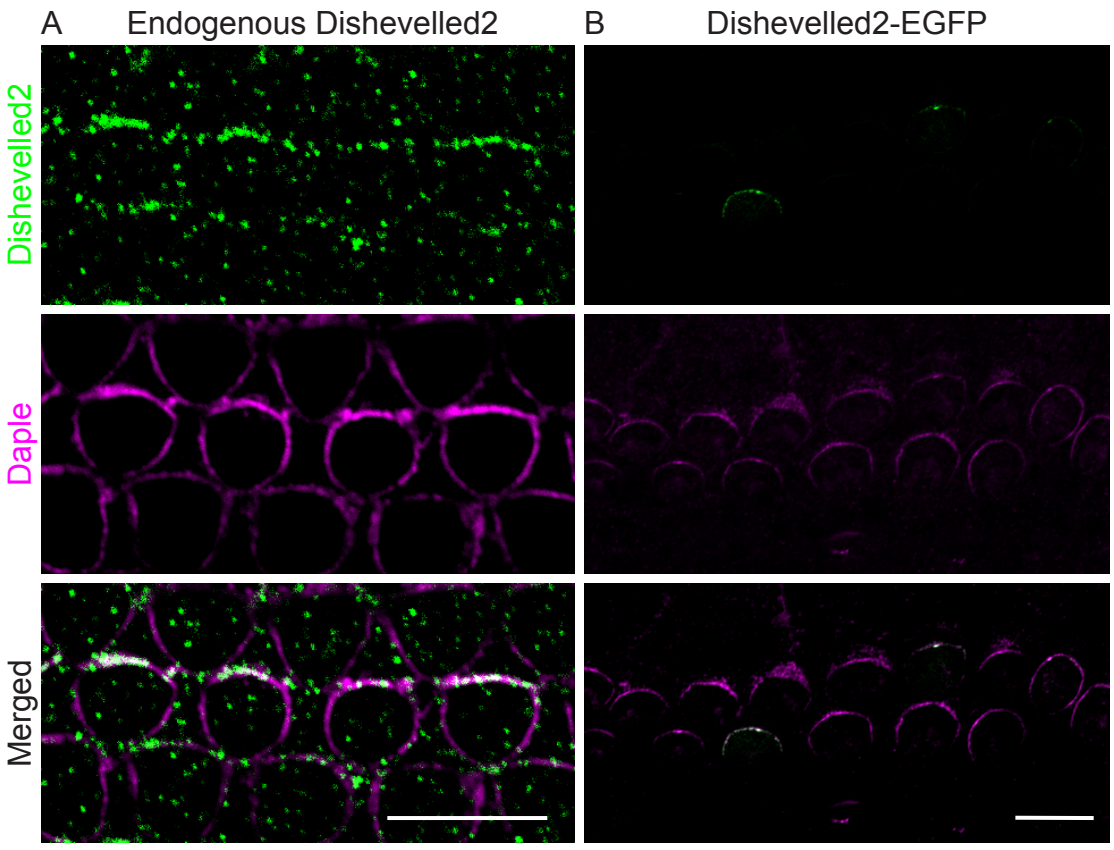
A
Endogenous Dishevelled2
B
Dishevelled2-EGFP
Dishevelled2
Daple
Merged

Daple and Gαi3 occupy adjacent subcellular compartments.

Because *Daple*$^{-/-}$ mutants exhibit defects in cell-intrinsic polarity, we characterized the relationship between Daple and Gαi3 during development. At P2 both proteins occurred at the abneural side of a hair cell but did not co-localize (Figure 5.5A); instead, Gαi3 lay more apically than Daple. The subcellular localization of each protein was more precisely determined by comparison to the tight-junction label zonula adherens 1 (ZO-1). Daple overlapped with and extended below the junction, whereas Gαi3 did not colocalize with ZO-1 and labelled the apical membrane (Figure 5.5B,C). Daple and Gαi3 therefore occupy distinct but adjacent subcellular compartments.

Subcellular patterning of Daple closely correlates with cell-intrinsic signals in embryonic mice.

The subcellular patterning of Daple was closely correlated with G-protein signals during embryonic development. Daple and Gαi3 were visible in some apical hair cells as early as E16.5; in a subset of immature cells, both proteins occurred at the neural cellular boundaries. Par-3 displayed an identical pattern. The localization of the three proteins was refined as hair cells matured from the apex to the base of the cochlea, adopting an abneural distribution in mature hair cells (Figure 5.6A,B). Daple and other cell-intrinsic polarity signals thus developed similar subcellular asymmetry in each region of the cochlea. Furthermore, Daple clearly colocalized with Par-3 in both apical and basal hair cells, confirming that Daple associates with junctional cell-intrinsic signals (Figure 5.6B).

Figure 5.5 Subcellular distributions of Daple and cell-intrinsic markers in postnatal hair cells (A) A projection of a Z-stack in the XY plane demonstrates the immunohistochemical localizations of Gαi (green) and Daple (magenta) at the apical surface of a P2 hair cell (top). Phalloidin labels the hair bundle (blue). A projection of the same stack in the XZ plane at the position of the yellow line demonstrates that Gαi localizes more apically than Daple, which occurs at the level of the intercellular junctions (bottom). (B) Immunolabeling of ZO-1 (green) and Daple (magenta) confirms that Daple is junctional (top). A projection of the stack in the XZ plane at the position of the yellow line suggests that Daple colocalizes with ZO-1 and extends more basally (bottom). (C) Immunolabeling of ZO-1 (green) and Gαi (magenta) establishes that Gαi is excluded from the intercellular junctions (top). A projection of the stack in the XZ plane at the position of the yellow line establishes that Gαi is restricted to the apical surface of the hair cell (bottom). Scale bars, 2 μm.

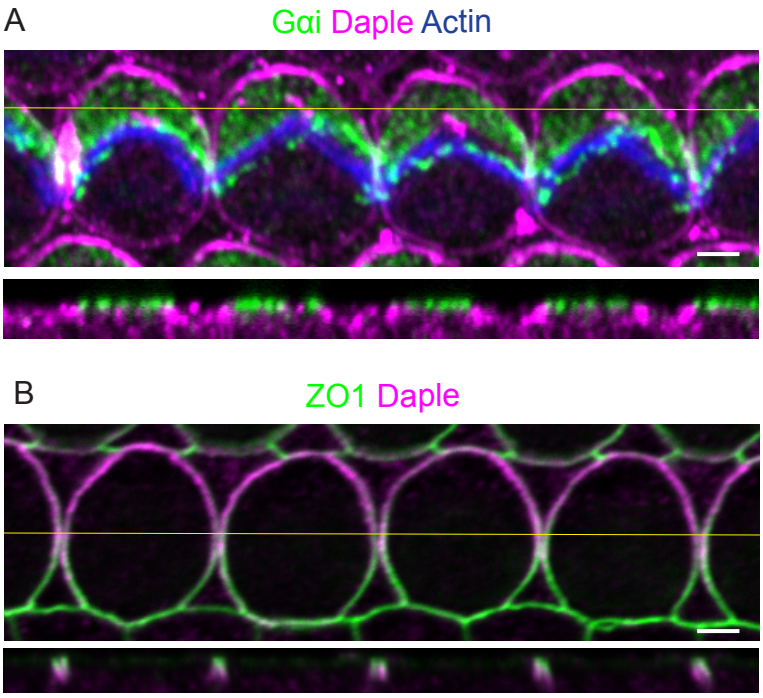
A
Gαi Daple Actin
B
ZO1 Daple
C
ZO1 Gαi

Figure 5.6 Localization of Daple and cell-intrinsic markers during hair-cell development (A) In an E17.5 cochlea immunolabeled for Daple (magenta), Gαi (green), and acetylated tubulin (blue), many immature hair cells near the cochlear apex express Daple and Gαi (top row). The distributions of the two proteins are closely correlated (yellow arrows, top row). In a subset of hair cells both proteins occur at the neural edge (white arrows, top row). In the middle of the cochlea, Daple and Gαi are confined to the abneural halves of some hair cells (arrows, middle row). Near the base of the cochlea Daple and Gαi are closely correlated, and their domains extend neurally (bottom row). (B) Near the apex of an E17.5 cochlea immunolabeled for Daple (magenta) and Par-3 (green), the two proteins are enriched at the neural edges of three outer hair cells (arrows, left three panels). Near the base Daple and Par-3 are distributed abneurally (right three panels). Par-3 is also expressed in supporting cells. Scale bars, 10 μm.

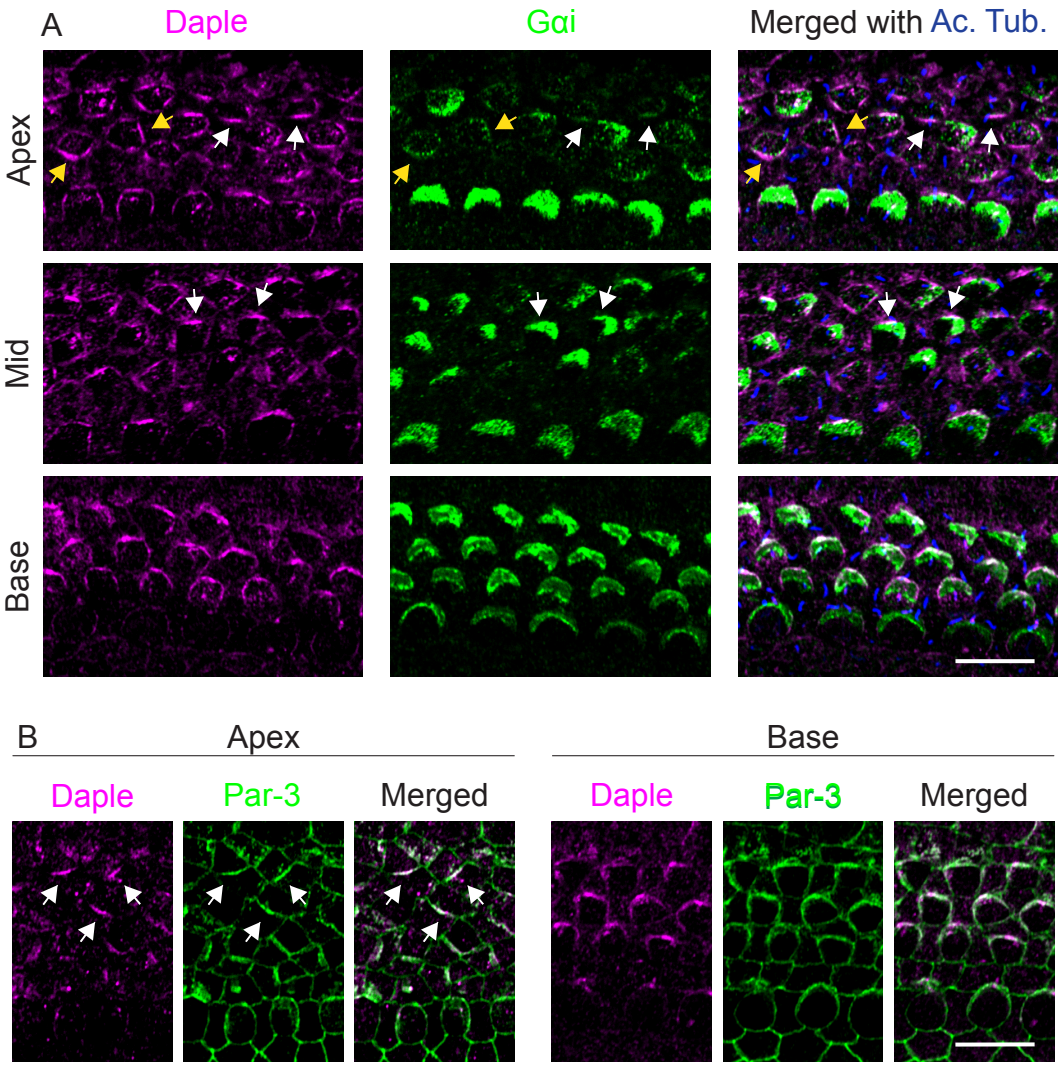
A
Daple
Gαi
Merged with Ac. Tub.
Apex
Mid
Base
B
Apex
Base
Daple
Par-3
Merged
Daple
Par-3
Merged

Daple localizes cell-intrinsically.

Developmental changes in expression implicated Daple as a cell-intrinsic signal, so we asked whether Daple localizes with cell-intrinsic factors in misoriented hair cells. Because the transcription factor Atoh1 induces the development of hair cells, electroporation of *Atoh1-IRES-EGFP* plasmids into cochlear explants produced hair cells in the greater epithelial ridge of the cochlea (Figure 5.7A), a region neural to the organ of Corti that is normally devoid of hair cells[43]. Although these ectopic hair cells were not aligned consistently along any axis, the subcellular localizations of Daple and Gαi3 remained closely correlated. In a subset of ectopic hair cells neither protein was asymmetrically distributed (Figure 5.7B): Daple associated with junctions at the circumference of the cell whereas Gαi3 expanded across the apical surface. In the remaining cells both Daple and Gαi3 were asymmetrically distributed as in endogenous hair cells (Figure 5.7C). Daple therefore associated with cell-intrinsic markers in the absence of directional cues. Consistent with this result, the distribution of Daple was reversed over the line of symmetry reversal in the utricle (Figure 5.7D). This observation clearly differentiated the effects of Daple from those of core PCP proteins.

Gαi3 and LGN regulate the asymmetric localization of Daple.

Because cell-intrinsic signals appeared sufficient to specify Daple's asymmetry, we inquired whether G-protein signals are necessary for the localization of Daple at hair-cell junctions. We first performed immunohistochemistry in $LGN^{-/-}$ mice. In the absence of LGN, Gαi and mInsc are depleted from the apical surface[18]. Daple maintained an

asymmetric, abneural distribution in LGN mutants but was noticeably diminished at hair-cell junctions (Figure 5.8A). Daple instead appeared near the base of the kinocilia.

Daple interacts with Dishevelled, so core PCP signals might also regulate the localization of Daple. Because pertussis toxin inactivates G-protein signaling in hair cells without disrupting PCP signals[18, 19, 26], we used a *Foxg1-cre* promoter to express the toxin throughout the embryonic cochlea. Gαi3 was highly depleted but detectable at apical hair-cell surfaces (Figure 5.8B). As in the absence of LGN, Daple occurred asymmetrically but was diminished at intercellular junctions. The expression of pertussis toxin inverted the first two rows of outer hair cells so that the tall edges of their hair bundles faced neurally (Figure 5.8B)[19]. Daple expression was also inverted in those cells. This observation suggests that Daple localization is regulated primarily by G-protein signals rather than by core PCP proteins[18].

We further tested this hypothesis by expressing Gαi3 ectopically. Because the protein Crumbs occurs uniformly throughout the apical surface of an epithelial cell, the electroporation of a Crumbs-Gαi3 fusion construct into a hair cell distributes Gαi3 and LGN uniformly throughout the apical surface[18]. The expression of a Crumbs-myc fusion protein in hair cells did not perturb the asymmetric distribution of either LGN or Daple (Figure 5.8C). In contrast, Daple was absent from the junctions of hair cells that expressed Crumbs-Gαi3. This result further supported the hypothesis that Gαi regulates the localization of Daple.

Dishevelled may interact with cell-intrinsic signals in the absence of core PCP.

Our results raised the possibility that Dishevelled is affected by cell-intrinsic polarity signals. To characterize the localization of Dishevelled in misoriented hair cells, we co-electroporated *Atoh1-IRES-EGFP* and *Dvl2-EGFP* plasmids into cochlear explants (Figure 5.9A). Daple and Dvl2-EGFP co-localized in the resultant ectopic hair cells, suggesting that Daple provided a link between G-protein signals and Dishevelled.

We therefore asked whether the expression of pertussis toxin perturbed the distribution of Dishevelled. In postnatal cochleas, however, Dishevelled occurred at the abneural edges of some pertussis toxin-treated hair cells that were oriented neurally (Figure 5.9B). Although a subset of treated hair cells did not exhibit abneural Dishevelled, this observation is likely due to inconsistent immunolabeling and requires further study.

Figure 5.7 Cell-intrinsic localization of Daple (A) Electroporation of an *Atoh1-IRES-EGFP* plasmid into cochlear explants induces ectopic hair cells in the greater epithelial ridge. The dotted white line denotes the transition between the four endogenous rows of outer hair cells and the greater epithelial ridge. Hair cells are immunostained for Daple (magenta) and Gαi3 (green). The yellow rectangle captures two ectopic hair cells that are magnified in panel *B*. (B-C) Daple (magenta) and Gαi (green) are immunolabeled in ectopic hair cells induced by the electroporation of *Atoh1-IRES-EGFP* plasmids into cochlear explants. (B) Neither Daple nor Gαi3 is asymmetrically localized in two ectopic hair cells. (C) Most ectopic hair cells are misoriented and exhibit asymmetric localizations of Daple and Gαi3. The labeling of the kinocilia is non-specific. (D) In the utricle, immunohistochemistry against Daple (magnenta) and Gαi3 (green) demonstrates that the distributions of both proteins reverse over the line of polarity reversal. Scale bars, 10 μm.

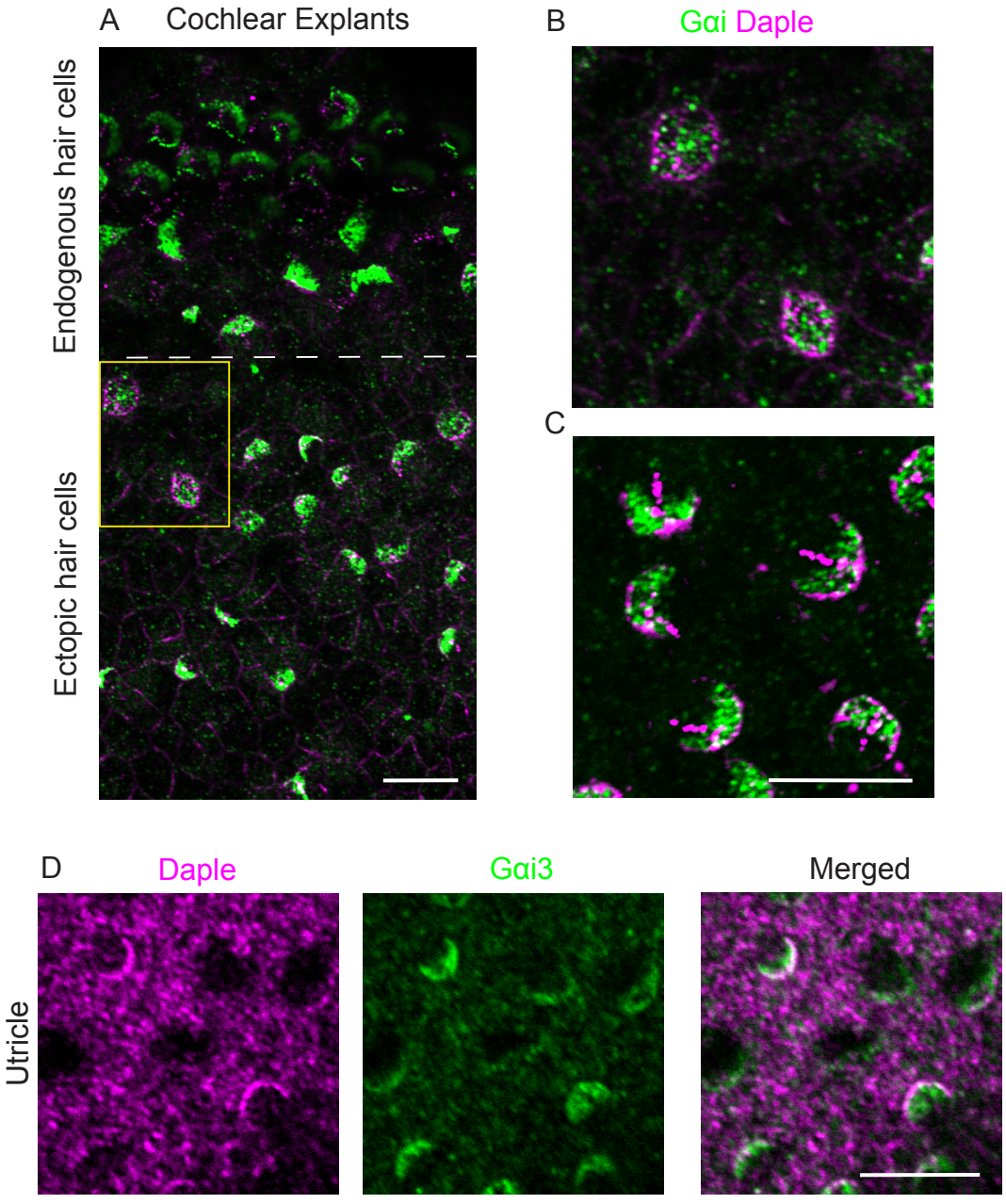
A
Cochlear Explants
Endogenous hair cells
Ectopic hair cells
B
Gαi Daple
C
D
Daple
Gαi3
Merged
Utricle

Figure 5.8 The regulation of Daple by LGN and Gαi (A) Daple is immunolabeled in P1 wild-type (left) and $LGN^{DEL/DEL}$ cochleas (right). Daple is depleted from the intercellular junctions of $LGN^{DEL/DEL}$ hair cells and enriched near the bases of the kinocilia. (B) When pertussis toxin is expressed in E18.5 cochleas with a Foxg1-cre promoter, wild-type (left column) and toxin-expressing (right column) cochleas are immunolabeled for Gαi (green) and Daple (magenta). Both proteins occur at the abneural edges of wild-type hair cells but are depleted from the apical surfaces by pertussis toxin. The toxin also inverts the first two rows of outer hair cells as well as the domains of Gαi and Daple expression. The labeling of the kinocilia is non-specific. (C) Because Crumbs is distributed uniformly across the apical surface, hair cells were electroporated with either a *Crumbs-myc* fusion protein (arrows, left) or a *Crumbs-Gαi3* fusion protein (arrow, middle and right). Immunohistochemistry demonstrates that the distributions of LGN (green) and Daple (magenta) are unaffected by apical Myc protein. In contrast, a uniform distribution of Gαi3 distributes LGN across the apical surface (middle) and eliminates Daple from hair-cell junctions (middle and right). Scale bars, 10 μm.

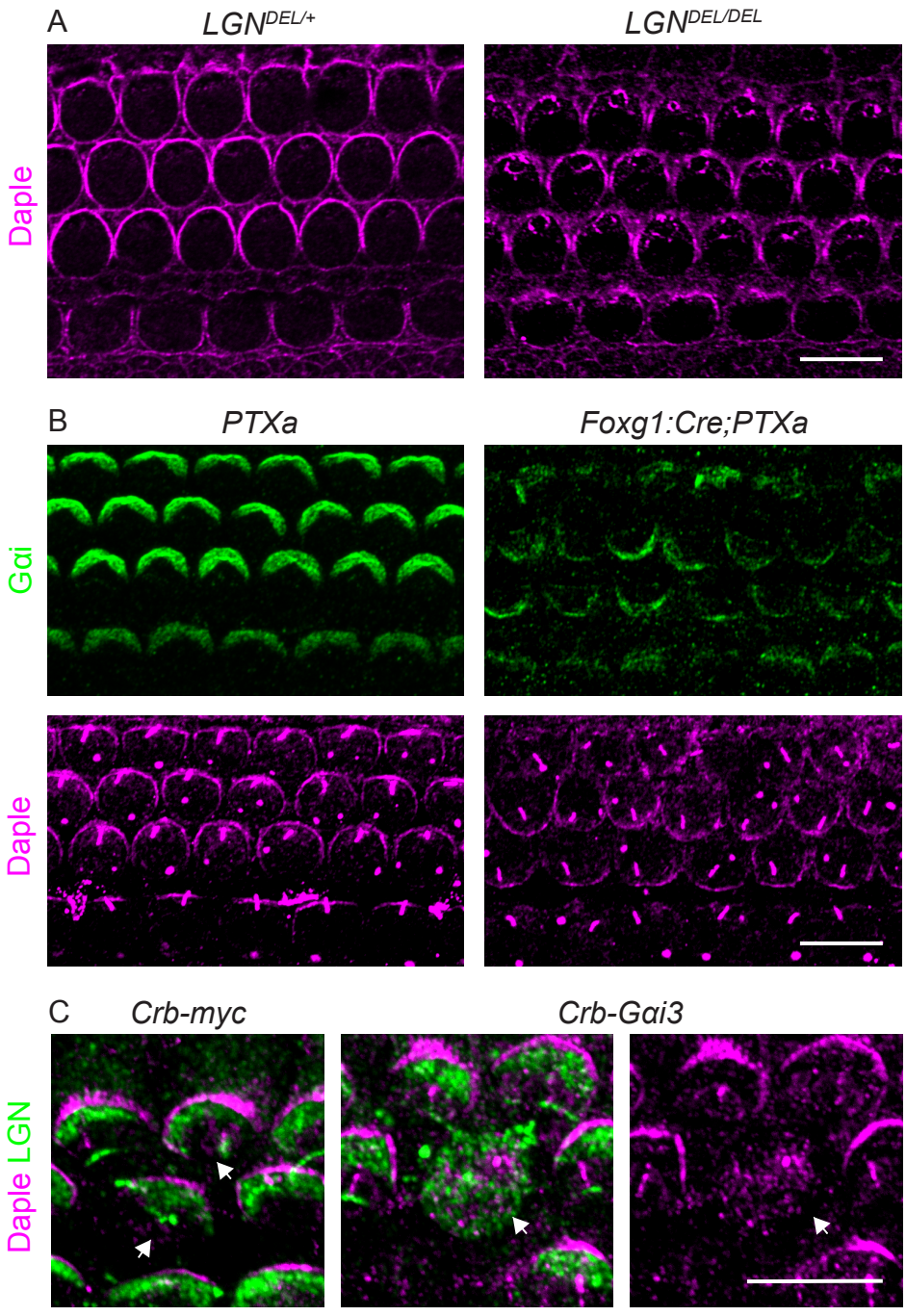
A
LGN^DEL/+
LGN^DEL/DEL
Daple
B
PTXa
Foxg1:Cre;PTXa
Gαi
Daple
C
Crb-myc
Crb-Gαi3
Daple LGN

Figure 5.9 Dishevelled and cell-intrinsic signals (A) Electroporation of *Atoh1* and *Dvl2-EGFP* plasmids into cochlear explants generates ectopic hair cells expressing fluorescently tagged Dishevelled protein. Dishevelled-2 (green) and Daple (magenta) colocalize in these ectopic hair cells. (B) Pertussis toxin is expressed in P1 hair cells with an *Atoh1-Cre* promoter. Phalloidin (gray) labels hair bundles (top). In a more basal plane from the same Z-stack (middle and bottom), immunohistochemistry demonstrates that Dishevelled-2 (magenta) occurs at the abneural edges of misoriented hair cells (arrows). ZO1 (green) labels cellular junctions. Scale bars, 10 μm.

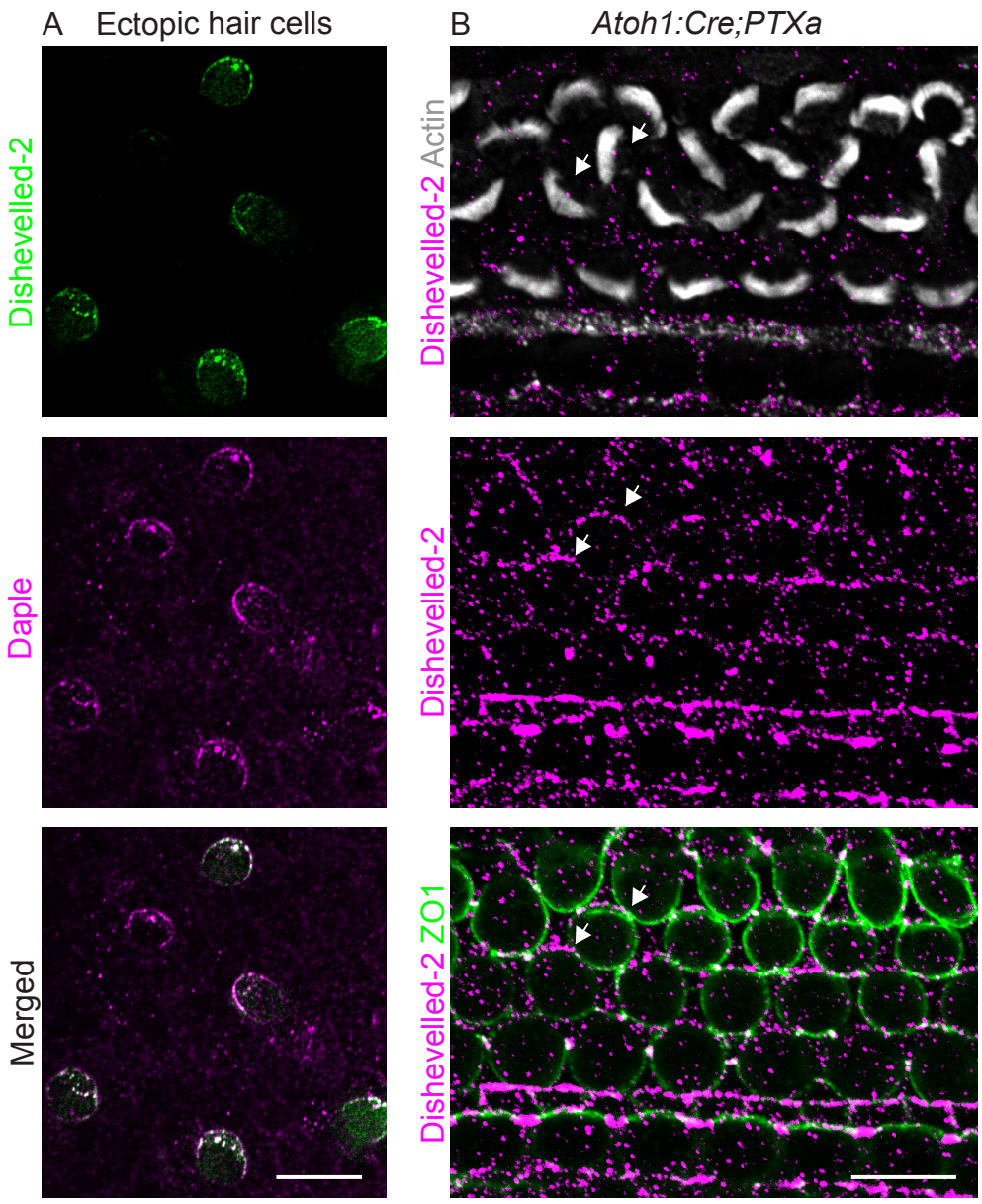
A Ectopic hair cells
B Atoh1:Cre;PTXa
Dishevelled-2
Daple
Merged
Dishevelled-2 Actin
Dishevelled-2
Dishevelled-2 ZO1

Discussion

Because Daple localizes between junctional Dishevelled and apical Gαi, it is well positioned to link the core PCP and cell-intrinsic signals that regulate polarity in the cochlea. Although Daple does not appear to co-localize with Gαi in postnatal hair cells, the two proteins are found in adjoining subcellular compartments and might interact at the boundaries of their expression domains. We also have not ruled out that the two proteins interact earlier in development. Their subcellular patterning is tightly correlated in embryonic hair cells.

My immunolabeling of Daple in ectopic hair cells and in the utricle suggests that Daple is a cell-intrinsic polarity factor. The protein co-localizes with Par-3. The protein's abneural distribution also appears to be regulated by G-protein signals. The mechanism by which Gαi and LGN localize Daple remains unclear. In the absence of LGN, Daple appears to accumulate near the base of the kinocilium. This observation suggests that Gαi or LGN transports Daple to cell junctions through the microtubule network. Daple does not occur at the junctions of hair cells that express a Crumbs-Gαi3 fusion protein. Although a more complex mechanism may underlie this result, the Crumbs moiety might simply disrupt the biochemical interaction of Daple and Gαi3. This interpretation requires further experimentation but is consistent with the hypothesis that Gαi physically transports Daple to the apical surface.

Daple also interacts with the core PCP protein Dishevelled. Daple maintains the abneural distribution of Dishevelled in endogenous hair cells and might also recruit Dishevelled in misoriented ectopic hair cells. Previous studies have suggested that the localization of a Dvl2-EGFP fusion protein differs from that of other core PCP proteins.

Whereas Frizzled-3 fails to localize in the absence of Vangl-2, Dvl2-EGFP in Vangl-2 *Looptail* mutants is diminished but asymmetrically distributed[44]. This pattern might reflect the cell-intrinsic polarity of core PCP mutants and agrees with our observation that Dvl2-EGFP localizes with cell-intrinsic signals in ectopic hair cells. Daple might therefore provide a channel through which cell-intrinsic signals affect the distribution of a core PCP factor.

The physiological relevance of this channel remains unclear. Preliminary results suggest that Dishevelled localizes normally in pertussis-toxin expressing hair cells. In *Atoh1:Cre;PTXa* cochleas, the core PCP protein is found at the abneural edges of hair cells that orient neurally. Because this distribution of Dishevelled might reflect expression in supporting cells rather than in hair cells, the result requires confirmation. Nevertheless the observation implies that the core PCP pathway overrides the cell-intrinsic pathway to distribute Dishevelled in endogenous hair cells. Notably, Daple diverges from Dishevelled and occurs at the neural edges of inverted pertussis toxin-treated hair cells. This result strengthens my hypothesis that Daple is primarily a cell-intrinsic factor.

Chapter Six: A yeast-two hybrid screen reveals potential partners of Daple.

The microtubule network is mispositioned but intact in the absence of Daple.

The mechanism by which Daple positions the kinocilium remains unclear. In the absence of Daple, the microtubule network is mispositioned but evidently intact (Figure 6.1). Daple therefore does not appear to perturb the kinocilium by simply disrupting the microtubule network. A similar observation has been made after pertussin-toxin treatment, which also disrupts the localization of the microtubule aster[19].

A yeast two-hybrid approach identifies potential partners of Daple in the inner ear.

To identify further potential partners of Daple in the core PCP and cell-intrinsic pathways, I initiated a second yeast two-hybrid screen. Murine Daple comprises 2009 amino acids, of which roughly half at the amino terminus contains the HOOK and coiled-coil domains. Because the second half of the protein contains the Gαi- and Dishevelled-binding regions, I cloned a cDNA encoding only the carboxy-terminal half of Daple to use as bait. The company Hybrigenics isolated 66 candidates, including Gαi3 and Gαi2 (Table 6.2). Among the most frequently detected candidates were the three Dishevelled proteins. Because the assay additionally revealed two isoforms of Par-3, the immunohistochemical co-localization of Daple and Par-3 likely reflected a legitimate biochemical interaction.

Daple also interacted with Fcho1, which localized at the apical surfaces of hair cells and is thought to promote membrane remodeling during endocytosis[45, 46] (Figure 6.2A). In addition, the screen identified microtubule-associated proteins such as Dynactin and Wwc1 (Figure 6.2 B-C). Wwc1 additionally localized to the tips of stereocilia.

Figure 6.1 Microtubule asters in the absence of Daple Immunohistochemical labeling of microtubule end-binding protein 1 (EB1, red) reveals microtubule asters in wild-type cochleas (top two panels) and *Daple*$^{-/-}$ cochleas (bottom two panels). Phalloidin staining labels hair bundles (gray). Scale bar, 10 μm.

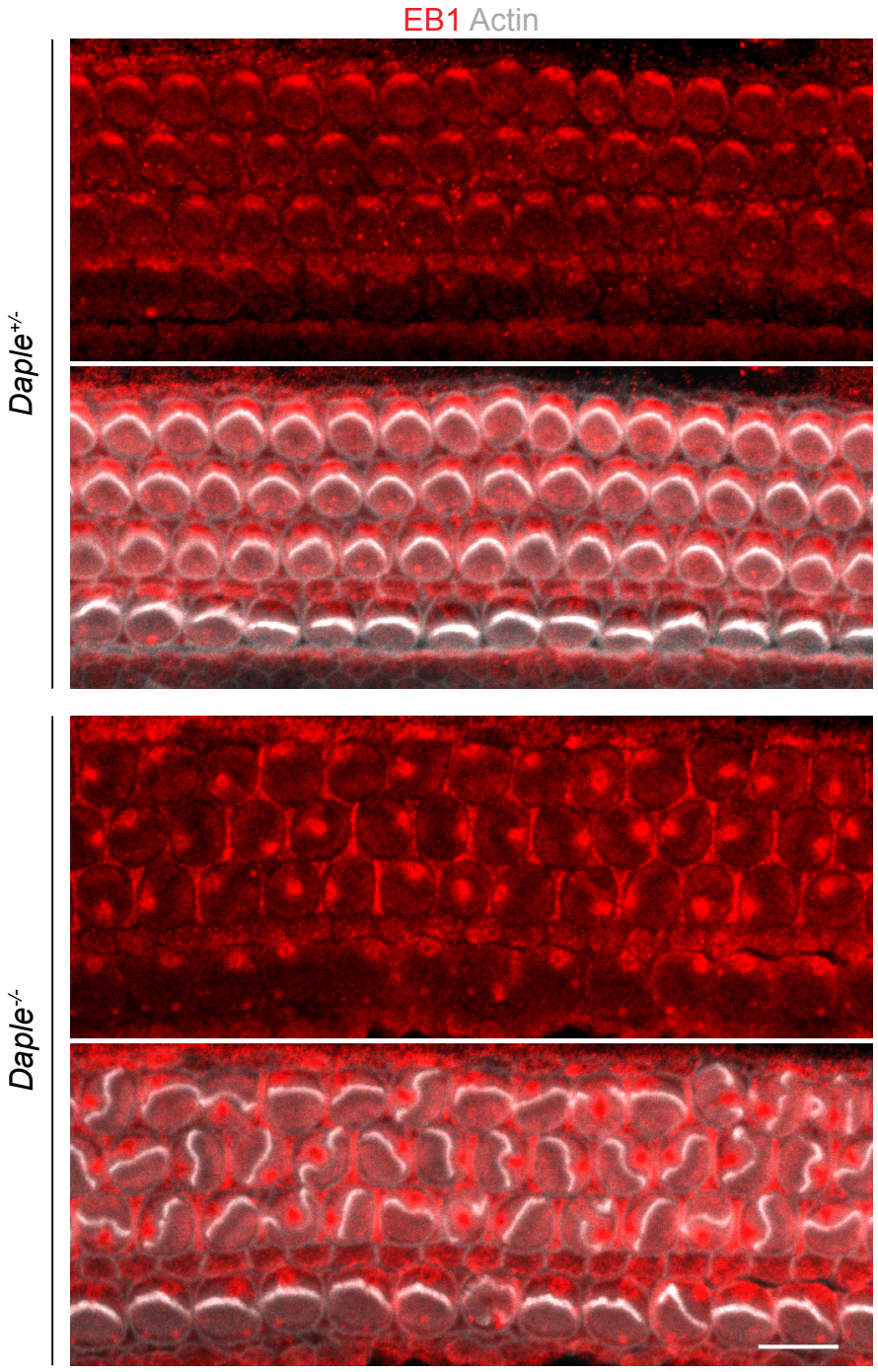
EB1 Actin
Daple+/-
Daple-/-

Table 6.1 Candidates revealed by a yeast two-hybrid screen of Daple

Gene symbol	Gene name	Accession number	Score
Dvl1	Dishevelled segment polarity protein 1	NM_010091.4	A
Dvl3	Dishevelled segment polarity protein 3	NM_001347176.1	A
Fcho1	FCH domain only 1	NM_028715.3	A
Gαi3	Guanine nucleotide binding protein	NM_010306.3	A
Hspg2	Heparan sulfate proteoglycan 2	NM_008305.3	A
Wwc1	WW, C2 and coiled-coil domain containing 1	NM_170779.1	A
Phldb2	Pleckstrin homology-like domain, family B, member 2	NM_153412.4	A
Zfp746	Zinc finger protein 746	NM_001347142.1	A
Cars2	Cysteinyl-tRNA synthetase 2	NM_024248.1	B
Dnlz	DNL-type zinc finger	NM_026828.3	B
Dst	Dystonin	NM_001276764.1	B
Dvl2	Dishevelled segment polarity protein 2	NM_007888.3	B
Lrig1	Leucine-rich repeats and immunoglobulin-like domains 1	NM_008377.2	B
Nup160	Nucleoporin 160	NM_021512.2	B
Plekhf1	Pleckstrin homology domain containing, family F	NM_024413.2	B
Rreb1	Ras responsive element binding protein 1	NM_001039188.1	B
Stag2	Stromal antigen 2	NM_021465.4	B
Ccdc151	Coiled-coil domain containing 151	NM_001163787.1	C
Sp2	Sp2 transcription factor	NM_030220.3	C
Sp7	Sp7 transcription factor	NM_130458.3	C

Spnb2	Spectrin beta 2	NM_009260.2	C
Zbtb4	Zinc finger and BTB domain containing 4	NM_029348.2	C
Zfp128	Zinc finger protein 128	NM_153802.4	C
2810422J05Rik	2810422J05Rik	NM_029366.2	D
Apobec2	Apolipoprotein B mRNA editing enzyme, catalytic polypeptide 2	NM_009694.3	D
Ccdc40	Coiled-coil domain containing 40	NM_175430.4	D
Chadl	Chondroadherin-like	NM_001164320.1	D
Clip2	CAP-GLY domain containing linker protein 2	NM_009990.3	D
Clip3	CAP-GLY domain containing linker protein 3	NM_001081114.1	D
Dctn1	Dynactin 1	NM_001198866.1	D
Emc2	ER membrane protein complex subunit 2	NM_025736.2	D
Flii	Flightless I actin binding protein	NM_001302207.1	D
Fscn2	Fascin actin-bundling protein 2	NM_172802.4	D
Ftl1	Ferritin light chain 1	NM_010240.2	D
Galnt6	UDP-N-acetyl-alpha-D-galactosamine: polypeptide N-acetylgalactosaminyltransferase 6	NM_001161768.1	D
Gnai2	Guanine nucleotide binding protein	NM_008138.4	D
Haus8	HAUS augmin-like complex, subunit 8	NM_001163042.1	D
Kif19a	Kinesin family member 19A	NM_001102615.1	D
Kif1b	Kinesin family member 1B	NM_207682.2	D
Lrrc45	Leucine rich repeat containing 45	NM_153545.2	D
Mospd3	Motile sperm domain containing 3	NM_030037.2	D
Myzap	Myocardial zonula adherens protein	NM_001033208.4	D

Nfs1	Nitrogen fixation gene 1	NM_010911.2	D
Nid1	Nidogen 1	NM_010917.2	D
Npnt	Nephronectin	NM_033525.3	D
Obsl1	Obscurin-like 1	NM_178884.5	D
Pard3	Par-3 family cell polarity regulator	NM_001013581.2	D
Pard3b	Par-3 family cell polarity regulator beta	NM_001081050.2	D
Psme3	Proteaseome (prosome, macropain) 28 subunit, 3	NM_011192.3	D
Rcor3	REST corepressor 3	NM_144814.3	D
Shroom4	Shroom family member 4	NM_001313764.1	D
Smc6	Structural maintenance of chromosomes 6	NM_025695.4	D
Smchd1	SMC hinge domain containing 1	NM_028887.3	D
Spred1	Sprouty protein with EVH-1 domain 1, related sequence	NM_033524.3	D
Sptbn5	Spectrin beta, non-erythrocytic 5	XM_006500537.2	D
Tax1bp1	Tax1 (human T cell leukemia virus type I) binding protein 1	NM_025816.3	D
Tbx18	T-box18	NM_023814.4	D
Trim37	Tripartite motif-containing 37	NM_197987.2	D
Zbtb44	Zinc finger and BTB domain containing 44	XM_006510215.3	D
Zfp219	Zinc finger protein 219	NM_001253694.1	D
Zfp32	Zinc finger protein 324	NM_178732.3	D
Zfp382	Zinc finger protein 382	XM_993935.1	D
Zfp462	Zinc finger protein 462	XM_017320199.1	D
Zfp467	Zinc finger protein 467	NM_020589.2	D
Zfp523	Zinc finger protein 523	NM_172617.3	D
Zfp655	Zinc finger protein 655	NM_028298.3	D

Figure 6.2 Candidates revealed by a yeast two-hybrid screen with Daple (A-C) Immunohistochemistry reveals the localizations of three candidate Daple-binding proteins in the cochlea. Maximal intensity projections of Z-stacks are shown. (A) Fcho1 (green) occurs at the apical surfaces of wild-type hair cells. Phalloidin staining (gray) reveals hair bundles. In some hair cells Fcho1 appears brighter near cellular boundaries (arrow). (B) Dctn1 (green) and Wwc1 (magenta) co-localize at or near the microtubule aster. Phalloidin (blue) labels hair bundles. (C) In hair cells and supporting cells, immunolabeling of Wwc1 (magenta) reveals membrane-bounded organelles in each cell body. (D) Wwc1 (magenta) occurs near the center of each hair cell in a pattern consistent with the tips of stereocilia. Phalloidin labeling (blue) reveals hair bundles. Scale bar, 10 μm.

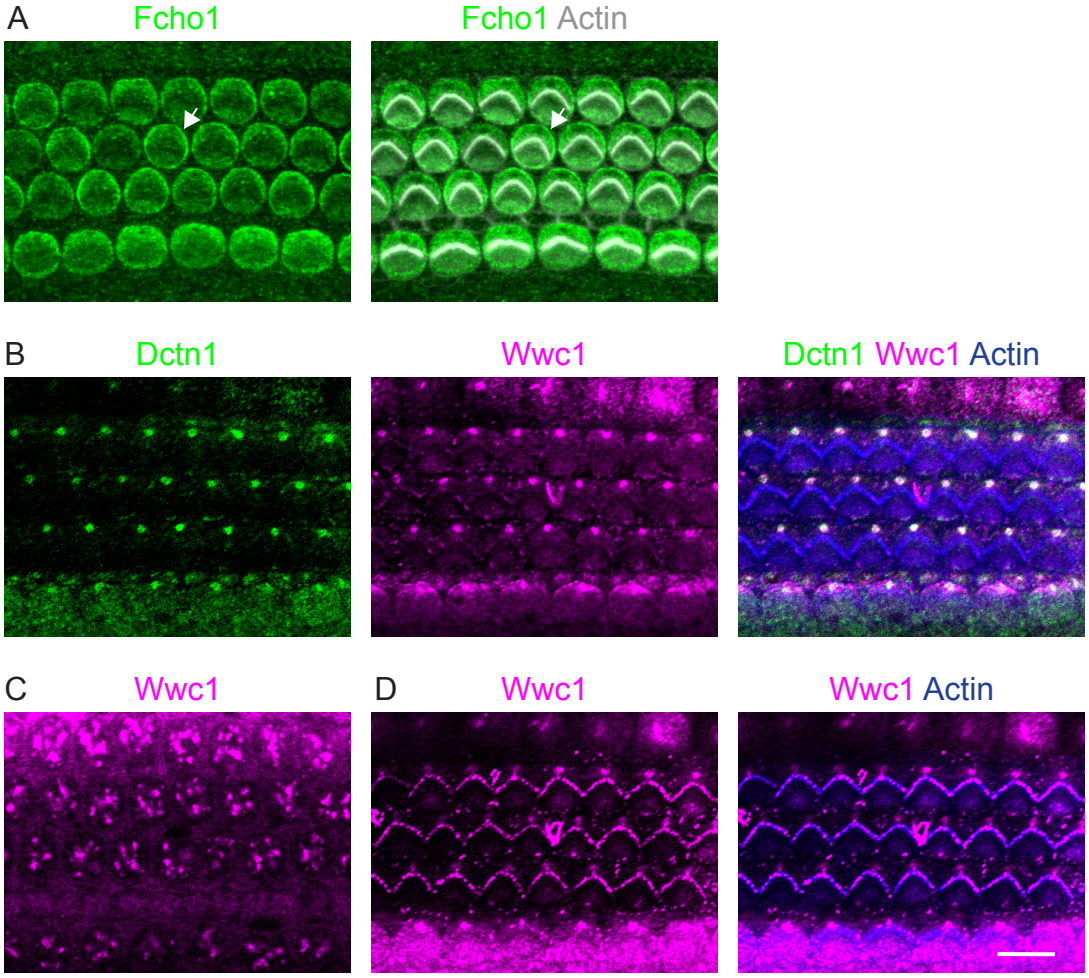
A
Fcho1
Fcho1 Actin
B
Dctn1
Wwc1
Dctn1 Wwc1 Actin
C
Wwc1
D
Wwc1
Wwc1 Actin

Discussion

Of the six core PCP proteins, only the Dishevelled isoforms interact with Daple in a yeast two-hybrid assay. In contrast, Daple appears to bind multiple members of the cell-intrinsic pathway, including two Gαi isoforms and Par-3. In light of its role in mammalian asymmetric cell division, the Dynein activator Dynactin-1 might also regulate cell-intrinsic polarity. The yeast two-hybrid results therefore support the hypothesis that Daple is primarily a cell-intrinsic factor.

Although Daple's interactions with Dishevelled and Gαi3 have been described previously[38, 39, 41], the other yeast two-hybrid candidates have not been validated. Immunohistochemistry shows that Daple and Par-3 co-localize (Figure 5.6). One study suggests that Dynein occurs at the abneural cortex of cochlear hair cells[19]; Dynactin-1 might distribute similarly and thereby localize near Daple. My own immunolabeling, however, demonstrates Dynactin-1 only along microtubules. This discrepancy necessitates further experimentation.

The yeast-two hybrid screen identified other microtubule-associated proteins, including two proteins in the Kinesin family. WW, C2 and coiled-coil domain containing 1 (Wwc1) also localizes along microtubules in the cochlea. An upstream regulator of the Hippo pathway, Wwc1 regulates the Dynein light chain 1 protein[47-49]. Daple might anchor microtubules through interactions with these proteins. Alternatively, because Daple occurs near the microtubule aster in the absence of LGN, microtubule-associated proteins may play a role in transporting Daple to apical junctions. Wwc1 additionally occurred at the tips of stereocilia and is therefore an intriguing candidate for further study.

Chapter Seven: Concluding remarks

In summary, Daple is a cell-intrinsic polarity factor that interacts with the core PCP protein Dishevelled. The characterization of *Daple*$^{-/-}$ mutants has shed light on two aspects of hair-bundle development. First, my observations provide striking evidence that the kinocilium or an associated organelle influences the extension of G-protein signals across the apical surface. Second, G-protein signals and the kinocilium must be properly coordinated to shape hair bundles. Although a previous study suggested that Gαi and LGN provide the blueprint for hair-bundle development, the kinocilium also appears to play an important role. Daple moreover coordinates these divergent signals.

The relationship between the G-protein crescent and migration of the kinocilium

An open question regarding planar polarity is how tissue-wide orientation and cell-intrinsic polarity are reconciled. One possibility is that tissue-wide cues regulate the abneural enrichment of Gαi and LGN, which directs the migration of the kinocilium. Consistent with this hypothesis, Daple is evidently regulated by these two proteins and required to position the kinocilium. Gαi is moreover enriched in an abneural crescent independently of Daple in immature hair cells. This observation suggests that the loss of Daple does not affect tissue-wide PCP and instead severs the connection between the crescent of G-protein signals and the migration of the kinocilium.

In this scenario, Daple's function might resemble the role of NuMA in mitotic spindle orientation. Daple may determine basal-body positioning through its putative interaction with Dynactin. The simultaneous binding of Gαi and a microtubule-associated

protein would permit Daple to anchor the kinocilium at the hair-cell surface. Alternatively, Daple might regulate Gαi activity directly. Yeast two-hybrid data and the subcellular proximity of the two proteins suggest a physiological interaction between Daple and Gαi. Although LGN attaches to GDP-bound Gαi, the GTP-bound state of Gαi is also important for the orientation of mitotic spindles; the guanine nucleotide exchange factor RIC-8 facilitates asymmetric cell division in *Cænorhabditis elegans*[50, 51]. The putative nucleotide-exchange activity of Daple may similarly contribute to kinociliary positioning in the cochlea. Unlike the loss of Daple, however, the absence of Ric-8 depletes the asymmetric localization of G-protein signals.

Some evidence suggests that Gαi and LGN are not necessary to direct the initial migration of kinocilium. In wild-type cells, the early crescent of G-protein signals does not perfectly correlate with the initial shift of the kinocilium[18]. Frequently the kinocilium is found at the abneural edge of a cell in which the crescent of Gαi expression is misoriented. My results additionally demonstrate that Daple is not required for the initial shift of the kinocilium away from the center of a hair cell. In embryonic cochleas, even those kinocilia opposite the crescent of Gαi are found near cellular boundaries. These observations raise the possibility that a second pathway regulates the migration of the kinocilium, and Daple aligns this system with the apical crescent of Gαi and LGN. Tissue-wide PCP signals might then separately regulate the abneural enrichment of Gαi and the positioning of the kinocilium.

Thus rather than linking Gαi and Dynactin, Daple might associate with Par-3 and Dynactin to position the kinocilium. Although suggested by the yeast two-hybrid screen,

these interactions have yet to be validated. However, Daple co-localizes with Par-3 early in development. Dishevelled might also play a role in positioning the kinocilium.

Notably, the loss of either Gαi or LGN affects the distribution of Daple. These results suggest that Daple operates downstream of cell-intrinsic polarity signals. Therefore, even if the apical crescent of G-protein signals does not directly generate force on the kinocilium, G-protein signaling is essential in immature hair cells to couple the kinocilium with the crescent of Gαi or LGN.

Potential implications of the interaction between Daple and Dishevelled

Dishevelled has been shown to regulate mitotic-spindle orientation and might likewise mediate kinociliary positioning in the cochlea[52]. Although the shape of the hair bundle does not appear significantly perturbed in Dishevelled double mutants, a triple knockout of the three Dishevelled homologs has not been described. Moreover the *Daple*$^{-/-}$ mutation constitutes a hair cell-specific interruption of Dishevelled function rather than a tissue-wide disruption of core PCP signaling, which may produce distinct effects. A study of *Ptk7* mutants, for example, suggests that hair-cell orientation requires a balance of contractile tension among cochlear epithelial cells[53]. The hair-cell specific loss of Dishevelled might similarly disrupt this balance. However, the loss of Ptk7 does not significantly disrupt the cell-intrinsic polarity of the hair bundle.

Dishevelled might also act independently of the core PCP pathway in hair-cell orientation. In a wound-healing assay, Daple facilitates the co-localization of Dishevelled and aPKC to activate Rac[39]. Dishevelled and aPKC do not co-localize in the cochlea and instead are found on opposite sides of the hair bundle. Nevertheless, Rac and its

downstream effectors the p21-activated kinases (PAK) affect hair-bundle development[16, 54]. Immunochemistry demonstrates activated PAK at the abneural edges of wild-type hair cells. Because I was unable to replicate this observation with my own immunolabeling, I have not yet investigated whether PAK is activated in the absence of Daple.

Because the core PCP proteins are distributed similarly on both sides of the utricle, a potential limitation of these hypotheses is that Daple likely localizes with Dishevelled on only one side of the utricle. Pertussis toxin affects orientation in only the Emx2-positive population of vestibular hair cells[26]; Daple might similarly affect Dishevelled in only one population of hair cells. Although a preliminary experiment (not shown) suggested that the line of polarity reversal is established in the absence of Daple, future work should include a closer examination of orientation defects on both sides of the utricle. Alternatively, the interaction between Daple and Dishevelled may be relevant only in the absence of core PCP signals.

To address this issue we electroporated two Daple constructs, each tagged with an amino-terminal GFP tag. The first construct contains full-length Daple; the second construct is missing the Dishevelled-binding domain. Unfortunately, the electroporation of both constructs into cochlear explants appeared lethal to hair cells (not shown). Although an amino-terminal tag has previously been used to visualize Daple in cell culture[39], we might remove the tag to investigate whether its presence is harmful to the hair cell. Future experiments might incorporate the electroporation of other Daple variants, including deletion of the Gαi-binding domain or the HOOK domain. A strategic analysis of Daple's functional domains may be necessary to dissect its likely complex role in hair-cell polarity.

Appendix A: Notch signaling orients hair cells in the zebrafish lateral line.

Introduction

The zebrafish lateral-line system comprises a series of sensory organs termed neuromasts that rely upon hair cells to detect local fluid flow. The hair cells of the lateral line are strikingly similar to those of the inner ear, but their location at the surface of the transparent zebrafish larva facilitates visualization and experimental manipulation. The planar polarity of the neuromast resembles that of the mammalian vestibular system: Each neuromast contains roughly equal numbers of oppositely oriented hair cells.

To achieve this organization, hair-cell precursors in the neuromast divide to produce sister cells that polarize in opposite directions. Whereas the anterior sister cell polarizes posteriorly, the posterior sister polarizes anteriorly (Figure 1A)[55]. The early neuromast thereby develops two columns of hair cells that are separated by a line of polarity reversal[56]. The arrangement becomes more complex as the neuromast matures, but pairs of hair cells remain visible. The localization of Vangl2 does not reflect this mirror symmetry but is similar in all hair cells[57].

Prior to establishment of mirror symmetry and shortly after precursor division, sister hair cells undergo rotational rearrangements[56, 57]. In 71% of observations, these rearrangements terminate in position reversal of the two cells. Such rearrangements do not occur in nascent supporting cells of the neuromast. Additionally, both core PCP and Notch signaling affect this process. In zebrafish *trilobite* larvae, which are deficient in Vangl2, hair cells orient randomly instead of anteriorly or posteriorly. Prior to planar polarization, rearrangements last over twice as long as in wild-type fish, and sister hair

cells undergo reversals in only 25 % of observations. In wild-type zebrafish, inhibition of Notch signaling with the γ-secretase inhibitor *N*-[*N*-(3,5-difluorophenacetyl-L-alanyl)]-*S*-phenylglycine *t*-butyl ester (DAPT) does not significantly affect duration of rearrangements, but position reversal again occurs for only about 25 % of hair-cell pairs. Moreover, both DAPT treatment and Vangl2 overexpression lead to an orientation bias within a neuromast; anteroposteriorly oriented neuromasts often display an anterior bias.

These results suggest that an asymmetry between sister cells induces cellular rearrangements to override an intrinsic preference for uniform orientation. Because Notch is known to mediate asymmetric cell division, Notch signaling between sister cells might similarly regulate cell-autonomous polarity in the neuromast. This hypothesis necessitates further examination, however. DAPT treatment inhibits Notch signaling not only in hair cells but throughout the neuromast. Notch is required for multiple steps of neuromast development, including the specification of dorsal and ventral regions of the neuromast from which hair-cell precursors arise[56]. Notch inhibition additionally generates supernumerary hair cells. Thus the disruption of polarity observed upon DAPT treatment might reflect a mispatterning of the neuromast that interrupts global orientation cues. Furthermore, potential downstream signals that specify cell-autonomous orientation in the neuromast have yet to be identified.

Materials and methods

Zebrafish transgenic lines

Zebrafish were maintained and bred with standard procedures. The following transgenic lines were used: *myo6b:Gff, brn3c:Gal4, UAS:GFP, myo6b:β-actin-GFP*[58] and *UAS:NICD-myc*[59].

Immunohistochemistry

Zebrafish were fixed between 3 and 5 days post fertilization in phosphate-buffered saline (PBS) with 4% paraformaldehyde and 0.2% Tween. After overnight fixation at 4°C, larvae were washed three times in PBS with 1% Tween and blocked at room temperature for 1 hr in PBS with 2 mg/mL bovine serum albumin, 5% normal goat serum, 1% dimethyl sulfoxide (DMSO), and 0.2% Tween. Primary antibody was diluted in PBS with 0.2% tween and incubated with the larvae overnight at 4°C. The next day larvae were washed three times in PBS with 0.2% Tween. Secondary antiserum was diluted in fresh washing solution and incubated with the larvae overnight at 4°C. Phalloidin-488 was added to the secondary antiserum at 1:40 to visualize actin-filled hair bundles. Primary antibodies used included anti-myc (1:1000, Covance 9E10) and anti-Gαi1 (1:100, GeneTex 128082).

Imaging

Zebrafish were mounted at 2 or 3 dpf in 1% low-melting-point agarose in Tricaine and E3. Time-lapse imaging was performed using a 63X/NA1.4 oil-immersion objective lens on an inverted microscope (Axiovert 200, Carl Zeiss Microscopy, Thornwood, NY) with a spinning-disk confocal system (Ultraview, Perkin-Elmer, Waltham, MA). Z-stacks were collected at 5- or 10-minute intervals.

Results

Gαi1 specifies hair-cell orientation in the zebrafish lateral-line system.

The signals that regulate cell-intrinsic polarity in the zebrafish lateral line remain unknown. Because G-protein signals have recently been associated with cell-intrinsic polarity in the mammalian inner ear, I speculated that this system is conserved in zebrafish. At least three isoforms of Gαi are present in the zebrafish genome. Unpublished RNA-Seq data from lateral-line hair cells suggested that Gαi1 is the most highly expressed among these isoforms. I therefore performed immunohistochemistry against Gαi1 in the zebrafish neuromast.

As in the mammalian inner ear, Gαi was expressed in a crescent at the apical surface of each zebrafish hair cell. Moreover, this crescent was adjacent to the kinocilium and therefore inverted in oppositely oriented cells. (Figure 1B). Gαi was asymmetrically distributed even in immature hair cells with an underdeveloped apical surface. This result suggests that Gαi plays an instructive role in shaping both zebrafish and mammalian hair bundles.

Notch specifies hair-cell orientation in the zebrafish lateral-line system.

To confirm that the effects of DAPT treatment on planar polarity reflect a hair-cell specific function of Notch, I used the Gal4-UAS system to drive constitutive expression of the Notch intracellular domain (NICD) in zebrafish hair cells (Figure 2A). The NICD was tagged with a myc epitope for immunohistochemistry. Although 51 % of hair cells oriented anteriorly in wild-type animals, 97 % of hair cells oriented anteriorly in myc-positive animals (Figure 2B). Neuromasts in myc-positive and wild-type fish contain a similar number of hair cells, suggesting that the specification of hair cells was unaffected (Figure 2C).

Hair cells moreover oriented anteriorly when either the *myo6b* promoter or *brn3c* promoter activated expression of the NICD (Figure 2, Figure 3A,B). Whereas the *myo6b promoter* was active in hair-cell precursors prior to mitosis, the *brn3c* promoter did not induce strong expression in hair-cell precursors or rearranging hair cells (Figure 3C,D). Evidently high levels of Notch expression were not required in hair-cell precursors or immature hair cells to induce an anterior orientation.

Figure A.1 Gαi1 expression in neuromast hair cells (A) A schematic diagram demonstrates that sister hair cells exhibit opposite orientations in the neuromast. The posterior hair cell is anteriorly oriented; the anterior hair cell is posteriorly oriented. The kinocilium (black) lies at the apex of each bundle (green). (B) For two different neuromasts (top and bottom), immunohistochemistry demonstrates that Gαi1 (magenta) is expressed in an apical crescent that denotes the orientation of each hair cell. Phalloidin (green) labels hair bundles. Gαi1 is asymmetrically distributed even in immature hair cells (arrows, top). Scale bar, 2 μm.

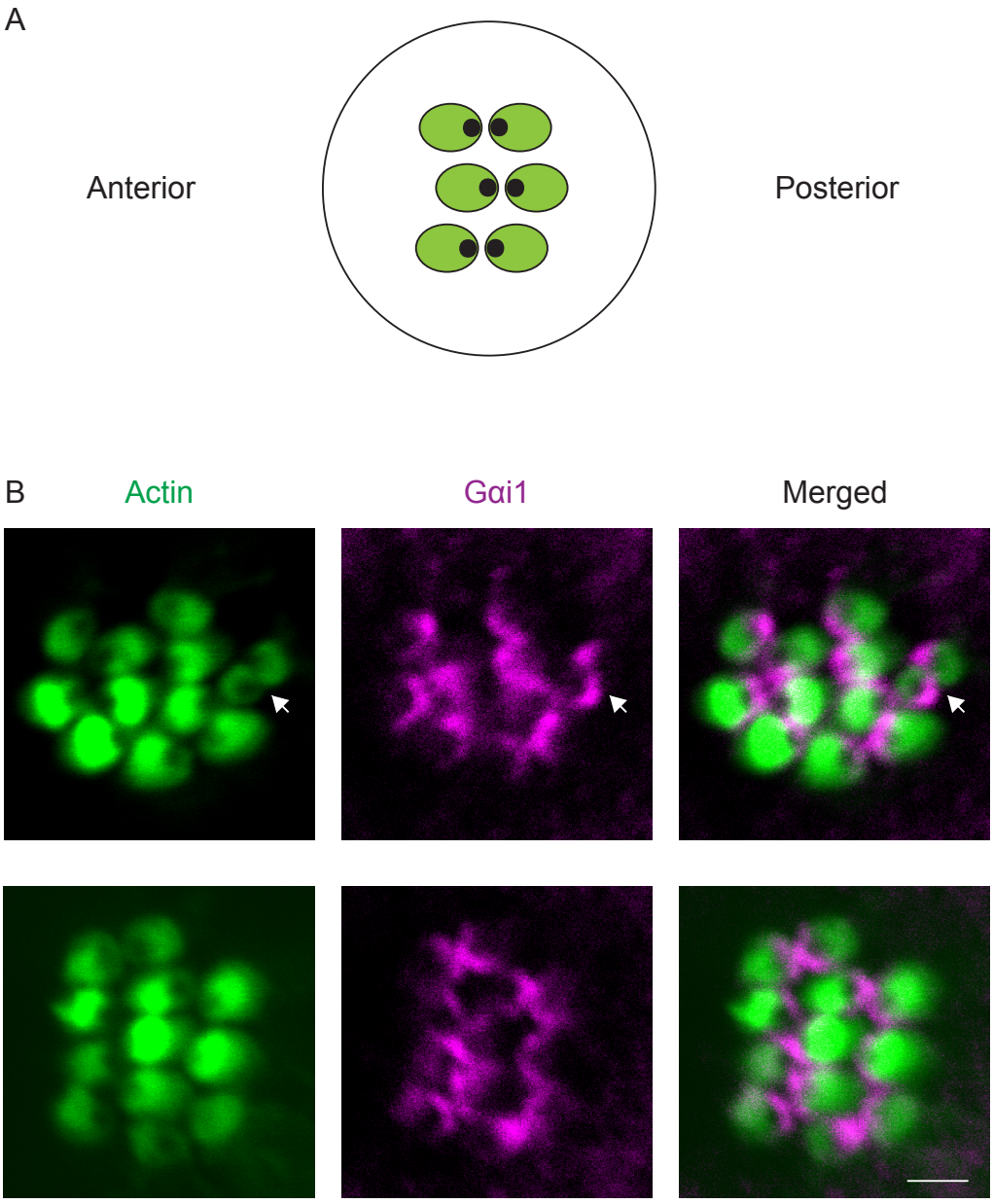
A
Anterior
Posterior
B
Actin
Gαi1
Merged

Figure A.2 Overexpression of the Notch intracellular domain in zebrafish hair cells Zebrafish of the *myo6b:Gff* transgenic line were crossed with *UAS:NICD-myc* zebrafish. Larvae were fixed at 4 days post fertilization and immunolabeled for myc expression (magenta). (A) Phalloidin labeling (green) reveals hair-bundle orientation in wild-type (left) and myc-positive (right) neuromasts. The yellow arrow indicates the anterior direction. Scale bar, 10 μm. (B) Hair-cell orientations are summarized in a pie chart. Blue denotes anteriorly oriented cells; pink denotes posteriorly oriented cells. Although 51% of hair cells orient anteriorly in *myo6b:Gff* fish (left, N = 303), 97% of hair cells orient anteriorly in *myo6b:Gff;UAS:NICD-myc* fish (right, N = 270) (C) On average, each neuromast contains approximately 15 hair cells in both genetic backgrounds.

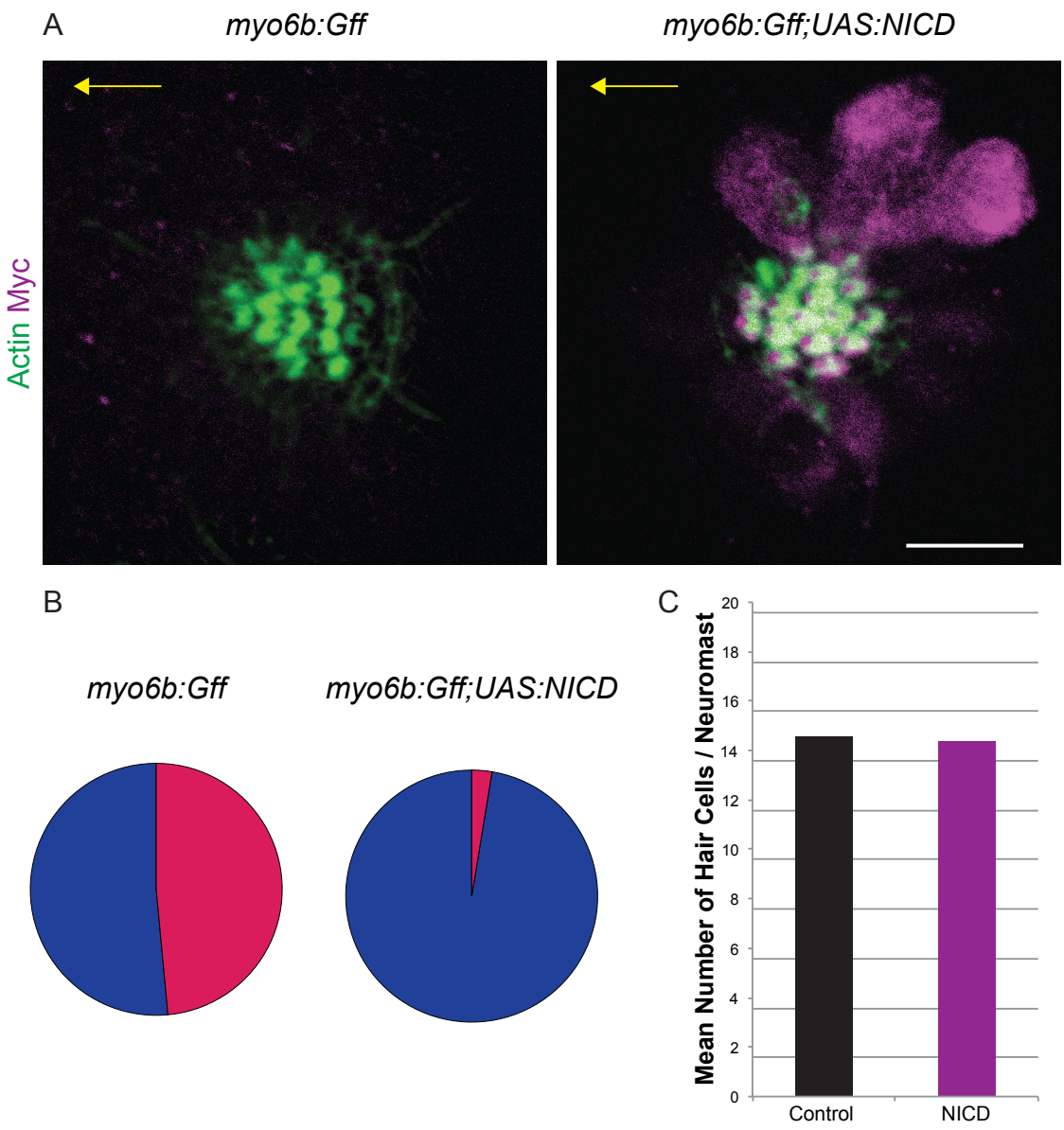
A
myo6b:Gff
myo6b:Gff;UAS:NICD
Actin Myc
B
myo6b:Gff
myo6b:Gff;UAS:NICD
C
Mean Number of Hair Cells / Neuromast
0
2
4
6
8
10
12
14
16
18
20
Control
NICD

Figure A.3 Overexpression of the NICD at different stages of hair-cell development (A) Phalloidin staining (green) reveals hair bundles in a *brn3c:Gal4* transgenic fish (left). The yellow arrow indicates the anterior direction. The neuromast exhibits equal numbers of oppositely oriented hair cells. Scale bar, 2 μm. (B) Phalloidin staining (green) reveals hair bundles in a *brn3c:Gal4;UAS:NICD* transgenic fish. The yellow arrow indicates the anterior direction. Hair cells that express NICD-myc (magenta) are oriented anteriorly. (C) Time-lapse imaging of a *brn3c:Gal4;UAS:GFP* neuromast demonstrates that GFP first appears after sister cells become visible and show a clear separation (arrowheads, t=0 min and t=100 min), an indication that the cells have completed rearrangements. (D) Time-lapse imaging of *myo6b:β-actin-GFP* fish demonstrates that GFP expression is already visible at precursor division (arrowhead, t=0 min). Rearrangements between developing sister cells are clearly visualized (arrowhead, t=70 min).

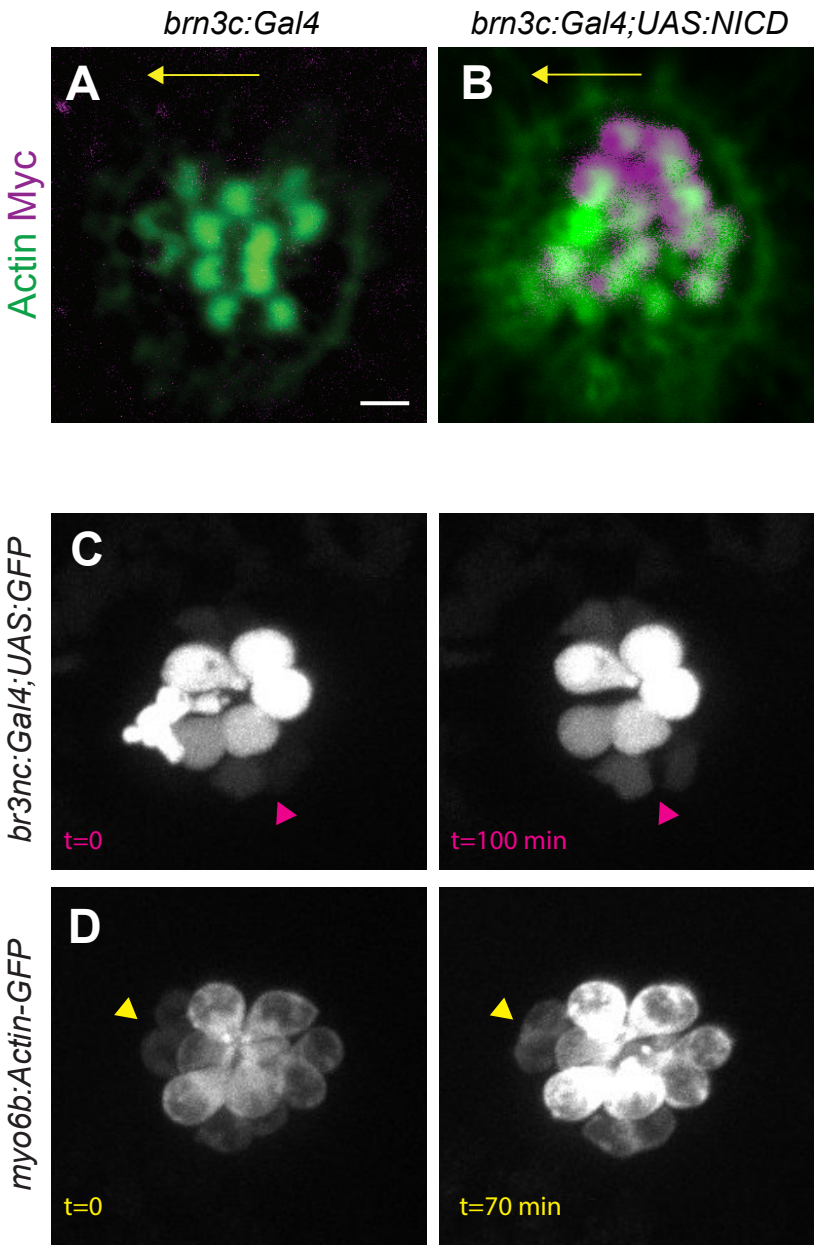
brn3c:Gal4
brn3c:Gal4;UAS:NICD
A
B
Actin Myc
C
br3nc:Gal4;UAS:GFP
t=0
t=100 min
D
myo6b:Actin-GFP
t=0
t=70 min

Discussion

Here I show that overexpression of the Notch intracellular domain causes hair cells to orient anteriorly. This effect is observed when either the *myo6b* promoter or the *brn3c* promoter activates overexpression. Notch therefore does not need to be expressed at high levels in hair-cell precursors or very immature hair cells to induce an anterior orientation. Surprisingly, DAPT treatment also induces an anterior bias, suggesting that an intermediate level of Notch signaling is necessary to specify hair-cell orientation. Alternatively the DAPT treatment of a zebrafish larva, which affects the entire neuromast, may disrupt hair-cell polarity through a separate mechanism.

In general, Notch signaling specifies the fate of a cell by activating transcription factors. A recent study of the mammalian utricle and saccule determined that Emx2 specifies the orientations of hair cells on one side of the line of polarity reversal in these tissues[26]. The authors additionally demonstrate that the role of Emx2 is conserved in zebrafish; the transcription factor is expressed in posteriorly oriented hair cells. Emx2 may specify orientation by regulating G-protein signals, and I show that Gαi likely specifies hair-cell orientation in zebrafish. Emx2 is therefore an excellent candidate to mediate Notch signaling in the zebrafish lateral line. Because my preliminary immunohistochemistry demonstrated Emx2 expression in both *myo6b:Gff* and *myo6b:Gff;UAS:NICD* hair cells (not shown), however, this relationship requires further characterization.

My observations suggest a multi-step model for the specification of hair-cell orientation. First, hair cells adopt a default orientation with respect to global polarity cues. The core PCP pathway may provide these cues. Second, sister hair cells maintain

close contact after mitosis and communicate with lateral Notch inhibition to adopt opposite orientations. This model predicts that a hair cell adopts the default orientation in the absence of cues from its sister cell. To test this prediction, I collaborated with Pavak Shah, a postdoctoral fellow in Zhirong Bao's group, who developed a real-time laser ablation and cell tracking system. The system permits high-throughput laser ablation of sister hair cells shortly after mitosis. The preliminary results are described in a manuscript that is currently under revision with *Developmental Cell*. In seven of nine ablations, the remaining sister cell adopted an anterior orientation. Although not yet statistically significant, this result is consistent with our current understanding of hair-cell polarity.

References

1. Hudspeth, A.J. Integrating the active process of hair cells with cochlear function. *Nat Rev Neurosci* **15**, 600-614 (2014).
2. Simons, M. & Mlodzik, M. Planar cell polarity signaling: from fly development to human disease. *Annual review of genetics* **42**, 517-540 (2008).
3. Yang, Y. & Mlodzik, M. Wnt-Frizzled/planar cell polarity signaling: cellular orientation by facing the wind (Wnt). *Annu Rev Cell Dev Biol* **31**, 623-646 (2015).
4. Wu, J., Roman, A.C., Carvajal-Gonzalez, J.M. & Mlodzik, M. Wg and Wnt4 provide long-range directional input to planar cell polarity orientation in Drosophila. *Nature cell biology* **15**, 1045-1055 (2013).
5. Ezan, J. & Montcouquiol, M. Revisiting planar cell polarity in the inner ear. *Seminars in cell & developmental biology* (2013).
6. Montcouquiol, M. *et al.* Identification of Vangl2 and Scrb1 as planar polarity genes in mammals. *Nature* **423**, 173-177 (2003).
7. Montcouquiol, M. *et al.* Asymmetric localization of Vangl2 and Fz3 indicate novel mechanisms for planar cell polarity in mammals. *The Journal of neuroscience : the official journal of the Society for Neuroscience* **26**, 5265-5275 (2006).
8. Copley, C.O., Duncan, J.S., Liu, C., Cheng, H. & Deans, M.R. Postnatal refinement of auditory hair cell planar polarity deficits occurs in the absence of Vangl2. *The Journal of neuroscience : the official journal of the Society for Neuroscience* **33**, 14001-14016 (2013).
9. Wang, Y., Guo, N. & Nathans, J. The role of Frizzled3 and Frizzled6 in neural tube closure and in the planar polarity of inner-ear sensory hair cells. *The Journal of neuroscience : the official journal of the Society for Neuroscience* **26**, 2147-2156 (2006).
10. Qian, D. *et al.* Wnt5a functions in planar cell polarity regulation in mice. *Developmental biology* **306**, 121-133 (2007).
11. Deans, M.R. *et al.* Asymmetric distribution of prickle-like 2 reveals an early underlying polarization of vestibular sensory epithelia in the inner ear. *The*

Journal of neuroscience : the official journal of the Society for Neuroscience **27**, 3139-3147 (2007).

12. Goetz, S.C. & Anderson, K.V. The primary cilium: a signalling centre during vertebrate development. *Nature reviews. Genetics* **11**, 331-344 (2010).
13. Simons, M. *et al.* Inversin, the gene product mutated in nephronophthisis type II, functions as a molecular switch between Wnt signaling pathways. *Nature genetics* **37**, 537-543 (2005).
14. Ross, A.J. *et al.* Disruption of Bardet-Biedl syndrome ciliary proteins perturbs planar cell polarity in vertebrates. *Nature genetics* **37**, 1135-1140 (2005).
15. Jones, C. *et al.* Ciliary proteins link basal body polarization to planar cell polarity regulation. *Nature genetics* **40**, 69-77 (2008).
16. Sipe, C.W. & Lu, X. Kif3a regulates planar polarization of auditory hair cells through both ciliary and non-ciliary mechanisms. *Development* **138**, 3441-3449 (2011).
17. May-Simera, H.L. *et al.* Ciliary proteins Bbs8 and Ift20 promote planar cell polarity in the cochlea. *Development* **142**, 555-566 (2015).
18. Tarchini, B., Jolicoeur, C. & Cayouette, M. A molecular blueprint at the apical surface establishes planar asymmetry in cochlear hair cells. *Developmental cell* **27**, 88-102 (2013).
19. Ezan, J. *et al.* Primary cilium migration depends on G-protein signalling control of subapical cytoskeleton. *Nature cell biology* **15**, 1107-1115 (2013).
20. Knoblich, J.A., Jan, L.Y. & Jan, Y.N. Asymmetric segregation of Numb and Prospero during cell division. *Nature* **377**, 624-627 (1995).
21. Gonczy, P. Mechanisms of asymmetric cell division: flies and worms pave the way. *Nature reviews. Molecular cell biology* **9**, 355-366 (2008).
22. Williams, S.E., Beronja, S., Pasolli, H.A. & Fuchs, E. Asymmetric cell divisions promote Notch-dependent epidermal differentiation. *Nature* **470**, 353-358 (2011).
23. Williams, S.E., Ratliff, L.A., Postiglione, M.P., Knoblich, J.A. & Fuchs, E. Par3-mInsc and Galphai3 cooperate to promote oriented epidermal cell divisions through LGN. *Nature cell biology* **16**, 758-769 (2014).

24. Bhonker, Y. *et al.* The GPSM2/LGN GoLoco motifs are essential for hearing. *Mamm Genome* **27**, 29-46 (2016).
25. Forge, A., Taylor, R.R., Dawson, S.J., Lovett, M. & Jagger, D.J. Disruption of SorCS2 reveals differences in the regulation of stereociliary bundle formation between hair cell types in the inner ear. *PLoS genetics* **13**, e1006692 (2017).
26. Jiang, T., Kindt, K. & Wu, D.K. Transcription factor Emx2 controls stereociliary bundle orientation of sensory hair cells. *Elife* **6** (2017).
27. Tarchini, B., Tadenev, A.L., Devanney, N. & Cayouette, M. A link between planar polarity and staircase-like bundle architecture in hair cells. *Development* **143**, 3926-3932 (2016).
28. Mauriac, S.A. *et al.* Defective Gpsm2/Galphai3 signalling disrupts stereocilia development and growth cone actin dynamics in Chudley-McCullough syndrome. *Nature communications* **8**, 14907 (2017).
29. Vojtek, A.B. & Hollenberg, S.M. Ras-Raf interaction: two-hybrid analysis. *Methods Enzymol* **255**, 331-342 (1995).
30. Bartel, P.L., Chien, C.-T., Sternglanz, R., and Fields, S. Using the two- hybrid system to detect protein-protein interactions. *Cellular Interactions in Development: A Practical Approach (Hartley, D.A., ed.), Oxford University Press, Oxford*, 153-179 (1993).
31. Fromont-Racine, M., Rain, J.C. & Legrain, P. Toward a functional analysis of the yeast genome through exhaustive two-hybrid screens. *Nature genetics* **16**, 277-282 (1997).
32. Formstecher, E. *et al.* Protein interaction mapping: a Drosophila case study. *Genome Res* **15**, 376-384 (2005).
33. Rain, J.C. *et al.* The protein-protein interaction map of Helicobacter pylori. *Nature* **409**, 211-215 (2001).
34. Wojcik, J., Boneca, I.G. & Legrain, P. Prediction, assessment and validation of protein interaction maps in bacteria. *J Mol Biol* **323**, 763-770 (2002).
35. Cho, H., Kim, D.U. & Kehrl, J.H. RGS14 is a centrosomal and nuclear cytoplasmic shuttling protein that traffics to promyelocytic leukemia nuclear

bodies following heat shock. *The Journal of biological chemistry* **280**, 805-814 (2005).

36. Cho, H. & Kehrl, J.H. Localization of Gi alpha proteins in the centrosomes and at the midbody: implication for their role in cell division. *The Journal of cell biology* **178**, 245-255 (2007).
37. Fry, A.M. *et al.* C-Nap1, a novel centrosomal coiled-coil protein and candidate substrate of the cell cycle-regulated protein kinase Nek2. *The Journal of cell biology* **141**, 1563-1574 (1998).
38. Oshita, A. *et al.* Identification and characterization of a novel Dvl-binding protein that suppresses Wnt signalling pathway. *Genes Cells* **8**, 1005-1017 (2003).
39. Ishida-Takagishi, M. *et al.* The Dishevelled-associating protein Daple controls the non-canonical Wnt/Rac pathway and cell motility. *Nature communications* **3**, 859 (2012).
40. Ara, H. *et al.* Role for Daple in non-canonical Wnt signaling during gastric cancer invasion and metastasis. *Cancer Sci* **107**, 133-139 (2016).
41. Aznar, N. *et al.* Daple is a novel non-receptor GEF required for trimeric G protein activation in Wnt signaling. *Elife* **4**, e07091 (2015).
42. Ghosh, P., Rangamani, P. & Kufareva, I. The GAPs, GEFs, GDIs and...now, GEMs: New kids on the heterotrimeric G protein signaling block. *Cell cycle*, 1-6 (2017).
43. Zheng, J.L. & Gao, W.Q. Overexpression of Math1 induces robust production of extra hair cells in postnatal rat inner ears. *Nature neuroscience* **3**, 580-586 (2000).
44. Wang, J. *et al.* Dishevelled genes mediate a conserved mammalian PCP pathway to regulate convergent extension during neurulation. *Development* **133**, 1767-1778 (2006).
45. Henne, W.M. *et al.* FCHo proteins are nucleators of clathrin-mediated endocytosis. *Science* **328**, 1281-1284 (2010).
46. Henne, W.M. *et al.* Structure and analysis of FCHo2 F-BAR domain: a dimerizing and membrane recruitment module that effects membrane curvature. *Structure* **15**, 839-852 (2007).

47. Rayala, S.K. *et al.* Essential role of KIBRA in co-activator function of dynein light chain 1 in mammalian cells. *The Journal of biological chemistry* **281**, 19092-19099 (2006).
48. Traer, C.J. *et al.* SNX4 coordinates endosomal sorting of TfnR with dynein-mediated transport into the endocytic recycling compartment. *Nature cell biology* **9**, 1370-1380 (2007).
49. Wennmann, D.O. *et al.* Evolutionary and molecular facts link the WWC protein family to Hippo signaling. *Mol Biol Evol* **31**, 1710-1723 (2014).
50. Afshar, K. *et al.* RIC-8 is required for GPR-1/2-dependent Galpha function during asymmetric division of C. elegans embryos. *Cell* **119**, 219-230 (2004).
51. Couwenbergs, C., Spilker, A.C. & Gotta, M. Control of embryonic spindle positioning and Galpha activity by C. elegans RIC-8. *Current biology : CB* **14**, 1871-1876 (2004).
52. Segalen, M. *et al.* The Fz-Dsh planar cell polarity pathway induces oriented cell division via Mud/NuMA in Drosophila and zebrafish. *Developmental cell* **19**, 740-752 (2010).
53. Lee, J. *et al.* PTK7 regulates myosin II activity to orient planar polarity in the mammalian auditory epithelium. *Current biology : CB* **22**, 956-966 (2012).
54. Grimsley-Myers, C.M., Sipe, C.W., Geleoc, G.S. & Lu, X. The small GTPase Rac1 regulates auditory hair cell morphogenesis. *The Journal of neuroscience : the official journal of the Society for Neuroscience* **29**, 15859-15869 (2009).
55. Lopez-Schier, H. & Hudspeth, A.J. A two-step mechanism underlies the planar polarization of regenerating sensory hair cells. *Proceedings of the National Academy of Sciences of the United States of America* **103**, 18615-18620 (2006).
56. Wibowo, I., Pinto-Teixeira, F., Satou, C., Higashijima, S. & Lopez-Schier, H. Compartmentalized Notch signaling sustains epithelial mirror symmetry. *Development* **138**, 1143-1152 (2011).
57. Mirkovic, I., Pylawka, S. & Hudspeth, A.J. Rearrangements between differentiating hair cells coordinate planar polarity and the establishment of mirror symmetry in lateral-line neuromasts. *Biology open* **1**, 498-505 (2012).

58. Kindt, K.S., Finch, G. & Nicolson, T. Kinocilia mediate mechanosensitivity in developing zebrafish hair cells. *Developmental cell* **23**, 329-341 (2012).
59. Scheer, N. & Campos-Ortega, J.A. Use of the Gal4-UAS technique for targeted gene expression in the zebrafish. *Mechanisms of development* **80**, 153-158 (1999).